

“Estudo das Propriedades Magnéticas de Sistemas com Alta Correlação Eletrônica”

**Aluno: Pascoal José Giglio Pagliusso
Orientador: Carlos Rettori**

Este exemplar corresponde à
relação final da Tese de Doutorado
defendida pelo aluno Pascoal José
Giglio Pagliusso e aprovada pela
comissão julgadora.

26/5/99

Comissão Julgadora:

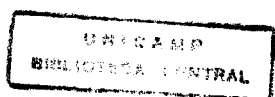
José Antonio Sanjurjo - IFGW/UNICAMP

Mário Eusébio Fóglia - IFGW/UNICAMP

Guillermo Gerardo Cabrera Oyarzún - IFGW/UNICAMP

Luiz Nunes de Oliveira - IF/USP-São Carlos

Paulo Pureur Neto - DF/URGS



TF 1189

UNIDADE	IFGW
N.º CHAMADA:	148e
V.	Ex.
TOMBO BC	39493
PROC.	229199
C	<input type="checkbox"/>
D	<input checked="" type="checkbox"/>
PESO	R\$ 11,00
DATA	17/11/99
N.º SPD	

m

CM-00136897-2

FICHA CATALOGRÁFICA ELABORADA PELA
BIBLIOTECA DO IFGW - UNICAMP

P148e

Pagliuso, Pascoal José Giglio

**Estudo das propriedades magnéticas de sistemas
com alta correlação eletrônica. - Campinas, SP : [s. n.],
1999.**

Orientador: Carlos Rettori.

**Tese (doutorado) - Universidade Estadual de
Campinas, Instituto de Física "Gleb Wataghin".**

- 1. Ressonância paramagnética eletrônica.**
- 2. Interações magnéticas. 3. Estrutura eletrônica.**
- 4. Interações elétron-íons. I. Rettori, Carlos.**
- III. Universidade Estadual de Campinas. Instituto de
Física "Gleb Wataghin". IV. Título.**



**Instituto de Física "Gleb Wataghin"
UNIVERSIDADE ESTADUAL DE CAMPINAS**

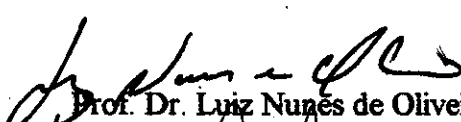
**MEMBROS DA COMISSÃO JULGADORA DA TESE DE DOUTORADO DO SR.
PASCOAL JOSÉ GIGLIO PAGLIUSO, RA 936231, APRESENTADA E
APROVADA AO INSTITUTO DE FÍSICA "GLEB WATAGHIN", DA
UNIVERSIDADE ESTADUAL DE CAMPINAS, EM 18 DE MAIO DE 1999.**

COMISSÃO JULGADORA:


Prof. Dr. José Antonio Sanjurjo
(Presidente da Banca Examinadora) – IFGW/UNICAMP
Nomeado pelo Prof. Dr. Carlos Rettori (afastado no exterior)


Prof. Dr. Mario Eusébio Foglio
IFGW/UNICAMP


Prof. Dr. Guillermo Gerardo Cabrera Oyarzún
IFGW/UNICAMP


Prof. Dr. Luiz Nunes de Oliveira
IF/USP-São Carlos


Prof. Dr. Paulo Pureur Neto
DF/UFRGS

Agradecimentos

Gostaria de agradecer especialmente o Professor Dr. Carlos Rettori pela orientação deste trabalho.

Agradecer sua paciência, sua amizade e os ensinamentos que me foram dados por ele durante todo este período.

Agradeço também aos meus companheiros de laboratório pela colaboração e amizade.

Agradeço a Fapesp pelo apoio financeiro a este trabalho.

Agradeço a toda minha família pelo apoio, e em especial a minha mulher Priscilla, pelo apoio e pela paciência.

Agradeço a Deus que sempre sinto ao meu lado.

E dedico este trabalho à minha filha que vai nascer.

RESUMO

Este trabalho de doutoramento apresenta, principalmente, uma sistemática de experimentos de Ressonância Paramagnética Eletrônica (RPE) e suscetibilidade magnética para estudos das propriedades magnéticas de diversos sistemas com alta correlação eletrônica, tais como:

- 1) Supercondutores de alta temperatura crítica (HTS)
- 2) Sistemas de Férmons pesados (HFS), Materiais tipo Kondo e Compostos de Valência Intermediária (IV).
- 3) Perovskitas que apresentam o fenômeno de magnetoresistência colossal (CMR).

Nos HFS de $\text{Eu}_{2-x}\text{Pr}_x\text{CuO}_4$, uma sistemática de experimentos de magnetização para $0 \leq x \leq 1$ em monocrstais crescidos em diferentes cadinhos, permitiu-nos estudar o aparecimento de uma componente de ferromagnetismo fraco (WF) neste materiais. Modos Raman “proibidos” foram somente observados em amostras que apresentam WF. Neste trabalho concluiu-se que para volumes de célula unitária menores que um volume crítico $V_C \approx 181.1 \text{ \AA}^3$ (próximo ao valor de V para Eu_2CuO_4 crescida em $\text{Al}_2\text{O}_3/\text{CuO}$), a estrutura T’ destes compostos apresenta distorções locais nos planos de CuO_2 dando origem a componente WF e aos modos Raman “proibidos”.

Para o caso dos HFS $\text{RNi}_2\text{B}_2\text{C}:Gd$ ($R = Y, Lu$), os valores obtidos para os parâmetros de troca $\langle J_{fs}^2(q) \rangle^{1/2}$, extraídos dos estudos da dependência a com temperatura da largura de linha de RPE do Gd^{+3} e do decréscimo de T_C com o aumento da concentração de impurezas magnéticas, coincidem dentro do erro experimental. Este resultado indica que os compostos $\text{RNi}_2\text{B}_2\text{C}$ ($R = Y, Lu$) comportam-se como um supercondutor BCS convencional.

Nestes compostos a interação de troca entre o Gd^{+3} e os elétrons de condução (c-e) mostrou-se dependende do vetor de onda q , e o parâmetro de troca $J_{fs}(0)$ foi encontrado positivo para ($R = Y, Lu$) indicando que a interação Gd^{+3} - c.e. é do tipo atômica. As interações elétron-elétron (relacionadas com o fator de Stoner), se mostraram significativas para as análises dos espectros de RPE.

Nos estudo de RPE do Gd^{+3} nos compostos IV de YbInCu_4 e no HFS de YbAgCu_4 e seus compostos de referência (Y, Lu)(In, Ag) Cu_4 , observamos um aumento do g-shift e da taxa de Korringa para os compostos de Yb em relação aos de referência. Este resultado é atribuído ao aumento da densidade de estados no nível de Fermi existente para os compostos de Yb.

Para ambos os sistemas acima, a dependência da interação de troca Gd^{+3} e os c-e com vetor de onda q foi introduzida para analisar os dados de RPE. No entanto, somente para o composto de IV, $YbInCu_4$, interações elétron-elétron, se mostrou significativa para as análises dos espectros de RPE.

Para o estudo dos compostos $LuInNi_4:Gd$ e Nd , uma contribuição tipo multibanda foi necessária para as análises de RPE. O valor da interação de troca entre a RE e os c-e é negativo para a banda-d (J_{fd}) é positivo para a banda-s (J_{fs}). O valor de J_{fs} é maior para o Nd^{3+} em relação ao Gd^{3+} para ambos os compostos, provavelmente devido ao maior contato com os c.e., resultado de um maior raio das camadas 4f para o Nd^{3+} . A banda eletrônica d para o caso do compostos de Ni, é provavelmente proveniente das camadas 3d incompletas do íon de Ni.

No composto $YBiPt$, o ajuste dos dados de susceptibilidade magnética e estudos de RPE nos permitiram obter os parâmetros de campo cristalino cúbico A_4 e A_6 para os compostos $Y_{0.9}Nd_{0.1}BiPt$ e $Y_{0.9}Yb_{0.1}BiPt$. Um limite superior para o parâmetro de campo cristalino $|b_4| \sim 1$ Oe, obtido da largura de linha, para o caso Gd, foi estimado. Nossos resultados sugerem que pequenos valores $|b_4|$ podem ser característicos de semicondutores da gap pequeno ou semimetais com baixa densidade de portadores.

Para as diferentes amostras $R_{1-x}A_xMnO_3$ ($R = La, Pr$; $A = Ca, Sr$) e também para os cristais CMR de $La_{1.2}Sr_{1.8}Mn_2O_7$, os "loops" de histerese e os "splittings" de linha de RPE ou linhas FMR observados foram associados à inhomogeneidades das amostras provenientes de uma distribuição não aleatória de vacâncias, defeitos e conteúdo de oxigênio, gerando principalmente uma distribuição de T_C nas amostras, ou para o caso das "layers" a fases extrínsecas provavelmente provenientes de fases de $La_{n+1}Mn_nO_{3n+1}$ com $n \neq 2$.

ABSTRACT

In this PhD work, we have performed systematic Electron Paramagnetic Resonance (EPR) and magnetic susceptibility studies in several Highly Correlated Electron Systems, such as: i) High-T_C Superconductors (HTS), ii) Heavy Fermions (HFS), Kondo Materials and Intermediate Valence compounds (IV) and iii) Colossal Magnetoresistance Perovskites (CMR).

For the HFS Eu_{2-x}Pr_xCuO₄ ($0 < x < 1$) compounds, our results of magnetization and Raman experiments were interpreted in terms of local distortions within the CuO₂ planes. Two forbidden Raman Modes (fMR) were observed in crystals showing a Weak-Ferromagnetic (WF) component.

We conclude that the Pt impurities and/or the reduction of the lattice cell volume, V , beyond a critical value, are the origin of orthorombic distortions which in turn are responsible for the fMR and WF observed in these compounds.

In the rare-earth nickel borocarbides RNi₂B₂C (R = Y, Lu), EPR of Gd³⁺ in normal state ($T > T_C$) allowed us to obtain the exchange parameter between the rare-earth localized magnetic moment and the conduction electrons. This parameter depends on the conduction electrons momentum transfer $|k_f^{in} - k_f^{out}| = q$, i.e. $J_{fs}(q)$.

The temperature dependence of the EPR linewidth yields a value for one of the exchange parameters, $\langle J_{fs}(q)^2 \rangle^{1/2}$, which is in agreement with that estimated from the slope of the initial linear decrease of T_C by the Gd³⁺ impurities. These results indicated that the R_{1-x}Gd_xNi₂B₂C (R = Y, Lu) compounds behave as conventional BCS superconductors.

In the EPR of Gd³⁺ studies in IV YbInCu₄ and the HFS YbAgCu₄ and their reference compounds, the larger g-shift and Korringa rate were interpreted in terms of the enhancement of the density of states at the Fermi level for the Yb-based. The extracted exchange interaction parameter was found to be q -dependent for all compounds. From the EPR and magnetic susceptibility data the electron-electron exchange enhancement factor for the YbInCu₄ was obtained. For the others compounds, including YbAgCu₄, the electron-electron interactions were negligible.

For the intermetallic LuInA₄ (A = Cu, Ni) compounds, our results of EPR of diluted Gd³⁺ and Nd³⁺ indicate a density of states at the Fermi level built up of a single s-band for the Cu-based compound and a multiple (s and d) bands for Ni-based system. The

susceptibility and specific heat data show negligible electron-electron exchange enhancement for both compounds.

For the Cu-based system the exchange interaction between the rare-earth local moment and the conduction electrons depends on the conduction electron wave-vector.

EPR and magnetic susceptibility experiments in the rare-earth ($R = Nd$, Yb and Er) doped cubic semiconducting $YBiPt$ allow us to estimate the fourth (A_4) and sixth (A_6) order crystal field parameters for this compound. It is found that these parameters are of the same order for all the R studied. On the other hand, no crystal field effects were found for Gd^{3+} doped single crystal system. Consistent with the small gap semiconducting character of the $YBiPt$ intermetallic compound, a Dysonian ESR lineshape with no g-shift and Korringa broadening was observed.

For the CMR $R_{1-x}A_xMnO_3$ ($R = La$, Pr ; $A = Ca$, Sr) and $La_{1.2}Sr_{1.8}Mn_2O_7$, the hysteresis loops and the resonance line splittings or the FMR lines observed above T_c are interpreted as inhomogeneities in the samples, probably, originated from a non-random distribution of vacancies, defects and oxygen content. The origin of the FMR lines in the layered $La_{1.2}Sr_{1.8}Mn_2O_7$ compounds was attributed to the presence of extrinsic Ruddlesden -Popper phases with $n \neq 2$.

INDICE

1. Introdução Geral

1.1 Supercondutores de Alta Temperatura Crítica.....	5
1.1.1 Compostos de $\text{Eu}_{2-x}\text{Pr}_x\text{CuO}_4$ ($0 \leq x \leq 1$) crescidos sob diferentes condições (Cadiños de Pt e Al_2O_3 e fluxos de CuO e PbO).....	5
1.1.2 Supercondutores Quaternários Intermétálicos $\text{RNi}_2\text{B}_2\text{C}$ ($\text{R} = \text{Y}, \text{Lu}$).....	7
1.2 Sistemas de Férnions pesados (HFS) e Compostos de Valênciia Intermediária (IV).....	8
1.2.1 Compostos de Yb com estrutura AuBe_5	11
1.2.2 Compostos de Yb com estrutura MgAgAs	13
1.3 Perovskitas que apresentam o fenômeno de Magnetoresistência Colossal(CMR).....	14

2. Resultados e Análises

2.1 Estudos de Magnetização e Espectroscopia Raman em monocristais de $\text{Eu}_{2-x}\text{Pr}_x\text{CuO}_4$	17
2.2 Estudos de RPE de Gd^{3+} no estado normal dos supercondutores $\text{RNi}_2\text{B}_2\text{C}$ ($\text{R} = \text{Y}, \text{Lu}$).....	25
2.3 Estudos de RPE de Gd^{3+} no composto de Valênciia Intermediária YbInCu_4 e seus compostos de referência (Y, Lu) InCu_4	29
2.4 Estudos de RPE de Gd^{3+} no composto Tipo Rede de Kondo YbAgCu_4 e seus compostos de referência (Y, Lu) AgCu_4	38
2.5 Estudos de RPE de Gd^{3+} e Nd^{3+} no composto LuInA_4 ($\text{A} = \text{Ni}, \text{Cu}$) - (submetido para Phys. Rev. B em 04/01/1999 e resubmetido em 03/05/1999).....	43
2.6 Estudos de Efeitos de Campo Cristalino no composto semicondutor de gap pequeno YBiPt - (aceito para publicação na Phys. Rev. B em 07/04/1999).....	62
2.7 Efeitos de Inomogeneidade nas Propriedades Magnéticas dos compostos $\text{R}_{1-x}\text{A}_x\text{MnO}_3$ ($\text{R} = \text{La}, \text{Pr}; \text{A} = \text{Ca}, \text{Sr}$).....	80
2.8 Estudos de RPE e FMR (Ressonância Ferromagnética) nos compostos Laminares: $\text{La}_{1.2}\text{Sr}_{1.8}\text{Mn}_2\text{O}_7$ - (submetido para Phys. Rev. B em 17/02/1999).....	92
3) Conclusão Geral.....	103
Apêndice 1-Aparato Experimental.....	107
Referências.....	111

Capítulo 1

INTRODUÇÃO GERAL

1) INTRODUCÃO GERAL

Neste trabalho de doutoramento, foram desenvolvidos estudos das propriedades magnéticas de diversos sistemas com alta correlação eletrônica, tais como:

- 1) Supercondutores de alta temperatura crítica (HTS)**
- 2) Sistemas de Férmions pesados (HFS), Materiais tipo Kondo e Compostos de Valência Intermediária (IV)**
- 3) Perovskitas que apresentam o fenômeno de magnetoresistência colossal (CMR).**

As principais técnicas experimentais utilizadas para o estudo dos sistemas acima foram: experimentos de Ressonância Paramagnética Eletrônica (RPE) numa ampla faixa de temperaturas (0.5 K - 600 K) e frequências de 4.0, 9.0 e 34 GHz; experimentos de magnetização dc (magnetômetro Squid - Quantum Design) e susceptibilidade ac (magnetômetro PPMS - Quantum Design). Experimentos de Espectroscopia de Espalhamento Raman e Difração de raios-X, foram realizados por colaboradores na própria Unicamp, e foram acompanhadas de perto neste trabalho. No entanto, toda a sistemática de crescimento e caracterização das amostras, bem como as medidas de propriedades de transporte, foram realizadas pelo grupo do Prof. Dr. John Sarrao, em Los Alamos – NM – USA.

Por fim, este trabalho de doutoramento resultou em uma sistemática de resultados, análises e conclusões a respeito das propriedades magnéticas macroscópicas e microscópicas destes sistemas de alta correlação eletrônica que estão dispostos nesta tese de acordo ao que se segue.

Nesta Introdução Geral serão encontrados sub-capítulos que descrevem cada um dos sistemas estudados, apresentando um resumo de suas propriedades físicas, dos estudos mais relevantes publicados a respeito e da motivação que nos levou a incluí-los neste trabalho.

O que se segue, no segundo capítulo, é a parte de resultados e análises que, nesta tese, será substituída pelos trabalhos de minha autoria ou co-autoria, publicados e submetidos para

publicação em revistas científicas no idioma exigido pelo veículo de divulgação. Este procedimento foi permitido, a critério do orientador, pelo artigo 2º da deliberação da CCPG - 001/98.

O terceiro capítulo, intitulado Conclusão Geral, será composto por um resumo de todas as conclusões obtidas nos estudos dos diversos sistemas, além dos possíveis desdobramentos futuros que estes estudos podem seguir.

Na sequência temos a secção de referências e finalmente um apêndice. Neste apêndice serão encontrados detalhes das montagem e dos aparatos experimentais utilizados para os experimentos de RPE para auxiliar aqueles que não são familiarizados com esta técnica.

Passamos agora, portanto, aos subcapítulos da Introdução Geral.

1.1) Supercondutores de alta temperatura crítica (HTS)

Duas classes de supercondutores HTS foram estudados neste trabalho:

1.1.1) Compostos de $\text{Eu}_{2-x}\text{Pr}_x\text{CuO}_4$ ($0 \leq x \leq 1$) crescidos sob diferentes condições (Cadiños de Pt e Al_2O_3 e fluxos de CuO e PbO).

Após a descoberta, por Bednorz e Müller,¹ de que o composto La_2CuO_4 quando dopado torna-se supercondutor (SC), um grande número de experimentos foram realizados a fim de caracterizar suas propriedades físicas e procurar sintetizar novos materiais com temperatura crítica ainda mais alta.² Muitos modelos teóricos têm sido propostos para explicar o mecanismo da supercondutividade nos HTS.³ Uma dificuldade comum a todos estes compostos está associada à necessidade de um alto nível de dopagem para que a supercondutividade se faça presente, resultando em amostras que nem sempre são homogêneas. Portanto amostras bem caracterizadas são fundamentais para o estudo desses HTS. Para minimizar este problema, nós realizaremos, quando possível, medidas em monocrystalis de alta qualidade.

Já é conhecido que correlações magnéticas em 2D entre os átomos de Cu nos planos de Cu-O estão presentes nos compostos precursores dos HTS. Eles experimentam um ordenamento antiferromagnético (AF) 3D a $T_N < 300$ K, com os spins dos átomos de Cu basicamente alinhados nos planos de Cu-O.⁴⁹ T_N diminui nestes cupratos quando estes são dopados com elétrons ou buracos. De acordo com o tipo dopagem, SC tipo-p ou tipo-n podem ser obtidas. Portanto qualquer mecanismo de emparelhamento para explicar a SC nestes materiais deverá levar em conta a correlação magnética entre os átomos de Cu e os portadores de carga.

Os compostos ortorrômbicos $(La_{1-x-y}A_xGd_y)_2CuO_{4+\delta}$ pertencem aos HTS tipo-p. Nestes sistemas o íon de Gd^{3+} é a sonda de RPE com $y \approx 0.002 - 0.01$, e A = Sr, Ba, com $x \approx 0 - 0.15$ e δ (teor de oxigênio) são os elementos dopantes de buracos. Nossa grupo, estudando os compostos isolantes precursores dos HTS $(La_{1-x}Gd_x)_2CuO_{4+\delta}$ com $x = 0.005$, encontrou que os espectros de RPE do Gd^{3+} levam a um parâmetro de campo cristalino (CFP) de segunda ordem muito grande, b_{20} (~ 1600 Oe). Além disto, foram observados linhas extras (splittings) da estrutura fina do espectro do Gd^{3+} abaixo de $T_N \sim 255$ K.¹⁰ Estes “splittings” foram analisados em termos de um campo magnético de origem dipolar atuando no sítio da RE e associado ao ordenamento AF 3D dos spins dos Cu em $T_N \sim 255$ K. Destes dados, o número de magnetons de Bohr associado aos Cu foi determinado. Esse número está de acordo com os dados de difração de neutrons, $\sim 0.5\mu_B/Cu$. Amostras dopadas com Sr confirmaram que T_N diminui conforme aumenta a concentração de Sr. O “splitting” das linhas de RPE apareceram a temperaturas mais baixas, de acordo com a diminuição de T_N .¹⁰

Os compostos de $(Ln_{1-x-y}A_xGd_y)_2CuO_{4+\delta}$, com $Ln = Pr, Nd, Sm, Eu$; A = Ce, Th (elementos dopantes de elétrons) e Gd (sonda de RPE) são tetragonais e pertencem aos HTS tipo-n. Nossa grupo realizou trabalhos também com os compostos $(Eu_{1-x}Gd_x)_2CuO_4$,¹¹ medindo os CFP, encontrando linhas de RPE com “splittings” abaixo de T_N , como no caso de $(La_{1-x}Gd_x)_2CuO_{4+\delta}$. Neste composto também associou-se o “splitting” ao campo interno devido ao ordenamento AF criado pelos spins dos Cu. O composto $(Eu_{1-x}Gd_x)_2CuO_4$ tem um comportamento magnético muito complicado abaixo de T_N . Em cristais crescidos em cadinhos

de Pt e fluxo de PbO, os espectros de RPE dependem da maneira pela qual se resfriam as amostras, ou seja, com ou sem campo magnético aplicado. Este comportamento está associado ao ferromagnetismo fraco (WF) observado nestes cristais. Esse efeito não foi encontrado em cristais crescidos em cadinhos de alumina e fluxo de CuO.¹² Não obstante, o “splitting” das linhas de RPE do Gd³⁺ foi observado para T < T_N.

Portanto, uma sistemática de experimentos de magnetização em Eu_{2-x}Pr_xCuO₄ (0 ≤ x ≤ 1) crescidos em cadinhos de Pt e de Al₂O₃ com fluxos de CuO e PbO, foi proposta neste doutoramento com o objetivo de estudar a aparecimento desta componente WF (cap. 2.1). Modos Raman “proibidos” foram observados somente em amostras que apresentam WF. Neste trabalho concluiu-se que para volumes de célula unitária menores que um volume crítico V_C ≈ 181.1 Å³ (próximo ao valor de volume (V) do composto de Eu₂CuO₄ crescido em Al₂O₃/CuO) a estrutura T’ destes compostos apresentam distorções locais nos planos de CuO₂, dando origem à componente WF e as modos Raman “proibidos”. No entanto para as amostras crescidas em Pt, as impurezas de Pt substitucionais ao Cu, favorecem as distorções locais nos planos de CuO₂ permitindo valores de V_C de 183.5 Å³ ≤ V_C ≤ 185.5 Å³ (cap. 2.1).

1.1.2) Supercondutores Quaternários Intermétálicos RNi₂B₂C (R = Y,Lu).

A nova série de supercondutores quaternários intermetálicos RNi₂B₂C (R = terra-rara)¹³ tem atraído grande interesse da comunidade científica, devido a estes materiais apresentarem supercondutividade com temperaturas críticas relativamente altas. (T_C = 16.6 K para R = Lu e T_C = 15.5 K para R = Y).¹⁴ Anisotropia magnética e coexistência entre supercondutividade (SC) e antiferromagnetismo (AF) associado às terras-raras R (com T_N < T_C ou T_N > T_C)¹⁵⁻¹⁷ é motivo de grande interesse nos estudo destes materiais, alguns deles chegando a apresentar inclusive reentrância no estado normal.

A estrutura magnética modulada, obtida por experimentos de difração de nêutrons, no composto HoNi₂B₂C¹⁵⁻¹⁷ para temperaturas entre T_N ≈ 5 K e T_C ≈ 7.5 K, e a supressão da SC

com a substituição de Dy por Lu em $DyNi_2B_2C$ foram interpretados em termos de um “pair breaking” magnético para os compostos RNi_2B_2C ($R = Er, Dy$).

A estrutura destes compostos é tetragonal (grupo espacial $I4/mmm$) com camadas de Ni perpendiculares ao eixo-c. Esta estrutura é similar à estrutura dos óxidos supercondutores de Alta- T_c . No entanto, nenhum ordenamento AF ou correlações magnéticas entre os spins de Ni foram encontradas nestes compostos. Além disso, cálculos de Estrutura de Banda Eletrônica sugerem que os compostos RNi_2B_2C são metais 3D “d-band” e que a SC é mediada via mecanismo convencional BCS elétron-fónon. Evidências experimentais para isto são dadas por experimentos de Espectroscopia de Tunelamento¹⁸ e efeito isotópico.¹⁹

É conhecido que estudos de RPE de terras-raras (Gd^{+3}) como impurezas magnéticas diluídas, no estado normal de supercondutores tipo BCS, possibilitam determinar parâmetros de troca entre o momento localizado da impureza e os elétrons de condução (c-e). E sabe-se também que este parâmetro de troca obtido da variação da largura de linha de RPE com a temperatura é o mesmo extraído pela variação de T_c com a concentração de impurezas magnéticas de acordo com a teoria de Abrikosov and Gorkov (AG).^{20,21}

Tendo isto em mente, planejamos e realizamos estudos de ESR de Gd^{+3} no estado normal dos compostos $R_{1-x}Gd_xNi_2B_2C$ ($R = Y, Lu$). (cap. 2.2)

1.2) Sistemas de Férmons pesados (HFS) e Compostos de Valência Intermediária (IV).

Uma classe de materiais metálicos muito interessante que vem sido estudada há vários anos,²² são os férmons pesados (HFS) ou metais de elétrons pesados. Em alta T seu comportamento é indistinguível de outros compostos de terras-raras (RE) ou actinídeos com momentos localizados proveniente de camadas eletrônicas parcialmente preenchidas. Quando a T diminui eles não se ordenam magneticamente como usualmente acontece, mas alguns dos elétrons f tornam-se itinerantes formando uma espécie de estado metálico.

A problemática teórica sobre como esse estado aparece a partir dos elétrons f continua sendo um problema muito estudado no momento. A questão fundamental é como uma banda

de elétrons pesados pode ser descrita. Momentos localizados ativos em RPE, colocados em matrizes HFS, podem resultar numa sonda magnética de muita utilidade para esclarecer a natureza destes materiais. Apesar do grande esforço teórico e experimental que tem sido realizado ainda está em falta o entendimento completo das propriedades dos HFS.

Em baixas T, os HFS são caracterizados por um comportamento anômalo na dependência com a temperatura do calor específico que tem os valores da contribuição eletrônica, γ , largamente aumentados, o que é normalmente atribuído a um grande aumento na densidade de estados eletrônicos no nível de Fermi, $\eta(E_F)$. Quando impurezas magnéticas são diluídas num metal simples, tal como a Ag, a linha de RPE possui um deslocamento do valor de g (g-shift) proporcional a $J \cdot \eta(E_F)$, e uma relaxação para os spins dada pela relação de Korringa $1/\gamma T_2 = \pi/h(J \cdot \eta(E_F))^2 k_B T$, onde J é o parâmetro de troca e $\eta(E_F)$ é a densidade de estados eletrônicos no nível de Fermi do metal hospedeiro.

Nos HFS pode haver uma banda eletrônica estreita com largura comparável a kT . Logo pode-se esperar que a relação de Korringa não seja mais válida, mas parte da alta densidade de estados poderia se manifestar na dependência com a temperatura nos dados de RPE. Não obstante pode acontecer que, qualquer que seja o mecanismo que resulte numa dependência forte com a temperatura da densidade de estado $\eta(E_F)$ obtida a partir do calor específico, ela não se manifeste na relaxação dos spins dos momentos localizados, como encontrou-se nos casos de UBe_{13} e UPt_3 dopados com Dy^{3+} , Er^{3+} e Gd^{3+} .²³⁻²⁵

Pode-se esperar uma grande redução efetiva na densidade de estados no sítio do U nos dados de RPE. Não foi encontrado mudança nem na posição da ressonância nem no comportamento de Korringa. Em resumo, parece que os momentos localizados substituindo o U em UBe_{13} e UPt_3 simplesmente não estão acoplados ao sistema de férmons pesados. Isto contradiz os experimentos de NMR no Be de MacLaughlin, et al.²⁶ Isto é surpreendente já que a interação de troca entre os momentos localizados e os elétrons de condução possuem atuações de maneira similar que a interação hiperfina do momento nuclear do Be com os elétrons de

condução. Em outras palavras os resultados de RPE não refletiam a situação real.

COS: A ideia física básica sugerida foi a de que os elétrons pesados nos sítios 4f e 5f estariam relativamente distantes dos momentos, para NMR $\sim 3 \text{ \AA}$ e para RPE $\sim (4\text{-}5) \text{ \AA}$. Não obstante para os núcleos leves, como Be, acoplados diretamente via a interação dipolar seria suficiente para providenciar uma relaxação suficientemente rápida devido a flutuação dos momentos 4f e 5f. Ele tem sugerido que o acoplamento dipolar anterior seria suficiente para explicar a relaxação em NMR do Be em CeBe₁₃ e UBe₁₃. Pelo contrário, o acoplamento dipolar não poderia explicar a relaxação de núcleos pesados, tal como ¹¹⁹Sn em CeSn₃, os quais possuem uma relaxação muito forte devida ao acoplamento no sítio com os elétrons de condução. Também não contribuiria para relaxação do Er³⁺ em UBe₁₃ e UPt₃ onde a contribuição principal deveria vir do acoplamento RKKY com os elétrons pesados e no sítio, pela interação de troca com os elétrons normais. Finalmente os cálculos sugerem que a falta de êxito, até o momento, no uso da técnica de RPE para o estudo dos elétrons pesados poderia ser eliminada naqueles compostos HFS com ordem magnética.²⁷

Simanek e Sasahara²⁸ tem calculado a relaxação de Korringa para momentos localizados em HFS utilizando o modelo de Yoshimori e Kasai.²⁹

Eles concluíram que a relaxação não seria afetada por férmons pesados renormalizados, em acordo com outros resultados.²³⁻²⁶

uma redução relativamente grande na densidade de estado no sítio da RE foi observado no RPE relativo aos compostos análogos de La. O mecanismo físico sugerido para este caso foi a hibridização entre os estados localizados de Ce-4f e a banda de condução. A hibridização produziria uma delocalização dos estados de Ce-4f e uma repulsão dos estados eletrônicos de condução nas vizinhanças dos estados Ce-4f.^{30,31} Não obstante não há um acordo total com respeito a esta explicação, já que em outros compostos de valência intermediária tais como CeBe₁₃,³² CeIr₂,³³ e YbCuAl,³⁴ a relaxação de Korringa das impurezas foi encontrada

inalterada ou ainda um pouco aumentada relativamente aos compostos de referência de valência não intermediária.

Enfim, foi proposto neste doutoramento pesquisar uma série de sistemas novos, cuidadosamente escolhidos, para que a técnica de RPE permita uma contribuição relevante ao destes sistemas de elétrons pesados. Passamos agora a uma descrição particular de cada um deles.

1.2.1) Compostos de Yb com estrutura de AuBe₅

A estrutura de AuBe₅ é cubica fcc, conhecida como fases cúbicas de Laves (C15b, F43m) com a formula genérica AB₂. Na estrutura C15, os átomos A ficam numa rede de diamante que pode ser pensada como duas redes fcc deslocadas em (1/4, 1/4, 1/4). Na estrutura AuBe₅, diferente da C15, uma das redes fcc é substituída por um terceiro átomo (e.g., X) para dar a subestrutura de zincoblenda AX com a formula genérica AXB₄. Propomos estudar uma série de compostos de Yb com a formula genérica YbXCu₄, para pesquisar as idéias acima discutidas.

Os dois materiais mais estudados neste grupo são YbInCu₄³⁵ e YbAgCu₄.³⁶ O primeiro apresenta uma transição de primeira ordem isoestrutural com uma expansão volumétrica a T = 40 K, o segundo é um composto classificado como rede de Kondo com temperatura característica de ~ 150 K. A descoberta da transição de primeira ordem isoestrutural com mudança de volume no YbInCu₄ foi feita por Felner e Nowik.³⁷ Eles encontraram que a transição se dava entre T = 40 K e 80 K na liga de Yb₄In₆Cu₂, suposta ser C15.³⁸ Os átomos de Índio substituem um sítio particular para formar o composto AXB₄, de tal maneira que experimentos podem ser realizados numa rede quimicamente melhor ordenada.³⁵ Felner e Nowik mostraram que a transição de fase produz uma expansão volumétrica de 0.45% ao esfriar o composto sem mudança estrutural. Simultaneamente, uma grande queda na resistividade elétrica e susceptibilidade magnética, χ , de uma lei do tipo Curie-Weiss a altas temperaturas, com momento magnético perto do esperado para um íon na configuração f¹³, J =

7/2, para um paramagnetismo de Pauli a baixas temperaturas. Os valores da susceptibilidade χ , ~ 0.005 emu/mole-Yb e o calor específico³⁸ abaixo da transição ~ 55 mJ/mole-K², são consistentes com um ion-*f* de valência intermediária com temperatura característica de, T ~ 400 K - 500 K. Experimentos de NMR³⁹ também mostram uma abrupta mudança no acoplamento hiperfino. Finalmente resultados de absorção de raios-X L_{III} foram interpretados em termos da mudança da valência, de z = 2,9 acima da transição para z = 2,8 embaixo da transição.³⁸ Por outro lado o composto isoestrutural de YbAgCu₄ é um material tipo rede de Kondo que não apresenta a transição de fase de primeira ordem.³⁶ Sua temperatura característica é da ordem de 150 K. Foi interessante também estudar este sistema para ver como as propriedades mudam quando comparadas com aquelas do YbInCu₄.

As transições de fase de primeira ordem isoestruturais encontradas em YbInCu₄ e no Ce metálico são extremamente raras. Seria apropriado perguntar porque isto acontece. Como foi proposto para outros HFS, a energia ganha da condensação de Kondo não é suficiente para vencer a energia de deformação que aparece na mudança de volume. Os compostos de Yb formam uma ampla gama de materiais interessantes que possibilitam o estudo das propriedades físicas longe da transição de fase. Por outro lado estas transições de fase são acessíveis em temperatura e composição, além de que monocristais de alta qualidade podem ser preparados com relativa facilidade. Estes sistemas são mais simples que o do Ce metálico devido a que o Ce possui a fase-β de simetria mais baixa, e também a temperatura de transição é bem menor no YbInCu₄ que no Ce. A concentração de RE é mais diluída nos compostos de Yb. Portanto os resultados podem ser comparados com mais confiabilidade com os dos compostos de referência. Finalmente os problemas severos de oxidação do Ce não estão presentes nos compostos de Yb.

RPE de Gd³⁺ em YbXCu₄ com X = In, Ag e seus compostos de referência YxCu₄ e LuXCu₄ foram realizados para os estudos acima propostos. Nossos resultados de RPE de Gd³⁺ em RInCu₄ (R = Yb, Y, Lu) e RAgCu₄ (R = Yb, Y, Lu) mostraram um alargamento da largura de linha e um deslocamento do valor de g muito maiores para os compostos de Yb,

consistente com uma maior densidade de estados eletrônicos no nível de Fermi para estes compostos. (cap. 2.3, 2.4).

Além destes, outros compostos interessantes são os isostruturais $RInNi_4$. ($R = RE$). Recentemente, medidas de propriedades de transporte, susceptibilidade magnética em função da temperatura, pressão e campo, realizadas no composto $RInNi_4$ mostraram uma fase ferromagnética para $T < 3$ K, com um incremento do calor específico eletrônico a baixa temperatura além de fortes efeitos de campo cristalino.⁴⁰ Os estudos de calor específico eletrônico, magnetização e resistividade apontam um estado fundamental Γ_7 , com um "splitting" de campo cristalino da ordem de ~ 110 K.⁴⁰

Com o mesmo espírito dos discussões anteriores, medidas de RPE de Gd^{+3} e Nd^{+3} inicialmente nos compostos de referência $LuInNi_4$ (cap. 2.5) foram realizadas. Os resultados de RPE obtidos foram interpretados em termos de uma densidade de estados no nível de Fermi constituída por um sistema de multi-banda d e s . As medidas de calor específico e susceptibilidade magnética mostraram que as interações elétron-elétorn podem ser desprezadas para este sistema (cap. 2.5).

1.2.2) Compostos de Yb com estrutura de MgAgAs

O composto cúbico de $YbBiPt$ possui a estrutura cúbica do $MgAgAs$ (grupo espacial $F43m$), chamada ligas de Heusler.⁴¹ Esta estrutura contém uma fórmula por célula primitiva sendo a célula primitiva romboédrica preferida frente à célula unitária fcc.⁴² Os átomos estão localizados em três dos quatro sítios ao longo da diagonal [111] com simetria de grupo pontual tetraédrico e o quarto sítio pode ser pensado como uma vacância ordenada. Canfield e seus colaboradores⁴³⁻⁴⁶ estudaram $YbBiPt$ detalhadamente. Eles o chamaram “super-heavy fermion”, devido a que possui o maior coeficiente linear conhecido no calor específico, $\gamma = 8$ J/mol K², o qual é uma ordem de grandeza maior que os férmons pesados típicos⁴⁷ e três ordens de grandeza maior que os metais convencionais.

Devido ao composto de Yb, toda a série RBiPt ($R = RE$) foi recentemente muito estudada.⁴³⁻⁴⁶ A maioria destes materiais são semicondutores de gap pequeno ($\Delta = 0.1 - 0.01$ eV) que uma evolução para um comportamento metálico quando R é variado através das RE. Esta sistemática mudança de um comportamento semicondutor para as RE leves, para um comportamento metálico as RE pesadas é atribuído à diminuição do parâmetro de rede quando R é variado na sequência da série das RE. Portanto, é provável que os efeitos de campo cristalino sejam importantes para o entendimento das propriedades físicas deste material.

Experimentos de RPE das terras raras $R = Gd^{3+}$, Er^{3+} , e Nd^{3+} diluídos nos compostos $Y_{1-x}R_xBiPt$ foram realizados durante este doutorado. Sabendo-se que o quarteto $\Gamma_8^{(3)}$ é o estado fundamental do Er^{3+} em $YBiPt$,⁴⁸ enquanto para Nd^{3+} e Yb^{3+} os estados fundamentais obtidos foram um Γ_6 e um Γ_7 , respectivamente. (cap.2.4) Além destes estados fundamentais, medidas conjuntas de EPR e susceptibilidade magnética para $YBiPt$: Gd, Nd, Er permitiu-nos obter os parâmetros de campo cristalino cúbico A_4 e A_6 para $YBiPt$. (cap. 2.6) Estranhamente nenhum efeito de campo cristalino foi observado nos espectros do Gd^{3+} em $YBiPt$. Neste trabalho sugerimos que, aparentemente, algum mecanismo de blindagem se faz presente para o caso do Gd^{3+} em presença de um campo cristalino cúbico em uma matriz de características semicondutoras de gap-pequeno, onde é baixa a densidade de portadores.^{49, 50} Os estudos de RPE para Nd^{3+} e Gd^{3+} em $YBiPt$ não mostraram nenhuma variação da largura de linha com a temperatura e nenhum g-shift, consistente com o caráter semicondutor (gap pequeno) do composto. (cap. 2.6).

É válido afirmar que nenhuma ressonância do Yb^{3+} foi observado no composto $Y_{1-x}Yb_xBiPt$ ($x = 0.5, 1, 5$ e 10%), tampouco ressonâncias do Nd^{3+} no composto composto $Yb_{1-x}Nd_xBiPt$ ($x = 0.2$ e 0.5%). Possíveis explicações para isto são dadas no capítulo 2.4.

1.3) Perovskitas que apresentam o fenômeno de magnetoresistência colossal (CMR).

Recentemente um renovado interesse recaiu sobre as manganitas com estrutura das perovskitas $R_{1-x}B_xMnO_{3+\delta}$ onde $R = La$, Pr , Nd , e $B = Ca$, Sr , Ba , Pb devido a estas

apresentarem uma resposta gigante magnetoresistiva, chamada magnetoresistência colossal (CMR) que pode ser de grande interesse tecnológico.⁵¹ Experimentos realizados com filmes finos do composto $\text{La}_{0.67}\text{Ca}_{0.33}\text{MnO}_3$ ⁵² registraram um efeito de magnetoresistência ($\Delta R/R_H$) de até 3.300%.

O composto estequiométrico de LaMnO_3 é um semicondutor que se ordena antiferromagneticamente (AF) e muda para um metal ferromagnético (FM) na faixa de composições de $0.2 < x < 0.5$.⁵³ Foi sugerido há muitos anos que o FM nestes compostos pode ser explicado na base do modelo de Zener de dupla troca (double exchange (DE)) entre os pares de Mn^{3+} and Mn^{4+} .⁵⁴ Muitos trabalhos recentes afirmam que somente o mecanismo DE não é suficiente para explicar as propriedades físicas destes materiais.

A. J. Millis et al.⁵⁵ propuseram um forte acoplamento elétron-fónon proveniente de um “splitting Jahn-Teller” do nível *d* do átomo de Mn^{+3} , em adição ao modelo de dupla-troca para explicar o comportamento da resistividade dos compostos $\text{La}_{1-x}\text{Sr}_x\text{MnO}_3$.

H. Y. Hwang et al.⁵⁶ realizaram experimentos com estes compostos substituindo o átomo de La por outras terras raras, encontrando uma relação direta entre o raio atômico da terra rara, a temperatura de ordenamento (T_C), e a intensidade do efeito magnetoresistivo. Este resultado mostra que a noção de interação dupla-troca deve ser generalizada para incluir efeitos de rede, que causam mudanças nos parâmetros de “saltos” dos elétrons entre os átomos de Mn como resultado das mudanças no ângulo da ligação Mn-O-Mn.

A. Asamitsu et al.⁵⁷ mostraram que transições estruturais podem ser inclusive induzidas através da aplicação do campo magnético externo e, recentemente, outros autores acreditam que ordenamento de carga que ocorrem acima de T_C são importantes para o entendimento das propriedades físicas destes materiais.

Experimentalmente a relação de $\text{Mn}^{3+}/\text{Mn}^{4+}$ pode ser modificada mudando, através do nível da dopagem, *x*, ou do teor de oxigênio, *δ*, produzindo portanto uma variável muito interessante para o entendimento das propriedades físicas destes materiais. No entanto, em alguns casos estas variáveis podem gerar amostras bastantes inhomogêneas, com distribuição inhomogênea de oxigênio, vacâncias no sítio da terra-rara, entre outros defeitos. Muitas vezes

efeitos extrínsecos devido a presença de inhomogeneidades podem ser erroneamente atribuídas a propriedades intrínsecas do material. RPE pode ser um método muito útil e bastante sensível para avaliar a homogeneidade das amostras (caps. 2.7 e 2.8). Dentro deste trabalho, portanto, as medidas de RPE serviram apenas com "teste de qualidade" das amostras não nos permitindo portanto extrair e estudar parâmetros e propriedades intrínsecas a estes sistemas.

Ainda de dentro destas classes de matérias, passamos a estudar também as perovskitas laminares de $\text{La}_{1.8}\text{Sr}_{1.2}\text{Mn}_2\text{O}_7$. Estes materiais possuem estruturas tetragonais semelhantes aos supercondutores de alta- T_C com octaedros de Mn-O intercalados com planos de La_2O_2 .⁵⁸

Kimura et. al. observaram duas transições magnéticas neste material para $T_C \sim 125$ K e $T_C \sim 280$ K.⁵⁹ Estes atribuíram a transição de alta temperatura uma transição magnética bidimensional associados aos planos de Mn. Potter et. al. observando as mesmas transições interpretaram a transição de alta temperatura como proveniente de fases extrínsecas $\text{La}_{n+1}\text{Mn}_n\text{O}_{3n+1}$ com $n \neq 2$.⁶⁰

Como RPE é uma técnica muito sensível para a observação de fases espúrias magnéticas realizamos estudos de RPE em dois monocrystal crescidos de forma ligeiramente diferente de $\text{La}_{1.8}\text{Sr}_{1.2}\text{Mn}_2\text{O}_7$. Estas amostras foram trazidas por mim de Los Alamos e a conclusão destes estudos apontam para a existência de fases espúrias com volume de $\sim 0.03\%$ do volume total para uma amostra e $\sim 0.25\%$ para a outra (cap. 2.8).

Capítulo 2

RESULTADOS E ANÁLISES

Seção 2.1

2.1 Estudos de Magnetização e Espectroscopia Raman em monocristais de $\text{Eu}_{2-x}\text{Pr}_x\text{CuO}_4$

2.1) Estudos de Magnetização e Espectroscopia Raman em monocrystalis de $\text{Eu}_{2-x}\text{Pr}_x\text{CuO}_4$.



Physica B 253 (1998) 296–304

PHYSICA B

Weak ferromagnetism and Raman scattering in $\text{Eu}_{2-x}\text{Pr}_x\text{CuO}_4$

P.G. Pagliuso^{a,*}, E. Granado^a, J.A. Sanjurjo^a, C. Rettori^a, I. Torriani^a, D. Rao^b, S.B. Oseroff^b, J. Sarrao^c, Z. Fisk^c

^a Instituto de Física "Gleb Wataghin", UNICAMP, 13083-970, Campinas-SP, Brazil

^b San Diego State University, San Diego, CA 92182, USA

^c National High Magnetic Field Laboratory, Florida State University, Tallahassee, FL 32306, USA

Received 22 January 1998

Abstract

Magnetization and Raman experiments performed in single crystals of $\text{Eu}_{2-x}\text{Pr}_x\text{CuO}_4$ ($0 \leq x \leq 1$) are interpreted in terms of local distortions within the CuO_2 planes. We find that samples grown in Pt crucibles contain Pt impurities, that are partially responsible for these distortions. We observed: (i) the appearance of two *forbidden* Raman modes (fRM) and (ii) a weak-ferromagnetic (WF) component when the crystals are field cooled in the *ab*-plane. The WF component, the onset temperature where 3D long-range WF is first observed, T_{WF} , the coercive field, H_C , and the intensity of the fRM decrease as the Pt content decreases. For crystals with a similar Pt content, the above quantities are larger for samples with smaller lattice unit cell volume, V . The crystal with the highest Pt content and smallest V ($x = 0$) shows, for $T \rightarrow 0$, an average canted Cu moment of $5.5(3) \times 10^{-3} \mu_B/\text{Cu}$. The intensity of the fRM decrease with T , suggesting that the number of distortions decrease as V expands. This is consistent with recent neutron diffraction results in Eu_2CuO_4 , where a tetragonal to orthorhombic phase transition was observed at $T \lesssim 200$ K. We concluded that the Pt impurities and/or the reduction of V beyond a critical value, V_c , are the origin of these orthorhombic distortions which in turn are responsible for the fRM and WF observed in these compounds. © 1998 Elsevier Science B.V. All rights reserved.

PACS: 63.20.-e; 75.60.-d; 75.30.Gw; 74.72.Jt

Keywords: Ferromagnetism; Raman scattering; $\text{Eu}_{2-x}\text{Pr}_x\text{CuO}_4$

1. Introduction

Among the antiferromagnetic (AF) rare-earth (RE) cuprites, RE_2CuO_4 (RE = Pr, Nd, Sm, Eu and Gd) of T' -(14 mmm) tetragonal structure, Eu_2CuO_4 is particularly interesting because it is at the bound-

ary between superconductivity (SC) and weak-ferromagnetism (WF) [1,2]. The light RE compounds do not show WF, and become superconductors when appropriate electron doping ions are incorporated into the lattice ($\text{RE}_{2-x}\text{M}_x\text{CuO}_4$ with $\text{M} = \text{Ce}^{4+}$, Th^{4+} and $x \approx 0.15$) and treated in reducing atmospheres [3]. However, for Gd and heavier RE compounds, SC cannot be induced [1,4,5]. Instead, WF is observed in them [6–8].

* Corresponding author. Fax: +55 19 7882427; e-mail: sanjurjo@ifi.unicamp.br.

Eu_2CuO_4 grown in alumina crucibles and CuO flux shows no WF, and SC can be induced on it [9]. But, Eu_2CuO_4 grown in Pt crucibles and PbO flux shows WF when field cooled (FC) in the ab -plane, and SC is not observed [2]. Another property of these series is that for the heavier RE (from RE = Tb to Tm, and Y) the compounds can only be synthesized under high pressure [6-8]. These results show that there is a subtle instability of the T'-type structure at the middle of the RE series. In all the RE_2CuO_4 compounds, the Cu moments order AF in the ab -plane at $T_N \approx 240$ -290 K [5]. The presence of WF has been attributed to a canting of the Cu moments in the ab -plane, away from their perfect AF alignment. In the T'-(14mm) structure WF order is forbidden, and lattice distortions in the CuO_2 planes were invoked to account for it [2,10]. A displacement of the O(1) oxygen ions, perpendicular to the Cu-O bonds in the CuO_2 planes, occurs in these compounds [1]. These distortions result in

oxides in the following crucibles/fluxes: Pt/PbO, Pt/CuO and $\text{Al}_2\text{O}_3/\text{CuO}$ [12]. The single crystals were of plate-like shape, with the c-axis perpendicular to the large face. Typical crystal sizes were $4 \times 3 \times 0.3 \text{ mm}^3$. Electron-microprobe analysis shows Pt content of 2-5 at% of Cu, and no traces of Pb for crystals grown in Pt/PbO. For crystals grown in Pt/CuO the Pt content was found to be less than 1 at% of Cu. The Raman measurements were carried out in backscattering geometry with the samples mounted on the cold finger of a close-cycle He refrigerator. The 514.5 nm line of an Ar ion laser was used to excite the spectra. The scattered light was analyzed with a Jobin Yvon T64000 triple spectrometer equipped with a cryogenic charge-coupled device (CCD) camera. In all the measurements the spectral resolution was better than 4 cm^{-1} . A laser power of about 15 mW and a point focus of $\sim 50 \mu\text{m}$ in diameter was used in order to avoid heating of the samples. The samples

Dzyaloshinsky-Moriya exchange interaction between adjacent Cu moments, giving rise to the observed WF [6,11].

In a previous work [2] we showed that the observed *forbidden* Raman modes (fRM) and WF were related in the $\text{Eu}_{2-x}\text{Pr}_x\text{CuO}_4$ compounds. These results suggested that local distortions in the CuO_2 planes, due to the O(1) oxygen displacements, were the origin for the observed fRM and WF. In this report we present additional data taken in samples grown in different crucibles (Pt and Al_2O_3) and fluxes (PbO and CuO). Electron-microprobe analysis was used to determine the Pt and Pb contents. Results of microwave absorption experiments are also given. The analysis of these results lead us to conclude that Pt impurities and/or the reduction of the lattice unit cell volume beyond a critical value, V_c , are the origin of the distortions responsible for the fRM and WF observed in these compounds.

2. Experimental details

Crystals of $\text{Eu}_{2-x}\text{Pr}_x\text{CuO}_4$ were grown from nominal stoichiometric mixtures of the respective

increasing the T . The X-ray powder diffraction experiments were performed in a Rigaku R200 diffractometer at room T . The lattice parameters were calculated using a Rietveld profile refinement program and their values are given in Table 1. Magnetization measurements were made in a Quantum design DC SQUID magnetometer. The microwave absorption experiments were carried out in a Varian X-Band ESR spectrometer using a TE₁₀₂ room T cavity and a nitrogen flux cooling system.

3. Results and analysis

For the $\text{Eu}_{2-x}\text{Pr}_x\text{CuO}_4$ compounds studied, Fig. 1 shows the room T lattice unit cell volume, $V = ca^2 \text{ \AA}^3$, as a function of x . For comparison we included V for Gd_2CuO_4 crystals grown in Pt/PbO [12] and ceramics of $\text{Gd}_{2-x}\text{Sm}_x\text{CuO}_4$ grown in $\text{Al}_2\text{O}_3/\text{CuO}$ [13]. As expected from the Vegard's law, V increases as the substituting Pr ions increase ($x > 0$). The Eu_2CuO_4 samples grown in $\text{Al}_2\text{O}_3/\text{CuO}$, Pt/CuO, and Pt/PbO show, respectively, increasing V . For these samples, the relative change in the a and c lattice parameters are about 0.15% and 0.10%, respectively (see Table 1). Since the Pt

Table 1

Room T lattice parameters (\AA) of $\text{Eu}_{2-x}\text{Pr}_x\text{CuO}_4$ grown in $\text{Al}_2\text{O}_3/\text{CuO}$, Pt/CuO and Pt/PbO (see text). Values in parentheses are Rietveld analysis standard deviations

	$\text{Al}_2\text{O}_3/\text{CuO}$	Pt/CuO	Pt/PbO		
x	0.0	0.0	0.0	0.10	0.25
a	3.9021(2)	3.9021(1)	3.9084(2)	3.9081(4)	3.9112(10)
c	11.8948(5)	11.9067(4)	11.9093(2)	11.9422(16)	11.9404(8)
					0.50
					1.0
					3.9247(3)
					12.0522(8)

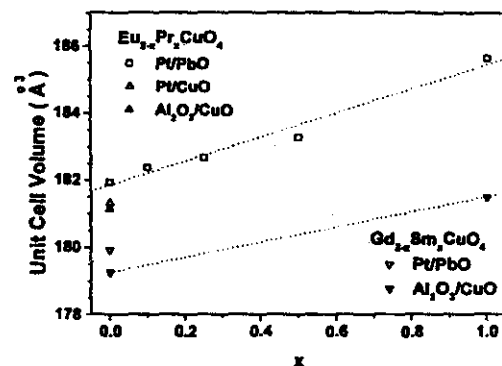


Fig. 1. Room T lattice unit cell volume, $V = ca^2 \text{\AA}^3$, as a function of x for $\text{Eu}_{2-x}\text{Pr}_x\text{CuO}_4$ grown in Pt/PbO , Pt/CuO and $\text{Al}_2\text{O}_3/\text{CuO}$. The V values for Gd_2CuO_4 crystals grown in Pt/PbO [12] and ceramic samples of $\text{Gd}_{2-x}\text{Sm}_x\text{CuO}_4$, grown in $\text{Al}_2\text{O}_3/\text{CuO}$ [13] are also included.

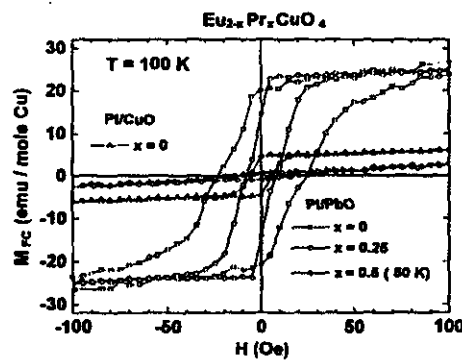


Fig. 2. Hysteresis loops of the ab -plane FC (50 kOe) total DC-magnetization, $M_{\text{FC}}(H_m, T)$, at $T = 100 \text{ K}$ between $H_s = \pm 100 \text{ Oe}$, for the samples showing WF. The data for the $x = 0.5$ sample were taken at $T = 80 \text{ K}$.

ionic radius is larger than that of Cu, and the electron-microprobe analysis shows that only Pt is incorporated into the compounds during the crystal growth, it is reasonable to assume that Pt substitutes the Cu ions in the CuO_2 planes.

The hysteresis loops of the ab -plane DC-magnetization obtained after FC in 50 kOe, $M_{\text{FC}}(H_m, T)$, at $T = 100 \text{ K}$ are shown in Fig. 2 for the applied field interval $H_s = \pm 100 \text{ Oe}$. WF is observed in all these samples. The WF disappears for $x > 0.5$ for crystals grown in Pt/PbO , and is not present for any value of x when they are grown in $\text{Al}_2\text{O}_3/\text{CuO}$. Magnetization data for FC and zero-field cooling (ZFC) up to $H_s = \pm 50 \text{ kOe}$ were reported previously in Ref. [2]. The values obtained for the remnant magnetization, $M'_{\text{FC}}(T)$, and the coercive

field, $H_C(T)$, are comparable to those found in other Gd-based compounds with similar V values [13]. Fig. 2 shows that $M'_{\text{FC}}(T)$ and $H_C(T)$ depends on the crystal preparation conditions. Larger values of $M'_{\text{FC}}(T)$ and $H_C(T)$ are obtained for crystals with: (i) higher Pt content ($x = 0$) and (ii) smaller V ($x \rightarrow 0$, and similar Pt content).

$M_{\text{FC}}(H_m, 100 \text{ K})$ shows a nearly linear increase with the applied field, H_m , for $H_m \gtrsim 30 \text{ Oe}$ (see Fig. 2 and Ref. [2]). That results from the RI's magnetic susceptibility, $dM_{\text{FC}}/dH_m \approx \chi_{\text{RI}}(100 \text{ K})$ [14]. Hence, for $H_m \gtrsim 30 \text{ Oe}$, $M_{\text{FC}}(H_m, T)$ can be approximated to [13]

$$M_{\text{FC}}(H_m, T) = M'_{\text{FC}}(T) + \chi_{\text{RI}}(T)H_m. \quad (1)$$

If we assume that the remnant magnetization, $M'_{\text{FC}}(T)$, is only the result of the WF component

due to the canting of the Cu moments in the *ab*-plane, $M_{\text{FC}}^{\text{Cu}}(T)$, Eq. (1) can be rewritten as

$$M_{\text{FC}}(H_a, T) = M_{\text{FC}}^{\text{Cu}}(T) + \chi_{\text{RE}}(T)H_a. \quad (2)$$

In Eq. (2) we have not considered the contribution from an internal field, $H_i(T)$, at the RE sites. It has been suggested that $M_{\text{FC}}^{\text{Cu}}(T)$ may lead to $H_i(T) \neq 0$ [13]. In that case the remnant magnetization is given by $M_{\text{FC}}^{\text{Cu}}(T) + \chi_{\text{RE}}(T)H_i(T)$ and $M_{\text{FC}}^{\text{Cu}}(T)$ will be only an upper limit for $M_{\text{FC}}^{\text{Cu}}(T)$. In a mean-field approximation $H_i(T) = \lambda M_{\text{FC}}^{\text{Cu}}(T)$, where λ involves the effective exchange interaction between the REs and neighbor Cu spins [6–8,13]. For Gd_2CuO_4 crystals grown in Pt/PbO it was found that $H_i(77\text{K}) \approx 900$ and $\approx 500\text{Oe}$ from magnetization and ESR data, respectively [6]. However, magnetization and ESR measurements on ceramic samples of $\text{Gd}_{2-x}\text{Sm}_x\text{CuO}_4$ grown in $\text{Al}_2\text{O}_3/\text{CuO}$ show that for $x \rightarrow 1$, $M_{\text{FC}}^{\text{Cu}}(T) \rightarrow 0$ and $H_i(T) \rightarrow 0$ [13]. In this system for $x \rightarrow 1$, $V \rightarrow 181.5\text{\AA}^3$ which is close to the V value of the Eu_2CuO_4 compounds (see Fig. 1). Besides, FC and ZFC ESR experiments in the *ab*-plane of Gd^{3+} in Eu_2CuO_4 crystals grown in Pt/PbO show no measurable shift of the spectra [14]. Moreover, the $\text{Eu}_{2-x}\text{Pr}_x\text{CuO}_4$ compounds are Van Vleck paramagnets with small values for $\chi_{\text{RE}}(T)$ [15]. Thus, we can assume that $\chi_{\text{RE}}(T)H_i(T) \ll M_{\text{FC}}^{\text{Cu}}(T)$ for the $\text{Eu}_{2-x}\text{Pr}_x\text{CuO}_4$ system.

For ZFC and neglecting the contribution from $\chi_{\text{RE}}(T)H_i(T)$, the *ab*-plane total DC-magnetization can be written as

$$M_{\text{ZFC}}(H_a, T) = M_{\text{ZFC}}^{\text{Cu}}(H_a, T) + \chi_{\text{RE}}(T)H_a. \quad (3)$$

Fig. 3 gives, for samples showing WF, the *ab*-plane ZFC DC-magnetization of the Cu ions, $M_{\text{ZFC}}^{\text{Cu}}(H_a, T) = M_{\text{ZFC}}(H_a, T) - \chi_{\text{RE}}(T)H_a$, at $T = 100\text{ K}$ between $H_a = \pm 50\text{kOe}$. For each sample, $\chi_{\text{RE}}(T)H_a$ was obtained from the high field of the $M_{\text{FC}}(H_a, T)$ data in Fig. 2. We find $M_{\text{ZFC}}^{\text{Cu}}(H_a, T)$ reversible and non-linear dependent on H_a . The data shows that crystals, with: (i) higher Pt content ($x = 0$), and (ii) smaller V ($x \rightarrow 0$, and similar Pt content) are easy to magnetize, i.e., show larger $M_{\text{ZFC}}^{\text{Cu}}(H_a, T)$.

Fig. 4 shows the T dependence of $M_{\text{FC-ZFC}}(H_a, T) = M_{\text{FC}}(H_a, T) - M_{\text{ZFC}}(H_a, T)$ for $H_a \leq 1\text{kOe}$. For these H_a values, $M_{\text{ZFC}}^{\text{Cu}}(H_a, T)$ is

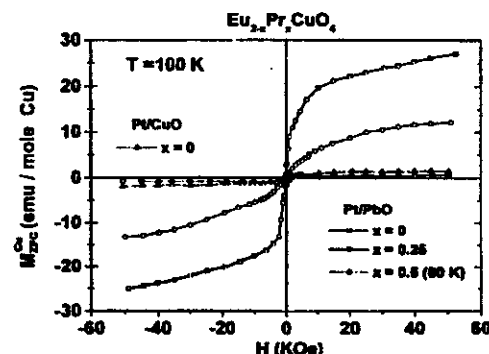


Fig. 3. Cu ions ZFC *ab*-plane DC-magnetization, $M_{\text{ZFC}}^{\text{Cu}}(H_a, T)$, at $T = 100\text{ K}$ between $H_a = \pm 50\text{kOe}$, for the samples showing WF. The data for the $x = 0.5$ sample were taken at $T = 80\text{ K}$.

negligible [2] (see Fig. 3) and $M_{\text{FC-ZFC}}(H_a, T)$, according to Eqs. (2) and (3), give an upper limit for the WF component of the Cu moments, $M_{\text{FC}}^{\text{Cu}}(T)$

$$\begin{aligned} M_{\text{FC-ZFC}}(H_a, T) &= M_{\text{FC}}^{\text{Cu}}(T) - M_{\text{ZFC}}^{\text{Cu}}(H_a, T) \\ &\approx M_{\text{FC}}^{\text{Cu}}(T). \end{aligned} \quad (4)$$

In all cases it was possible to fit the experimental data to

$$M_{\text{FC-ZFC}}(H_a, T) \approx M_{\text{FC}}^{\text{Cu}}(T) = M_{\text{FC}}^{\text{Cu}}[1 - (T/T_{\text{WF}})]^\beta, \quad (5)$$

where $M_{\text{FC}}^{\text{Cu}}$ is the saturation of the WF component at $T = 0$, T_{WF} is the T where 3D long-range FM correlations first appear, and β the exponent which was found to be $\approx 0.54(2)$. This suggest that mean-field theory accounts for the 3D long-range WF ordering of the Cu moments. From $M_{\text{FC}}^{\text{Cu}}$ we estimate the average number of Bohr magnetons per Cu ions to be $5.5(3) \times 10^{-3}\mu_B/\text{Cu}$ and $1.3(2) \times 10^{-3}\mu_B/\text{Cu}$ for the crystals with $x = 0$ grown in Pt/PbO and Pt/CuO, respectively. These values are of the order of those found for other heavier RE₂CuO₄ compounds [7,8,13]. It is known that T_N is ≈ 265 and $\approx 284\text{K}$ for Eu_2CuO_4 and Pr_2CuO_4 , respectively [16]. Although lower values for T_N were reported for crystals grown in Pt/PbO [15,17], our results suggest that $T_{\text{WF}} < T_N$ for our compounds. However, this should be taken with

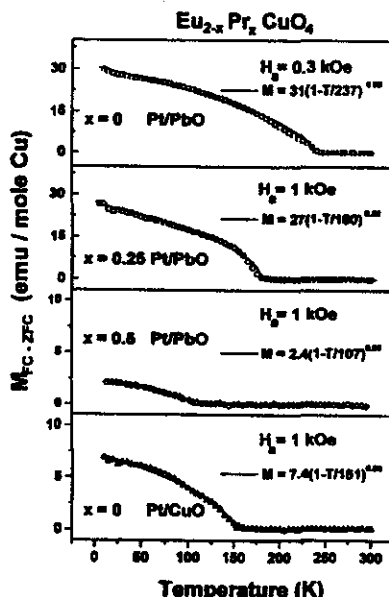


Fig. 4. T dependence of the Cu ions ab -plane DC-magnetization, $M_{\text{FC}-\text{zpc}}(H_0, T)$, for $H_0 \leq 1$ kOe, for samples showing WF. The solid lines are the best fitting to Eq. (5) (see text).

care since we have not measured T_N in our crystals. It is interesting to mention that magnetization measurements in Y_2CuO_4 , by Rouco et al. [8], suggested the existence of strong 2D short range AFM correlations above T_N and the persistence of 3D long range FM correlations above T_N . Hence, for these materials it may be expected that 3D long range FM correlations can appear at T different than T_N . Fig. 4 shows that $M_{\text{FC}}^{\text{OCu}}$ is smaller and T_{WF} lower for crystals with: (i) lower Pt content ($x = 0$), which is consistent with the absence of WF in samples grown in $\text{Al}_2\text{O}_3/\text{CuO}$ ($M_{\text{FC}}^{\text{OCu}} \rightarrow 0$; $T_{\text{WF}} \rightarrow 0$), and (ii) larger V ($x = 0.25, 0.50$, and similar Pt content). Notice that the crystal with the largest V ($x = 1$), shows no WF ($M_{\text{FC}}^{\text{OCu}} \rightarrow 0$; $T_{\text{WF}} \rightarrow 0$) [2].

For the tetragonal $\text{T}'-(\text{I}4/\text{mmm})$ structure of Eu_2CuO_4 it is expected four Raman-active modes: $\text{A}_{1g} + \text{B}_{1g} + 2\text{E}_g$. In our previous paper (Ref. 2) we have discussed the polarization selection rules of

the observed peaks. That lead us to the following results at 12 K: $\text{Y}(ZZ)\overline{Y}$ (A_{1g} , 229 cm^{-1}), $\text{Y}(ZX)\overline{Y}$ (E_g , 499 cm^{-1}) and $\text{Z}(XX)\overline{Z}$ or $\text{Z}(X'Y)\overline{Z}$ ($X' = \frac{1}{\sqrt{2}}(1,1)$, $Y' = \frac{1}{\sqrt{2}}(1, -1)$) (B_{1g} , 324 cm^{-1}). The spectra also showed the additional peaks at 413 and 388 cm^{-1} in the XX - and XY -polarizations, respectively. We have respectively labelled them as B_{1g}^* and $\text{B}_{2g}^*/\text{RM}$ due to their polarization selection rules in the D_{4h} point symmetry, despite the fact that the B_{2g}^* mode is forbidden in the $\text{T}'-(\text{I}4/\text{mmm})$ symmetry. Two anomalous peaks were also observed in Gd_2CuO_4 at 422 cm^{-1} (XX -polarization) by Laguna et al. [18] and at 380 cm^{-1} (XY -polarization) by Udagawa et al. [19]. Moreover, neutron scattering experiments in single crystals of Gd_2CuO_4 have shown the presence of a superstructure below 658 K in the T' -phase [20,21]. This superstructure, of an orthorhombic symmetry and space group Acam (D_{2h}^{18}), was attributed to squares of $\text{O}(1)$ oxygen atoms surrounding the Cu sites in the CuO_2 planes, rotated around the c -axis by $\sim 5.2^\circ$ at room T . Similar results were found in Eu_2CuO_4 at low T . In this case the angle of rotation measured at 9 K was about 2.2° [21]. This orthorhombic phase has 2 formula units per primitive cell, with the orthorhombic a and b axes rotated 45° respect to the tetragonal unit cell. Factor group analysis for the Raman-active modes yields to: $4\text{A}_g(XX, YY, ZZ) + 5\text{B}_{1g}(XY) + 4\text{B}_{2g}(XZ) + 5\text{B}_{3g}(YZ)$, where in parenthesis we indicate the allowed Raman tensor components for each mode. Correlation analysis and lattice dynamical calculation [22] give the following correspondence between the tetragonal zone center modes (Γ -point) and the orthorhombic modes: $\text{A}_{1g} \rightarrow \text{A}_g$ (229 cm^{-1} , stretching of Eu); $\text{B}_{1g} \rightarrow \text{B}_{1g}$ (324 cm^{-1} , z -bending of O(2) oxygens); $\text{E}_g \rightarrow \text{B}_{2g} + \text{B}_{3g}$ (499 cm^{-1} , in-plane vibration of O(2)). The expected splitting of the E_g mode was not observed. This result is consistent with neutron scattering experiments where the measured a and b lattice parameters were equal within the experimental error [21]. As the orthorhombic unit cell volume doubled that of the tetragonal one, new modes appear as a consequence of the folding of the first Brillouin zone. These modes are originating at the X-points zone border modes of the tetragonal

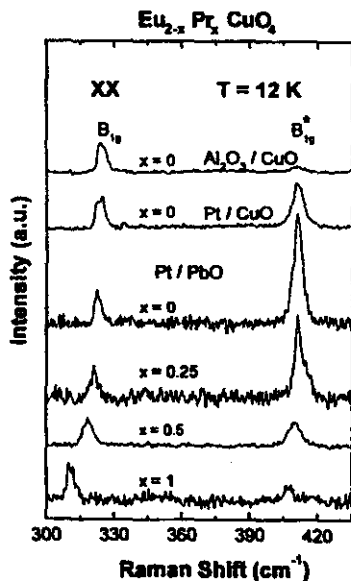


Fig. 5. XX-polarized Raman spectra at $T = 12 \text{ K}$ for the $\text{Eu}_{2-x}\text{Pr}_x\text{CuO}_4$ crystals studied in this work.

cell [22]. The anomalous 413 cm^{-1} peak (labelled B_{1g}^* in Ref. 2) belongs to this class and has B_{1g} symmetry ($X\bar{Y}$ -polarization, in-plane vibrations of the O(1) atoms) in the orthorhombic phase [22]. This mode that appears in XX -polarization in the tetragonal axes (see Fig. 1 in Ref. 2), corresponds to $X\bar{Y}$ -polarization in the orthorhombic axes, confirming its B_{1g} character. The 324 cm^{-1} anomalous peak (labelled B_{2g}^* in Ref. 2), that appears in $X\bar{Y}$ -polarization in the tetragonal axes corresponds, to an A_g symmetry mode in the orthorhombic axes.

Fig. 5 shows the XX -polarized Raman spectra at $T = 12 \text{ K}$ for the samples studied. The allowed Raman mode, B_{1g} , for the T'-structure [2] is observed at $\sim 324 \text{ cm}^{-1}$ in all our crystals. The relative intensity of the fRM at $\sim 413 \text{ cm}^{-1}$, B_{1g}^* , to that of the allowed B_{1g} peak, $I(B_{1g}^*)/I(B_{1g})$, strongly depends on the compound and the crystal preparation conditions [2]. Larger $I(B_{1g}^*)/I(B_{1g})$ ratios are found for crystals with: (i) higher Pt content ($x = 0$) and (ii) smaller V ($x \rightarrow 0$, and similar Pt content (see

Figs. 2–5). For Gd_2CuO_4 grown in $\text{Al}_2\text{O}_3/\text{CuO}$ and Pt/PbO ($179.2 \text{ \AA}^3 \leq V \leq 179.9 \text{ \AA}^3$), where highly correlated ordered orthorhombic distortions in the CuO_2 planes have been found [20], even larger $I(B_{1g}^*)/I(B_{1g})$ ratios [18] were observed. However, for Eu_2CuO_4 crystals grown in $\text{Al}_2\text{O}_3/\text{CuO}$ ($V \approx 181.1 \text{ \AA}^3$) a very small $I(B_{1g}^*)/I(B_{1g})$ ratio is found (see Fig. 5 and Ref. 2).

The fRM and WF features ($M'_{\text{FC}}(T)$, $H_c(T)$, $M''_{\text{FC}}(H_c, T)$, $M''_{\text{FC}}^{\text{CO}}(H_c, T)$, and T_{WF}) observed in these T'-structures were associated to the orthorhombic lattice distortions discussed above, involving the displacement of the O(1) oxygens away from their equilibrium positions [2]. Then, the above results of our fRM and WF measurements suggest that the Pt impurities and/or the reduction of V beyond a critical value, $V_c = V(\text{Eu}_2\text{CuO}_4) \approx 181.1 \text{ \AA}^3$ (see Fig. 1), are the origin of these distortions. Hence, the different fRM intensities and WF features found in these compounds may be caused by the presence of a different number of these distortions in the various crystals. In Gd_2CuO_4 the orthorhombic to tetragonal phase transition occurs around 658 K , and the T dependence of the lattice parameters yield a value of 181.9 \AA^3 for the lattice unit cell volume at this phase transition [21]. This is in good agreement with the critical value, $V_c \approx 181.1 \text{ \AA}^3$ found for Eu_2CuO_4 .

Fig. 6 presents the T dependence of the $I(B_{1g}^*)/I(B_{1g})$ ratio for the crystals grown in Pt/PbO ($T_{\text{WF}} \approx 237 \text{ K}$) and Pt/CuO ($T_{\text{WF}} \approx 151 \text{ K}$) with $x = 0$, and grown in Pt/PbO ($T_{\text{WF}} \approx 107 \text{ K}$) with $x = 0.5$. The data shows that the number of distortions, responsible for the B_{1g}^* peak, decreases as T increases and only a small number of distortions remain above T_{WF} . Therefore, only a small contribution to the magnetization is expected from the canting of the Cu moments at $T > T_{\text{WF}}$, in the AF phase. This is consistent with the results shown in Fig. 7 for $M_{\text{FC}-\text{ZFC}}(H_c, T)$ at high fields and high T obtained for two of the crystals shown in Fig. 6. Within the accuracy of the measurements we find $M_{\text{FC}}^{\text{CO}}(T) - M_{\text{ZFC}}^{\text{CO}}(H_c, T) \approx 0$ for $T > T_{\text{WF}}$. These results suggest that 3D long-range FM correlations are observed only above a critical number of distortions. Also, notice that Fig. 4 and Fig. 6 show that the 3D FM ordering appear at $I(B_{1g}^*)/I(B_{1g}) \approx 1$. This ratio may correspond to that critical number.

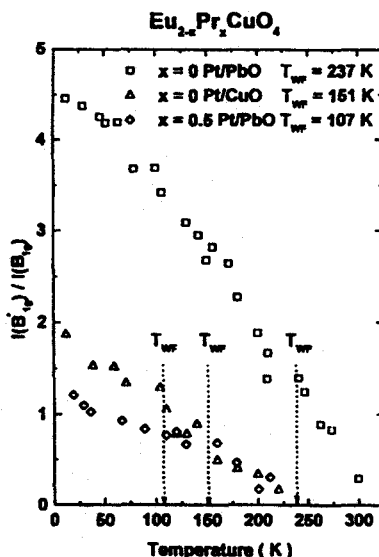


Fig. 6. T dependence of the $I(B_{1g}^*)/I(B_{1g})$ ratio for the $\text{Eu}_{2-x}\text{Pr}_x\text{CuO}_4$ crystals grown in Pt/PbO ($T_{wf} \approx 237$ K) and Pt/CuO, ($T_{wf} \approx 151$ K) with $x = 0$, and Pt/PbO ($T_{wf} \approx 107$ K) with $x = 0.5$.

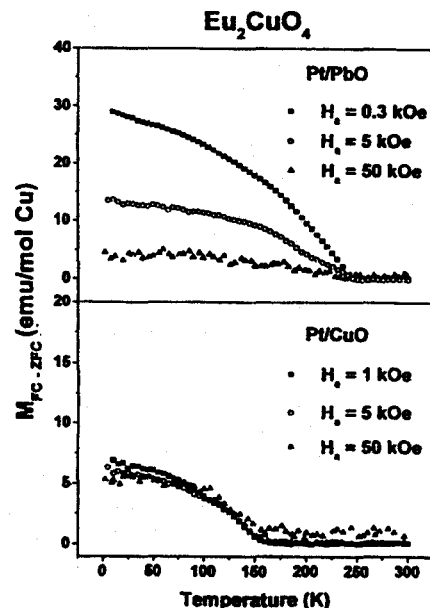


Fig. 7. T dependence of the Cu ions ab-plane DC-magnetization, $M_{rc-zrc}(H_m, T)$, for $H_m \geq 0.3$ kOe, for Eu_2CuO_4 grown in Pt/PbO and Pt/CuO.

It is interesting to mention that the T dependence of $I(B_{1g}^*)/I(B_{1g})$ in Eu_2CuO_4 , is similar to the T dependence of the orthorhombic superstructure reflection (2.5 1.5 2) measured in neutron scattering experiments [21]. They decrease rapidly above 80 K and vanish at about 200 K. These results suggest that the distortions, responsible for the f/RM and WF, may be also highly correlated at low T .

Microwave absorption experiments in our samples showed the zero-field absorption [6] only for the Eu_2CuO_4 crystal grown in Pt/PbO when FC, and no absorption for ZFC. This signal is observed at $T \leq T_{wf} = 237$ K. Within the sensitivity of our experiment, the mid-field resonance was not found [6] in any of our samples showing WF. The Eu_2CuO_4 crystal grown in Pt/PbO is the sample with the largest hysteresis loop (see Fig. 2). Thus, it is possible that the zero and mid-field absorptions may be associated to the magnetic domains structure of the WF in these materials.

4. Discussion

The B_{1g}^* and B_{2g}^*/RM arc always found at about the same energies, 413 cm^{-1} (422 cm^{-1} for Gd_2CuO_4) and 398 cm^{-1} (380 cm^{-1} for Gd_2CuO_4), respectively [2,18,19]. This indicates that their origin is the same, regardless the compounds and T where they are observed. Besides, our results show that there is a correlation between the intensity of the f/RM and the magnitude of the WF features (see Figs. 2–5, and Refs. 6 and 8). Thus, the origin of the f/RM and WF should be the same in these compounds, and it may be attributed to the presence of orthorhombic distortions caused by the O(1) oxygen displacements within the CuO_2 planes [1,2]. As mentioned above, we associate these distortions to the presence of Pt impurities and/or the reduction of V beyond a critical value $V_c \approx 181\text{ \AA}^3$. This reduction may be induced by changing the RE in

the T'-structure across the RE series or by lowering the T .

The increase of the B_{1g}^0 peak intensity at low T (see Fig. 6) may be associated to the thermal contraction of the T'-structure unit cell volume, $V(T)$, beyond V_c . A decrease of about 0.6% in $V(T)$ was reported in Pr_2CuO_4 between 10 and 300 K [23]. Notice that the difference in V at room T between Eu_2CuO_4 and Gd_2CuO_4 is of the same order, 0.5–1% (see Fig. 1).

5. Conclusions

The T'-structure compounds with a unit cell volume smaller than a critical value $V_c \approx 181.1 \text{ \AA}^3$ (close to the V value of Eu_2CuO_4 grown in $\text{Al}_2\text{O}_3/\text{CuO}$) present local distortions within the CuO_2 planes, allowing for WI and fRM [1,6,18]. However, if Cu ions are substituted by Pt impurities from the crucible, favoring the formation of local distortions in the CuO_2 planes, a slightly higher value for V_c is then found. For our $\text{Eu}_{2-x}\text{Pr}_x\text{CuO}_4$ crystals grown in Pt/PbO we find $183.5 \text{ \AA}^3 \leq V_c \leq 185.5 \text{ \AA}^3$, for $0.5 < x < 1$ (see Fig. 1).

The results of this work and that of our previous report [2], as well as those from others in $\text{Gd}_{2-x}\text{Sm}_x\text{CuO}_4$, Gd_2CuO_4 and Eu_2CuO_4 compounds [6,13,20,21], lead us to conclude that there is a delicate instability of the T'-structure at the middle of the RE series. Our data on Eu_2CuO_4 crystals grown by different techniques show that this instability appears at a critical lattice unit cell volume close to that of Eu_2CuO_4 grown in $\text{Al}_2\text{O}_3/\text{CuO}$ ($V_c \approx 181.1 \text{ \AA}^3$). Based on the X-ray [1] and neutron diffraction [20,21] results, we associate this instability with orthorhombic distortions involving a displacement of the O(1) oxygen atoms within the CuO_2 planes. Therefore, we claim that these distortions are responsible for the observed WI and fRM. Moreover, the T dependence of the intensities of the neutron diffraction elastic peak [21] and fRM observed below $T \approx 250$ K, suggest that a second order tetragonal to orthorhombic phase transition may take place at $V(T) \approx V_c$.

In summary, our Raman and magnetization measurements have shown that the distortions in

the T'-structure are caused by: (i) the reduction of the lattice unit cell volume beyond a critical value, V_c , and (ii) the substitution of Cu ions by Pt impurities incorporated from the Pt crucible during the crystal growth.

Acknowledgements

This work was supported by FAPESP Grant No 95/4721-4, São Paulo-SP-Brazil and NSF-DMR No 9117212, No 9016241, and No 9501529. C. Rettori acknowledges the financial support from FAPESP-Brazil.

References

- [1] T. Schultz, R. Smith, A. Fonfado, C. Maley, T. Beacom, P. Tinklenberg, J. Gross, C. Saylor, S. Oseroff, Z. Fisk, S.W. Cheong, T.E. Jones, *J. Appl. Phys.* 75 (1994) 6723; P. Gallez, P. Schweiss, G. Collin, R. Bellissent, *J. Less Common Metals* 164 165 (1990) 784.
- [2] A.D. Alvarenga, D. Rao, J.A. Sanjurjo, E. Granado, I. Torriani, C. Rettori, S. Oseroff, J. Sarao, Z. Fisk, *Phys. Rev. B* 53 (1996) 837.
- [3] Y. Tokura, H. Takegi, S. Uchida, *Nature (London)* 337 (1989) 345.
- [4] H. Okada, M. Takano, Y. Takeda, *Physica C* 166 (1990) 111.
- [5] P. Bordet, J.J. Capponi, C. Chailout, D. Chateigner, J. Chenavas, Th. Fournier, J.L. Hodeau, M. Marzio, M. Perroux, G. Thomas, A. Varela, *Physica C* 185 189 (1991) 539.
- [6] P. Bordet, J.J. Capponi, C. Chailout, D. Chateigner, J. Chenavas, Th. Fournier, J.L. Hodeau, M. Marzio, M. Perroux, G. Thomas, A. Varela, *Physica C* 193 (1992) 178; S.B. Oseroff, D. Rao, J. Wright, D.C. Vier, S. Schultz, J.D. Thompson, Z. Fisk, S.W. Cheong, M.F. Hundley, M. Tovar, *Phys. Rev. B* 41 (1990) 1934.
- [7] M. Tovar, X. Obradors, F. Pérez, S. Oseroff, R.J. Durn, J. Rivas, D. Chateigner, P. Borlet, J. Chenavas, *Phys. Rev. B* 45 (1992) 4729; A. Rouco, X. Obradors, M. Tovar, J. Appl. Phys. 78 (1995) 4608.
- [8] A. Rouco, X. Obradors, M. Tovar, F. Pérez, D. Chateigner, P. Bordet, *Phys. Rev. B* 50 (1994) 9924.
- [9] J.T. Markert, L.A. Early, T. Björnholm, S. Ghannat, B.W. Lee, J.J. Neumeier, R.D. Prior, C.L. Scanlan, M.B. Maple, *Physica C* 158 (1989) 178.
- [10] P. Adelmann, R. Ahrens, G. Czjzek, G. Roth, H. Schmidt, C. Steinleitner, *Phys. Rev. B* 46 (1992) 3619.
- [11] A.A. Stepanov, P. Wyder, T. Chattopadhyay, P.J. Brown, G. Filion, I.M. Vitebsky, A. Deville, B. Gaillard, S.N. Barilo, D.I. Zhigunov, *Phys. Rev. B* 48 (1993) 12979.
- [12] K.A. Kubat-Martin, Z. Fisk, R. Rayan, *Acta Crystallogr. C* 44 (1988) 1518.
- [13] L.B. Steren, M. Tovar, S.B. Oseroff, *Phys. Rev. B* 46 (1992) 2874; S. Skanthakumar, J.W. Lynn, J.L. Peng, Z.Y. Lu, *J. Appl. Phys.* 69 (1991) 4866.
- [14] R.D. Zysler, M. Tovar, C. Rettori, D. Rao, H. Shore, S.B. Oseroff, D.C. Vier, S. Schultz, Z. Fisk, S.-W. Cheong, *Phys. Rev. B* 44 (1991) 9467.
- [15] G.B. Martins, D. Rao, J.A. Valdivia, M.A. Pires, G.E. Barberis, C. Rettori, P.A. Venegas, S. Oseroff, Z. Fisk, *Phys. Rev. B* 51 (1995) 11909; C. Rettori, S.B. Oseroff, D. Rao, J.A. Valdivia, G.E. Barberis, G.B. Martins, J. Sarao, Z. Fisk, M. Tovar, *Phys. Rev. B* 54 (1996) 1123.
- [16] T. Chattopadhyay, J.W. Lynn, N. Rosov, T.E. Grigereit, S.N. Barilo, D.I. Zhigunov, *Phys. Rev. B* 49 (1994) 9944; I.W. Sumarlin, J.W. Lynn, T. Chattopadhyay, S.N. Barilo, D.I. Zhigunov, J.L. Peng, *Phys. Rev. B* 51 (1995) 5824.
- [17] P. Allenbach, S.-W. Cheong, A. Dommann, P. Fischer, Z. Fisk, A. Furrer, H.R. Ott, B. Rupp, Z. *Phys. B-Condens. Matter* 77 (1989) 185.
- [18] M.A. Laguna, M.I. Sanjuan, A. Butera, M. Tovar, Z. Fisk, P. Canfield, *Phys. Rev. B* 48 (1993) 7565.
- [19] M. Udagawa, Y. Nagaoaka, N. Ogita, M. Masada, J. Akimitsu, K. Ohbayashi, *Phys. Rev. B* 49 (1994) 585.
- [20] M. Braden, W. Paulus, A. Cousson, P. Vigoreux, G. Heger, A. Cioukassov, P. Bourges, D. Petitgrand, *Europhys. Lett.* 25 (1994) 625.
- [21] P. Vigoreux, Ph.D. Dissertation Thesis, University of Paris-SUD, U.F.R Scientific D'Orsay, France, June 1995.
- [22] M.A. Laguna, Ph.D. Dissertation Thesis, University of Zaragoza, Spain, 1996.
- [23] D.E. Cox, A.I. Goldman, M.A. Subramanian, J. Gopalakrishnan, A.W. Sleight, *Phys. Rev. B* 40 (1989) 6998.

Seção 2.2

2.2 Estudos de RPE de Gd^{3+} no
estado normal dos supercondutores

$\text{RNi}_2\text{B}_2\text{C}$ ($\text{R} = \text{Y}, \text{Lu}$).

2.2) Estudos de RPE de Gd³⁺ no estado normal dos supercondutores RNi₂B₂C (R = Y, Lu).

PHYSICAL REVIEW B

VOLUME 57, NUMBER 6

1 FEBRUARY 1998-II

Electron spin resonance of Gd³⁺ in the normal state of RNi₂B₂C (R=Y,Lu)

P. G. Pagliuso, C. Rettori, and S. B. Oseroff*

Instituto de Física "Gleb Wataghin," UNICAMP, 13083-970, Campinas-SP, Brazil

P. C. Canfield

Ames Laboratory and Department of Physics and Astronomy, Iowa State University, Ames, Iowa 50011

E. M. Baggio-Saitovitch and D. Sanchez
CBPF, R. Xavier Sigaud 150, 22290-180, Rio de Janeiro, Brazil

(Received 26 August 1997)

Electron spin resonance (ESR) of Gd³⁺ in the normal state ($T \gg T_c$) of $R_{1-x}Gd_xNi_2B_2C$ ($R = Y, Lu$) is reported. The results show that the exchange coupling between the rare-earth localized magnetic moment and the conduction electrons depends on the conduction electrons momentum transfer ($|k_F^0 - k_F^{xx}| = q$), i.e., $J_{f_z}(q)$. The temperature dependence of the ESR linewidth yields a value for one of the exchange parameters, $(J_{f_z}(q))_{F_z}^{1/2}$, which is in agreement with that estimated from the slope of the initial linear decrease of T_c by the Gd³⁺ impurities. These results indicate that the $R_{1-x}Gd_xNi_2B_2C$ ($R = Y, Lu$) compounds behave as conventional BCS superconductors, in agreement with previous reports.
[S0163-1829(98)02806-9]

I. INTRODUCTION

The series of quaternary intermetallic rare-earth nickel borocarbides RNi_2B_2C (R = rare earth) compounds¹ have recently attracted great interest due to their relatively high superconducting temperatures ($T_c = 16.6$ K for $R = Lu$ and $T_c = 15.5$ K for $R = Y$).² The magnetic anisotropy and coexisting superconductivity (SC) with the antiferromagnetic (AF) ordering associated to the magnetic rare-earths R elements ($T_N \lesssim T_c$),³⁻⁵ have strongly motivated the scientific community to study these materials. The interplay between SC and magnetism in these materials resembles that of the ternary $ErRh_4B_4$ and $HoMn_6S_8$ compounds.⁶ The incommensurate modulated magnetic structure shown by neutron diffraction experiments in $HoNi_2B_2C$ (Ref. 7) at temperatures between $T_N \sim 5$ K and $T_c \sim 7.5$ K, and the suppression of SC by the substitution of Dy by Lu in $DyNi_2B_2C$,⁸ were interpreted in terms of a magnetic pair breaking in the RNi_2B_2C ($R = Er, Dy$) compounds. The structure of the RNi_2B_2C compounds is a filled variant of the body-centered tetragonal (bct) $ThCr_2Si_2$ (space group I_{4}/mm) with Ni layers perpendicular to the c axis.⁹ This structure is qualitatively similar to that of the layered cuprate high- T_c superconductors. However, no local magnetic moment or AF spin correlations on the Ni sublattice have been found.¹⁰ In addition, electronic band structure calculations suggest that the RNi_2B_2C compounds are 3D d -band metals and that the SC is mediated by the conventional electron-phonon BCS mechanism.¹¹⁻¹³ Experimental support for this is given by tunneling spectroscopy¹⁴ and boron isotopic effect¹⁵ measurements in these materials.

It is known that by means of electron spin resonance (ESR) of dilute rare-earth magnetic impurities (i.e., Gd³⁺) in the normal state of BCS-type superconducting compounds, it is possible to determine the exchange parameters between the localized magnetic impurity and the conduction electrons (CE's).¹⁶ It was also shown that the exchange parameter obtained from the thermal broadening of the ESR linewidth

(Korringa rate), was comparable with that extracted from the slope of the initial linear decrease of T_c by the magnetic impurities, as predicted by the Abrikosov-Gorkov (AG) theory.^{16,17} The present work's goal is to measure, by means of ESR, the exchange parameters between the localized magnetic moment of Gd³⁺ and the CE's in the normal state of the RNi_2B_2C ($R = Y, Lu$) compounds, and to compare the value obtained from the Korringa rate with the one obtained from the reduction of T_c by the Gd³⁺ impurities.

II. EXPERIMENT

Single crystals of $Lu_{1-x}Gd_xNi_2B_2C$ ($x \sim 0.005$) were grown at the Ames Laboratory by the high-temperature flux growth method described elsewhere.¹⁸ The $Y_{1-x}Gd_xNi_2B_2C$ ($x \sim 0.005$) samples were made at the CBPF Laboratory in a polycrystalline form by the arc-melting technique.¹⁹ The structure and phase purity were checked by x-ray powder diffraction and the crystals orientation determined by the usual Laue method. The ESR experiments were carried out in a conventional Varian ESR spectrometer using a TE₁₀₂ room-temperature cavity. The sample temperature was varied using a helium gas flux temperature controller. To increase the ESR signal to noise ratio, the temperature dependences of the spectra were taken in powdered samples. Magnetization measurements have been done in a Quantum Design dc superconducting interference device magnetometer. The temperature dependence of the magnetic susceptibility in the normal state was measured increasing the temperature, after zero field cooling (ZFC), in a field of 5 kOe. Table I gives the Gd³⁺ concentration estimated from the fitting of the magnetic susceptibility data to a Curie-Weiss law.

III. EXPERIMENTAL RESULTS

Figure 1 shows the Gd³⁺ ESR powder spectra observed in the normal state at $T = 18$ K for $R_{1-x}Gd_xNi_2B_2C$ (R

TABLE I. Experimental parameters for Gd:(Lu,Y)Ni₂B₂C.

	<i>g</i>	<i>a</i>	<i>b</i>	<i>c</i>	γ	β	$\frac{\Delta T_c}{\Delta c}$
	Oe	Oe/K	%		$\frac{mJ}{mol K^2}$	$\frac{mJ}{mol K^4}$	K/%
Lu _{1-x} Gd _x Ni ₂ B ₂ C	2.035(7)	165(10)	13(1)	0.5(2)	19(2)*	$2.67(10) \times 10^{-4}$ *	-0.65(4)*
Y _{1-x} Gd _x Ni ₂ B ₂ C	2.03(3)	830(30)	11(2)	2.1(2)	18.7(5)*	$1.02(10) \times 10^{-4}$ *	~-0.43*

*See Refs. 8,34,38,39.

=Y, Lu) compounds with $x \approx 0.005$ for $R = \text{Lu}$ ($T_c \approx 16$ K) and $x \approx 0.02$ for $R = \text{Y}$ ($T_c \approx 15$ K). The spectra show the usual Dysonian type of line shape,²⁰ characteristic of metallic sample particles of dimensions much larger than the skin depth. The dashed lines in Fig. 1 are the best fit of the experimental spectra to a Lorentzian admixture of absorption and dispersion derivatives.²¹ From these fittings the linewidth ΔH and the *g* value are obtained.

Figure 2 presents the temperature dependence of the Gd³⁺ ESR linewidth for the samples of Fig. 1. The observed linear thermal broadening of ΔH indicates that the Gd³⁺ localized magnetic moment relax to the lattice via an exchange coupling with the CE's, known as the Korringa mechanism.⁶ The dashed lines are the best fit of the data to $\Delta H = a + bT$.

Several samples of Gd concentrations in the range between 0.5 to 2 % were measured. Within the accuracy of the measurements, the *b* and *g* values were concentration independent and the residual linewidth *a* increases with the Gd concentration. The *g* value was found to be temperature independent within the experimental error. Table I shows the experimental parameters obtained with $x \approx 0.005$ for the Lu-based sample and $x \approx 0.02$ for the Y-based sample.

We were unable to measure the ESR of Gd³⁺ in the superconducting state ($T < T_c$) of the R_{1-x} Gd_xNi₂B₂C ($R = \text{Y}, \text{Lu}$) compounds. This is usually an extremely difficult measurement due to (i) the large change in the loaded cavity quality factor (Q_i) between the normal and superconducting

state and (ii) the interaction between the vortices and the microwave magnetic field h_{rf} in the superconducting state. That results in a large frequency drift and nonresonant microwave absorption in the ESR detector system.

IV. ANALYSIS AND DISCUSSION

The exchange interaction $J_{fs}S \cdot s$ between a localized 4f electron spin (*S*) on a solute atom (Gd³⁺) and the free CE's spin (*s*) of the host metal, cause *g* shift (Knight shift)²² and thermal line broadening (Korringa rate)²³ of the ESR spectra. Conduction electron-electron exchange enhancement^{24,25} and the *q*-dependent exchange interaction $J_{fs}(q)$ (Ref. 26) are often used in the analysis of the ESR data.²⁷ $J_{fs}(q)$ is the Fourier transform of the spatially varying exchange coupling. In this case, and when "bottleneck" and "dynamic" effects are not present, the *g* shift (Δg) and Korringa rate (*b*) can be written as²⁸

$$\Delta g = J_{fs}(0) \frac{\eta(E_F)}{1 - \alpha} \quad (1)$$

and

$$b = \frac{d(\Delta H)}{dT} = \frac{\pi k}{g \mu_B} \langle J_{fs}^2(q) \rangle_{E_F} \eta^2(E_F) \frac{K(\alpha)}{(1 - \alpha)^2}, \quad (2)$$

where $J_{fs}(0)$ and $\langle J_{fs}^2(q) \rangle_{E_F}$ are the effective exchange parameters between the Gd³⁺ local moment and the CE's in the presence of CE's momentum transfer ($q = |\mathbf{k}_F^{in} - \mathbf{k}_F^{out}|$)

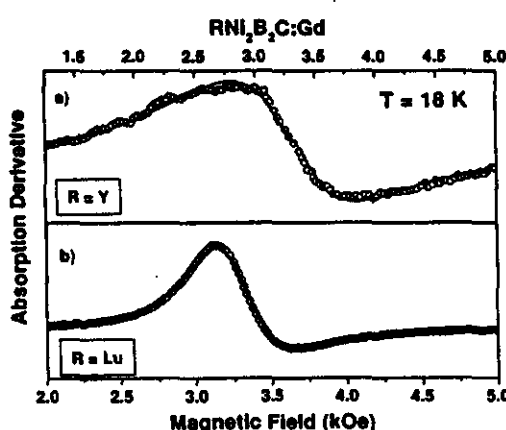


FIG. 1. ESR spectra of Gd³⁺ in (a) Lu_{1-x}Gd_xNi₂B₂C for $x = 0.005$ and (b) Y_{1-x}Gd_xNi₂B₂C for $x \approx 0.02$ and $T = 18$ K.

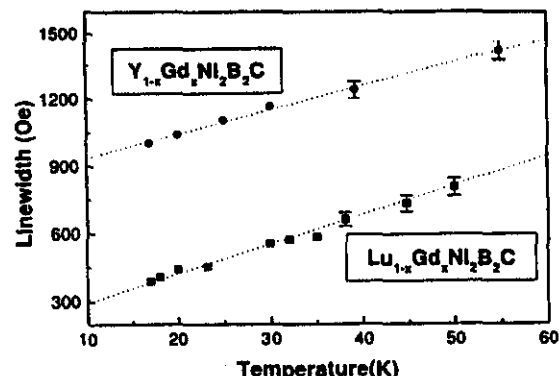


FIG. 2. Temperature dependence of the Gd³⁺ ESR linewidth for the two samples shown in Fig. 1.

TABLE II. Extracted parameters for Gd:(Lu,Y)Ni₂B₂C.

	$\eta(E_F)$ states eV mol spin	λ	θ_D	α	$K(\alpha)$	$J_{fs}(0)$	ESR	SC
							K	meV
Lu _{1-x} Gd _x Ni ₂ B ₂ C	2.20(7)	~0.8*	~345°	~0.2*	~0.8*	15(2)	10(4)	11(3)
Y _{1-x} Gd _x Ni ₂ B ₂ C	2.05(6)	~0.9*	~489°	~0.3*	~0.7*	13(2)	9(3)	10(2)

*See Refs. 33,4,35,36.

= $k_F[2(1-\cos\theta)]^{1/2}$.²⁶ Under these assumptions the Gd³⁺ g shift measures the CE's polarization ($q=0$), and the Korringa rate the CE's momentum transfer ($0 \leq q \leq 2k_F$) averaged over the Fermi surface.²⁶ ($1-\alpha$)⁻¹ and $K(\alpha)$ are the Stoner and the Korringa enhancement factors, respectively, due to the electron-electron exchange interaction.^{27,29,30} $\eta(E_F)$ is the "bare" density of states for one spin direction at the Fermi surface, k is the Boltzmann constant, μ_B is the Bohr magneton, and g is the Gd³⁺ g value.

Equations (1) and (2) are appropriated for the analysis of ESR data of diluted rare earths in metallic hosts with appreciable CE's spin-flip scattering, i.e., the *unbottleneck* regime. We found in this work that the g value and b parameter do not depend on the Gd³⁺ concentration. Hence, it is expected that the following relation would hold:^{27,28}

$$b = \frac{d(\Delta H)}{dT} = \frac{\pi k}{8\mu_B} \frac{\langle J_{fs}^2(q) \rangle_{E_F}}{J_{fs}^2(0)} (\Delta g)^2 K(\alpha). \quad (3)$$

In our analysis the contribution from different CE's bands will be neglected, because the measured thermal broadening of the linewidths are much smaller than those expected from the measured g shifts.³¹

In a superconductor the electron-phonon interaction enhances the CE's effective mass, and in turn the density of states at the Fermi level. Thus, the Sommerfeld's parameter is usually written as $\gamma=(2/3)\pi^2k^2(1+\lambda)\eta(E_F)$, where λ is the electron-phonon coupling constant.³² The RNi₂B₂C (R = Y,Lu) compounds have been classified as intermediate coupled electron-phonon-mediate superconductors, with $\lambda_Y \sim 0.9$ (Ref. 33) and $\lambda_{Lu} \sim 0.8$.³⁴ The electronic contribution to the heat capacity γ for the Lu- and Y-based compounds, were measured and their values are shown in Table I. Now, using the γ and λ values, the density of states at the Fermi level $\eta(E_F)$ can be estimated for the Y- and Lu-based compounds (see Table II). The extracted values for $\eta(E_F)$ are in good agreement with the theoretical ones obtained from band calculations.^{35,36} In addition, electron-electron exchange enhancement is important in these systems and has been evaluated by NMR measurements³⁵ for the Y-based compound and from theoretical calculations for the Lu-based compound.³⁶ The values of α , from the Stoner enhancement factor ($1-\alpha$)⁻¹ and $K(\alpha)$ are given in Table II.

Using in Eq. (3) the g value of Gd³⁺ in insulators as a reference, 1.993(2),³⁷ $\pi k/g\mu_B = 2.34 \times 10^4$ Oe/K, and the values of Δg , b , $\eta(E_F)$, α , and $K(\alpha)$ from Tables I and II, the exchange parameters between the Gd³⁺ local moment and the CE's in these two compounds were estimated. Table

II summarizes these parameters for Gd³⁺ in RNi₂B₂C (R = Y,Lu). Notice that the ratios $\langle J_{fs}^2(q) \rangle_{E_F}^{1/2}/J_{fs}(0)$, are about the same for both systems. This suggests similar wave-vector dependence of the exchange interaction for isomorphic compounds.

It is interesting to compare the exchange parameter $\langle J_{fs}^2(q) \rangle_{E_F}^{1/2}$ obtained in our ESR experiments and that obtained from the decrease of T_c by adding Gd³⁺ magnetic impurities, $\Delta T_c/\Delta c$. From the Abrikosov-Gorkov (AG) theory¹⁷ we have that

$$\left| \frac{\Delta T_c}{\Delta c} \right| = (\pi^2/8k_B) \langle J_{fs}^2(q) \rangle_{E_F} \eta(E_F) (g_J - 1)^2 J(J+1). \quad (4)$$

The values of $\Delta T_c/\Delta c$, for both compounds, were taken from the literature^{38,8} and are given in Table I. The values for $\langle J_{fs}^2(q) \rangle_{E_F}^{1/2}$, calculated using these data are in agreement with those obtained in this work (see Table II).

V. CONCLUSIONS

We have shown that R_{1-x} Gd_xNi₂B₂C (R = Y,Lu) dilute magnetic alloys behave as conventional three-dimensional superconductors as far as the ESR and superconducting results are concerned. Taking into account the CE mass enhancement due to the electron-phonon coupling λ and the electron-electron exchange enhancement α we found comparable effective exchange parameters $\langle J_{fs}^2(q) \rangle_{E_F}^{1/2}$ from the thermal broadening of the Gd³⁺ ESR linewidth (Korringa rate) and the decrease of T_c by the Gd³⁺ magnetic impurities (AG). This shows that the exchange coupling between the Gd³⁺ local moment and the CE's governs the impurity relaxation and pair-braking processes.

Our ESR results (g-shift and Korringa rate) show that the exchange interaction between the localized magnetic moments and the CE's involves only a single electronic conduction band. The exchange interaction is found to be strongly dependent on the CE's momentum transfer ($|k_F^{in} - k_F^{out}| = q$) and is of atomiclike [$J_{fs}(0) > 0$].

ACKNOWLEDGMENTS

This work was supported by FAPESP Grant Nos. 95/4721-4 and 96/12585-6, São Paulo-SP-Brazil, NSF-DMR No. 9705155, NPS-INT 9602928, and by the Director for Energy Research, Office of Basic Energy Sciences, U.S. Department of Energy by Iowa State University, Grant No. W-7405-Eng-82.

- ¹Current address: Department of Physics, San Diego State University, San Diego, CA 92182.
- ²R. Nagarajan, C. Mazumdar, Z. Illesheim, S. K. Dhar, K. V. Golpakrishnan, L. C. Gupta, C. Godart, B. D. Padalia, and R. Vijayaraghavan, Phys. Rev. Lett. **72**, 274 (1994).
- ³R.J. Cava, H. Takagi, B. Batlogg, H. W. Zandbergen, J. J. Krajewski, W. F. Peck, R. B. van Dover, R. J. Felder, T. Siegrist, K. Mmizuhashi, J. O. Lee, H. Eisaki, S. A. Carter, and S. Uchida, Nature (London) **367**, 146 (1994); **367**, 252 (1994); **367**, 282 (1994).
- ⁴B.K. Cho, M. Xu, P. C. Canfield, L. L. Miller, and D. C. Johnston, Phys. Rev. B **52**, 3676 (1995); B.K. Cho *et al.*, *ibid.* **52**, 3684 (1995).
- ⁵P.C. Canfield, B. K. Cho, D. C. Johnston, D. K. Finnemore, and M. F. Hundley, Physica C **230**, 397 (1994); K.D.D. Rathnayaka *et al.*, Phys. Rev. B **53**, 5688 (1996).
- ⁶B.K. Cho, P. C. Canfield, and D. C. Johnston, Phys. Rev. B **53**, 8499 (1996); B.K. Cho *et al.*, *ibid.* **53**, 2217 (1996).
- ⁷L.N. Bulaevskii *et al.*, Adv. Phys. **34**, 175 (1985).
- ⁸A.I. Goldman, C. Stassis, P. C. Canfield, J. Zarestky, P. Dernagras, B. K. Cho, D. C. Johnston, and B. Sternlieb, Phys. Rev. B **50**, 9668 (1994); T.B. Grigereit *et al.*, Phys. Rev. Lett. **73**, 2756 (1994).
- ⁹B.K. Cho, P. C. Canfield, and D. C. Johnston, Phys. Rev. Lett. **77**, 163 (1996).
- ¹⁰T. Siegrist *et al.*, Nature (London) **367**, 255 (1994).
- ¹¹B.J. Suh, F. Borsa, D. R. Torgeson, B. K. Cho, P. C. Canfield, D. C. Johnston, J. Y. Rhee, and B. N. Harmon, Phys. Rev. B **53**, 6022 (1996).
- ¹²L.F. Mattheiss, Phys. Rev. B **49**, 13 279 (1994); R. Coehoorn, Physica C **228**, 331 (1994); H. Kim *et al.*, Phys. Rev. B **52**, 4592 (1995).
- ¹³W.E. Pickett and D.J. Singh, Phys. Rev. Lett. **72**, 3702 (1994).
- ¹⁴J.I. Lee, T. S. Zhao, I. G. Kim, B. I. Min, and S. J. Youn, Phys. Rev. B **50**, 4030 (1994).
- ¹⁵T. Ekino, H. Fujii, M. Kosugi, Y. Zenitani, and J. Akimitsu, Phys. Rev. B **53**, 5640 (1996).
- ¹⁶D.D. Lawrie and J.P. Franck, Physica C **245**, 159 (1995).
- ¹⁷D. Davidov, R. Orbach, C. Rettori, D. Shaluel, L. J. Tao, and B. Ricks, Phys. Rev. B **5**, 1711 (1972); C. Rettori *et al.*, *ibid.* **7**, 1 (1973).
- ¹⁸A.A. Abrikosov and L.P. Gor'kov, Zh. Éksp. Teor. Fiz. **39**, 1781 (1960) [Sov. Phys. JETP **12**, 1243 (1961)].
- ¹⁹M. Xu, P. C. Canfield, J. H. Ostenson, D. K. Finnemore, B. K. Cho, Z. R. Wang, and D. C. Johnston, Physica C **227**, 321 (1994).
- ²⁰S.L. Bud'ko, M. Ilimassalam, M. B. Fontes, J. Mondragon, W. Vanoni, B. Giordanego, and E. M. Baggio-Saitovich, Physica C **243**, 183 (1995).
- ²¹G. Feher and A.I. Kip, Phys. Rev. **98**, 337 (1955); F.J. Dyson, *ibid.* **98**, 349 (1955).
- ²²G.L. Pake and H.M. Purcell, Phys. Rev. **74**, 1184 (1948).
- ²³K. Yosida, Phys. Rev. **106**, 893 (1957).
- ²⁴J. Korringa, Physica (Amsterdam) **16**, 601 (1950).
- ²⁵T. Moriya, J. Phys. Soc. Jpn. **18**, 516 (1963).
- ²⁶A. Narath, Phys. Rev. **163**, 232 (1967).
- ²⁷D. Davidov *et al.*, Solid State Commun. **12**, 621 (1973).
- ²⁸C. Rettori *et al.*, Phys. Rev. B **55**, 1016 (1997).
- ²⁹D. Davidov *et al.*, Phys. Lett. **35A**, 339 (1971); C. Rettori *et al.*, Phys. Rev. B **10**, 1826 (1974).
- ³⁰A. Narath and H.T. Weaver, Phys. Rev. **175**, 373 (1968).
- ³¹R.W. Shaw and W.W. Warren, Phys. Rev. B **3**, 1562 (1971).
- ³²W.L. McMillan, Phys. Rev. **167**, 331 (1968).
- ³³J.I. Lee, T. S. Zhao, I. G. Kim, B. I. Min, and S. J. Youn, Phys. Rev. B **50**, 4030 (1994).
- ³⁴S.A. Carter *et al.*, Phys. Rev. B **50**, 4216 (1994).
- ³⁵B. J. Suh, F. Borsa, D. R. Torgeson, B. K. Cho, P. C. Canfield, D. C. Johnston, J. Y. Rhee, and B. N. Harmon, Phys. Rev. B **53**, R6022 (1994).
- ³⁶Warren E. Pickett and David J. Singh, Phys. Rev. Lett. **72**, 3702 (1994).
- ³⁷A. Abragam and B. Bleaney, *EPR of Transition Ions* (Clarendon, Oxford, 1970).
- ³⁸M. El Massalami, S. L. Bud'ko, B. Giordanego, M. B. Fontes, J. C. Mondragon, and E. M. Baggio-Saitovich, Physica C **235-240**, 2563 (1994).
- ³⁹R. Movshovich, M. F. Hundley, J. D. Thompson, P. C. Canfield, B. K. Cho, and A. V. Chubukov, Physica C **227**, 381 (1994).

Seção 2.3

Estudos de RPE de Gd^{3+} no
composto de Valênciia
Intermediária YbInCu_4 e seus
compostos de referênciia
 $(\text{Y}, \text{Lu})\text{InCu}_4$

2.3) Estudos de RPE de Gd³⁺ no composto de Valência Intermediária YbInCu₄ e seus compostos de referência (Y, Lu)InCu₄.

PHYSICAL REVIEW B

VOLUME 55, NUMBER 2

1 JANUARY 1997 II

ESR of Gd³⁺ in the intermediate-valence YbInCu₄ and its reference compound YInCu₄

C. Rettori, S. B. Oseroff, and D. Rao
San Diego State University, San Diego, California 92182

P. G. Pagliuso and G. E. Barberis
Instituto de Física "Gleb Wataghin," UNICAMP, 13083-970, Campinas-SP, Brazil

J. Sarrao and Z. Fisk
National High Magnetic Field Laboratory, Florida State University, Tallahassee, Florida 32306

M. Hundley
Los Alamos National Laboratories, Los Alamos, New Mexico 87545
(Received 11 April 1996)

Electron-spin-resonance (ESR) experiments on Gd³⁺ in the intermediate-valence phase ($T < T_v$) of YbInCu₄ and in its reference compound YInCu₄ are interpreted in terms of an enhanced density of states at the Fermi level for the Yb-based compound. The Korringa rate and g shift measured in ESR and the susceptibility data allowed us to extract the electron-electron exchange enhancement factor σ for the Yb-based compound. The exchange interaction between the Gd³⁺ local moments and the conduction electrons ($c-e$) is $c-e$ wave-vector dependent in both compounds. [S0163-1829(97)00701-7]

I. INTRODUCTION

Many rare-earth intermetallic compounds present interesting physical properties associated with the hybridization between localized f -electron states and conduction electrons ($c-e$). This has motivated experimentalists and theoreticians for the last several decades to study strongly correlated electron phenomena in intermediate-valence (IV) and heavy-fermion (HF) systems.¹ The Ce- and Yb-based compounds are particularly well suited for these studies, since the $4f$ shell of Ce and Yb can contribute, at most, one electron or hole to the conduction band, respectively, simplifying the theoretical analysis. The cubic AuBe₃ (C15b, F43m)-type structure² of the YbInCu₄ compound is particularly interesting due to the first-order isostructural volume expansion phase transition found at $T_v \sim 50$ K.³ Extensive studies⁴ of susceptibility, specific heat, resistivity, Yb's Mossbauer, lattice parameter, L_{III} , x-ray absorption, and NMR (Refs. 5 and 6) are consistent with a 0.45% volume change² and a Yb valence change from $z \sim 2.9$ at high temperatures to $z \sim 2.8$ at lower temperature.⁴ This property characterizes this compound as an intermediate f -ion valence system at low temperatures. To further study the electronic properties of this compound, we have measured the low-temperature electron-spin resonance (ESR) of Gd³⁺ in YbInCu₄ ($T \leq 50$ K) and in its reference compound YInCu₄ ($T \leq 100$ K). Susceptibility and specific-heat measurements were also performed.

While our work was in progress, a paper by Altshuler *et al.*⁷ on Gd³⁺ in YbInCu₄ was published. They have analyzed their ESR data by focusing on the exchange coupling between the Gd³⁺ local moment and the "quasilocalized Yb³⁺ moment." Thus, their analysis is mainly concentrated on the high-temperature data ($T > 50$ K). Their results resemble those found for Gd³⁺ impurities in a stable-valence weak-magnetic metallic^{8,9} or insulator^{10,11} hosts. In such

compounds the observed temperature-dependent g shifts and rapid broadening of the linewidths are associated, respectively, with the temperature dependence of the host magnetic susceptibility and with the relaxation via excited crystal-field levels.⁸⁻¹¹ The magnetic moment of the Yb³⁺ ions, for the YbInCu₄ compound at $T \geq T_v$, is well defined. For $T \geq T_v$ the compound behaves as a magnetic host with well established crystal-field levels for the free Yb³⁺ ion ground state $^2F_{7/2}$.^{4,12} Thus, exchange and/or direct magnetic interactions result in a shift and broadening of the Gd³⁺ resonance. Therefore, an analysis of ESR data in a magnetic host should be carried out keeping in mind that a shift and a broadening of the resonance may have a variety of origins. Although our data in YbInCu₄ agree with those of Altshuler *et al.*,⁷ the aim of our work and analysis has been focused on the temperature region where the ESR of Gd³⁺ actually probes the IV state of YbInCu₄ ($T < T_v$). In this case it is important to use a reference compound that allows the extraction of the various intrinsic parameters. For this reason, we have also measured the ESR and susceptibility of Gd³⁺ in YInCu₄ and specific heat of YInCu₄.

II. EXPERIMENTAL DETAILS

Single crystals of (Yb,Y)_{1-x}Gd_xInCu₄ (0.0005 $\leq x \leq$ 0.002 nominal) were grown from a flux of excess InCu by the method described elsewhere.¹³ The crystals were of cubiclike shape with typical sizes of $4 \times 3 \times 1$ mm³. For the high-temperature ESR measurements, powdered crystals were used in order to increase the ESR signal-to-noise ratio. The ESR experiments were carried out in a Varian E-line X-band spectrometer, using a liquid-helium tail dewar (1.7–4.15 K) and a helium gas flux (7–100 K) adapted to a room-temperature TE₁₀₂ cavity. The susceptibility measurements



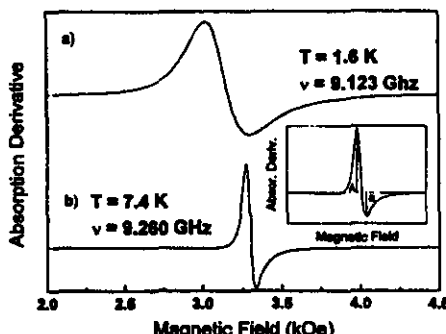


FIG. 1. ESR powder spectra of (a) 0.18% of Gd³⁺ in YbInCu₄ and (b) 0.25% of Gd³⁺ in YInCu₄. The inset shows the definition of *A* and *B* for a Dysonian line shape.

were made in a Quantum Design dc superconducting quantum interference device magnetometer. Specific-heat measurements were performed in a small-mass calorimeter system that employs a quasiadiabatic thermal relaxation technique.¹⁴ Samples employed here ranged in mass from 45 to 145 mg.

III. EXPERIMENTAL RESULTS

Figure 1 shows the ESR powder spectra of Gd³⁺ (~0.2%) in YbInCu₄ and YInCu₄ measured at $T \leq 7$ K. Typical Dysonian line shapes¹⁵ with $A/B \sim 2.2(2)$ were observed. This type of line shape is characteristic of localized magnetic moments in a lattice with a skin depth smaller than the size of the sample particles. For YbInCu₄ the Gd³⁺ resonance shows a decreasing A/B ratio as the temperature increases, in agreement with the increase of the resistivity observed for this compound.^{4,16} The *g* value and linewidth were obtained using the method of Peter *et al.*¹⁷ Figure 2 gives the temperature dependence of the linewidth for both compounds. For the Yb-based system for $T > 30$ K, an increase in the broadening of the linewidth and of the *g* value were observed. A departure from a linear broadening is seen in Fig. 2 and is in agreement with recently published data on

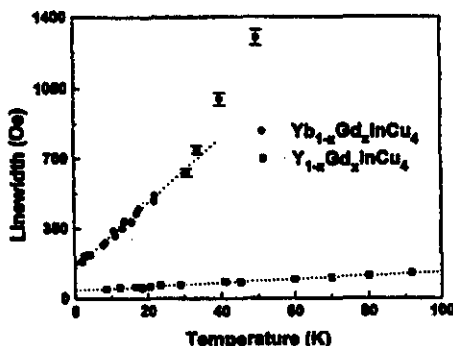


FIG. 2. Temperature dependence of the ESR linewidth for 0.18% of Gd³⁺ in YbInCu₄ (circles) and 0.25% of Gd³⁺ in YInCu₄ (squares). The dashed line is the best fit to $\Delta H = a + bT$.

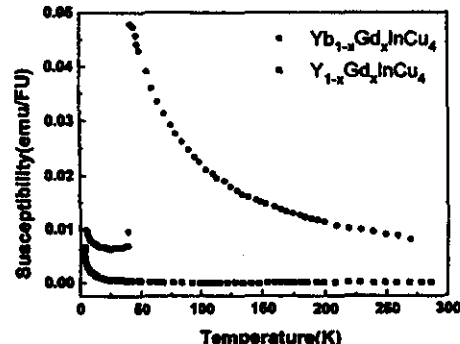


FIG. 3. Magnetic susceptibility as a function of temperature, measured at 1 kOe for 0.18% of Gd³⁺ in YbInCu₄ (circles) and 0.25% of Gd³⁺ in YInCu₄ (squares).

Yb_{1-x}Gd_xInCu₄.⁷ The linear dependence of the linewidth was fitted to the expression $\Delta H = a + bT$, with $a = 150(20)$ Oe, $b = 16(1)$ Oe/K and $a = 42(5)$ Oe, $b = 0.9(1)$ Oe/K for Gd³⁺ in YbInCu₄ and YInCu₄, respectively. Within the accuracy of the measurements, the *g* values were found to be temperature independent for $T < 30$ K. The measured low-temperature ($T < 7$ K) *g* values were 2.073(8) and 2.004(2) for the Yb- and Y-based compounds, respectively. For the low concentration samples ($\sim 0.05\%$) we measured similar values, within our experimental error. In single crystals the Gd³⁺ resonance did not show crystal-field features, i.e., fine structure and/or anisotropic linewidth.

Figure 3 shows the magnetic susceptibility, corrected for the compound core-diamagnetism, for the samples used in our ESR experiments. From the low-temperature tail ($T > 45$ K) we estimate the Gd concentration to be 0.18(2)% and 0.25(2)% for the Yb_{1-x}Gd_xInCu₄ and Y_{1-x}Gd_xInCu₄ compounds, respectively. From the high-temperature ($T > 50$ K) susceptibility of the Yb_{1-x}Gd_xInCu₄ we obtain $4.24(10)\mu_B/Yb$, in good agreement with previous reports,³⁻⁶ and close to the $4.54\mu_B/Yb$ expected for Yb³⁺ ($4f^{13}, 2F_{7/2}$). From the low-temperature data ($T < 45$ K) a temperature-independent contribution of $6(1) \times 10^{-3}$ emu/FU was estimated, in agreement with previous measurements.³⁻⁶

In Fig. 4 we present specific-heat measurements for the YInCu₄ compound in the temperature range between 2 K $< T < 20$ K. The low-temperature C/T data increase linearly with T^2 as seen in the inset of Fig. 4. The fitting parameters obtained from these data are $\gamma = 1.63(6)$ mJ/mol K² and $\beta = 0.327(2)$ mJ/mol K⁴. A Debye temperature $\theta_D = 330(5)$ K is also obtained.

In Table I we summarize the experimental parameters derived in the present work, and by other groups, for the YbInCu₄ and YInCu₄ compounds.

IV. ANALYSIS AND DISCUSSION

In the simplest treatment of the exchange interaction, $J_{fs}S_zs_z$, between a localized $4f$ electron spin (S) on a solute atom (Gd³⁺) and the free $c-e$ spin (s) of the host metal, the ESR *g* shift (Knight shift)¹⁸ and the thermal broadening of the linewidth (Korringa rate),¹⁹ when "bottleneck" and

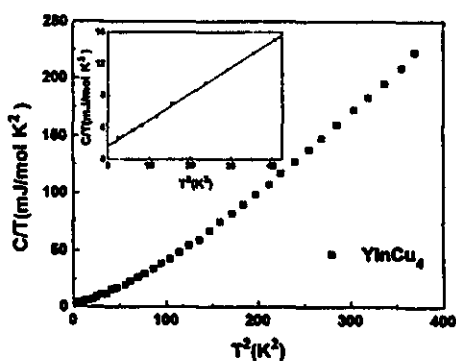


FIG. 4. Specific heat (C/T) as a function of T^2 for YInCu_4 . The inset shows the low temperature T^2 dependence of C/T . The solid line is the best fit to $C/T = \gamma + \beta T^2$, with $\gamma = 1.63(6)\text{mJ/mol K}^2$ and $\beta = 0.327(2)\text{mJ/mol K}^4$.

"dynamic" effects are not present,²⁰ can be written as

$$\Delta g = J_{fs} \eta(E_F), \quad (1)$$

and

$$\frac{d(\Delta H)}{dT} = \frac{\pi k}{g \mu_B} J_{fs}^2 \eta^2(E_F), \quad (2)$$

where J_{fs} is the effective exchange interaction between the Gd^{3+} local moment and the $c-e$ in the absence of $c-e$ momentum transfer,²¹ $\eta(E_F)$ is the "bare" density of states for one spin direction at the Fermi surface, k is the Boltzmann constant, μ_B is the Bohr magneton, and g is the Gd^{3+} g value.

Equations (1) and (2) are normally used in the analysis of ESR data for highly diluted rare-earths magnetic moments in intermetallic compounds with appreciable residual resistivity, i.e., large $c-e$ spin-flip scattering. In our case the ESR parameters are found to be independent of the concentration.²⁰ Hence, it is expected that the following relation would hold:

$$\frac{d(\Delta H)}{dT} = \frac{\pi k}{g \mu_B} (\Delta g)^2. \quad (3)$$

Using the g value of Gd^{3+} in insulators as 1.993(2),²² ($\pi k/g \mu_B = 2.34 \times 10^4 \text{ Oe/K}$), the measured g shifts and the thermal broadening of the linewidths b for the Gd^{3+} resonance in YbInCu_4 and YInCu_4 , we found (i) that for YbInCu_4 , when replacing $\Delta g \sim 0.08(1)$ in Eq. (3), a thermal broadening of $b \sim 150(40) \text{ Oe/K}$ is obtained. That value is much larger than the one measured, $b \sim 16(1) \text{ Oe/K}$, and (ii)

for YInCu_4 , when replacing $\Delta g \sim 0.011(4)$ in Eq. (3), we calculated a thermal broadening of $b \sim 3(2) \text{ Oe/K}$. That value is also larger than the one measured, $b \sim 0.9(1) \text{ Oe/K}$. Therefore, we conclude that the approximations made in Eqs. (1) and (2) are not valid for either compound, and conduction electron-electron correlations^{23,24} and q -dependent exchange interaction, $J_{fs}(q)$,²¹ must be considered in the analysis of our ESR data. $J_{fs}(q)$ is the Fourier transform of the spatially varying exchange. In our analysis we will only consider the contribution from a single $c-e$ band, because the measured thermal broadenings of the linewidths were found to be much smaller than those expected for the measured g shifts.^{25,26}

As mentioned above the electronic contribution to the heat capacity for the YInCu_4 compound yields a $\gamma = 1.63(6)\text{mJ/mol K}^2$. Assuming a free $c-e$ gas model for YInCu_4 , $\gamma = (2/3) \pi k^2 \eta(E_F)$, we calculate a density of states at the Fermi level, $\eta(E_F) = 0.34(2) \text{ states/eV mol spin}$. For this density of states, one would expect an electronic-spin susceptibility, $\chi_e = 2\mu_B \eta(E_F)$, of $\sim 0.03 \times 10^{-3} \text{ emu/FU}$. That is of the order of the "background" susceptibility (corrected for the core diamagnetism) measured at high temperatures for this compound (see Fig. 3). Hence, one can assume that electron-electron correlations are not important in YInCu_4 . Taking into account only the wave-vector dependence of the exchange interaction, $J_{fs}(q)$,²¹ in Eqs. (1) and (2) the exchange parameters should be replaced by $J_{fs}(0)$ and $\langle J_{fs}^2(q) \rangle$, respectively. At the Gd^{3+} site the g shift probes the $c-e$ polarization ($q = 0$) and the Korringa rate the $c-e$ momentum transfer ($0 \leq q \leq 2k_F$) averaged over the Fermi surface.²¹ Using $\eta(E_F) = 0.34(2) \text{ states/eV mol spin}$, $\Delta g = 0.011(4)$, and $b = 0.9(1) \text{ Oe/K}$, we found the exchange parameters between the Gd^{3+} local moment and the $c-e$ in YInCu_4 to be $J_{fs}(0) = 32(10) \text{ meV}$ and $\langle J_{fs}^2(q) \rangle^{1/2} = 18(5) \text{ meV}$.

For YbInCu_4 the low-temperature linear part of the heat capacity gives an electronic contribution of $\gamma = 50(5)\text{mJ/mol K}^2$.^{4,6,16} For a free $c-e$ gas we obtained $\eta(E_F) = 10(1) \text{ states/eV mol spin}$, about 30 times larger than that found for YInCu_4 . For this density of states, we obtained a $c-e$ spin susceptibility, $\chi_e = 2\mu_B \eta(E_F)$, of $\sim 0.7 \times 10^{-3} \text{ emu/FU}$. This is one order of magnitude smaller than the temperature-independent part of the susceptibility measured in this compound for $T < 45 \text{ K}$, $6(1) \times 10^{-3} \text{ emu/FU}$. This suggests that a strong electron-electron exchange enhancement contributes to the $c-e$ spin susceptibility in YbInCu_4 below its valence transition. It is known, that in the presence of such an electron-electron exchange enhancement, the host metal $c-e$ spin susceptibility can be approximated by^{23,24}

TABELA I. Experimental parameters for $\text{Gd}:(\text{Yb,Y})\text{InCu}_4$.

g	a Oe	b Oe/K	c %	γ	β mJ mol K ²
				mol K ²	
$\text{Yb}(\text{Gd})\text{InCu}_4$	2.073(8)	150(20)	16(1)	50(5) ^a	0.33(4) ^a
$\text{Y}(\text{Gd})\text{InCu}_4$	2.004(2)	42(5)	0.9(1)	1.63(6)	0.327(2)

TABLE II. Extracted parameters for Gd:(Yb,Y)InCu₄.

	$\eta(E_F)$ states eV mol spin	θ_D K	$J_{fs}(0)$ meV	$\langle J_{fs}^2(q) \rangle^{1/2}$ meV	$K(\alpha)$	α
Yb(Gd)InCu ₄	10(1) ^a	~ 276 ^a	2.4(1.5)	1.3(1.0)	0.36(20)	0.7(2)
Y(Gd)InCu ₄	0.34(2)	330(5)	32(10)	18(5)	~ 1	~ 0

^aSee Refs. 4, 6, and 16.

$$\chi_c = 2\mu_B^2 \frac{\eta(E_F)}{1-\alpha}, \quad (4)$$

where α accounts for the electron-electron interaction, $(1-\alpha)^{-1}$ is the Stoner enhancement factor, and $\eta(E_F)$ is the bare density of states for one spin direction at the Fermi level obtained from specific-heat experiments. An upper limit for α of ~ 0.9 is estimated assuming that the temperature-independent part of the susceptibility, $6(1) \times 10^{-3}$ emu/FU, is only due to an enhanced c-e spin susceptibility.

In the presence of electron-electron exchange enhancement and a q dependence of the exchange interaction, $J_{fs}(q)$, the g shift [Eq. (1)] and the thermal broadening of the linewidth [Eq. (2)] may be rewritten as^{20,21}

$$\Delta g = J_{fs}(0) \frac{\eta(E_F)}{1-\alpha}, \quad (5)$$

and

$$\frac{d(\Delta H)}{dT} = \frac{\pi k}{g \mu_B} \langle J_{fs}^2(q) \rangle \eta^2(E_F) \frac{K(\alpha)}{(1-\alpha)^2}, \quad (6)$$

where $K(\alpha)$ is the Korringa exchange enhancement

$$\frac{d(\Delta H)}{dT} = \frac{\pi k}{g \mu_B} \frac{\langle J_{fs}^2(q) \rangle}{J_{fs}(0)} (\Delta g)^2 K(\alpha). \quad (7)$$

Using $\Delta g = 0.08(1)$, $b = 16(1)$ Oc/K, and assuming that the wave-vector dependence of the exchange interaction in YbInCu₄ is the same as that of its isomorphic compound YInCu₄, i.e., $[(J_{fs}^2(q))/J_{fs}(0)] \sim 0.31(15)$, we calculated $K(\alpha) \sim 0.36(20)$ from Eq. (7). From the work of Shaw and Warren²⁹ this value corresponds to $\alpha \sim 0.7(2)$, which is compatible with the upper limit of ~ 0.9 estimated from the enhancement of the c-e spin susceptibility. Then, using

$\eta(E_F) = 10(1)$ states/eV mol spin, $\alpha \sim 0.7(2)$, and Eqs. (5) and (6) we obtain, $J_{fs}(0) \sim 2.4(1.5)$ meV and $\langle J_{fs}^2(q) \rangle^{1/2} \sim 1.3(1.0)$ meV for the exchange parameters between Gd³⁺ and the c-e in YbInCu₄. These values are at least ten times smaller than their respective values found for Gd³⁺ in YInCu₄, suggesting a much higher c-e localization for the Yb than for the Y-based compound. That is consistent with a large $\eta(E_F)$ associated with a "narrow" band at the Fermi level in IV and HF systems. Table II summarizes the parameters obtained in the present work for Gd³⁺ in (Yb,Y)InCu₄.

V. CONCLUSIONS

The ESR data presented for Gd³⁺ in the IV phase of YbInCu₄ ($T < T_c$) show that the large density of states at the Fermi level, characteristic of an IV and HF system, results in a g shift and a Korringa rate larger than those found in its reference compound YInCu₄. Our results also indicate that the high density of states of an IV system perturb the g shift and the Korringa rate in a different way. We found that these parameters are strongly dependent on the electronic properties of the chosen compound, such as electron-electron exchange interaction,²⁷ wave-vector dependence of the exchange interaction,²¹ band structure,²⁶ and the local-

In summary, our results show that ESR experiments can be used to monitor the high density of states in some of the highly correlated electron IV and HF systems. However, one should be aware that this property may not be observable for other strongly correlated electron systems when using the ESR technique.³⁰⁻³³

ACKNOWLEDGMENTS

This work was supported by Grant No. 91/0573-0 of FAPESP, São Paulo-SP-Brazil and NSF-DMR Grant Nos. 9117212, 9016241, and 9501529.

¹ See, *Valence Fluctuation in Solids*, edited by L.M. Falicov, W. Hanke, and M.B. Maple (North-Holland, Amsterdam, 1981); *Valence Instabilities*, edited by P. Wachter and H. Boppert (North-Holland, Amsterdam, 1982); *Valence Fluctuation*, edited by E. Müller-Hartmann, B. Roden, and D. Wohleben (North-Holland, Amsterdam, 1984); *Valence Fluctuations*, edited by G.B. Barberis, M.E. Foglio, J.H. Crow, and P. Schlottmann (North-Holland, Amsterdam, 1991).

² K. Kojima, Y. Nakai, T. Suzuki, H. Asano, I. Izumi, T. Fujita,

and T. Hihara, *J. Phys. Soc. Jpn.* **59**, 792 (1990).

³¹ I. Felner and I. Nowik, *Phys. Rev. B* **33**, 617 (1987); I. Felner and I. Nowik, *J. Magn. Magn. Mater.* **63-64**, 615 (1987).

⁴ I. Felner, I. Nowik, D. Vaknin, U. Potzel, J. Moser, G.M. Kalvius, G. Wortmann, G. Schmießer, G. Hilscher, U. Gratz, C. Schmitz, N. Pillmayr, K.G. Prasad, D. deWaard, and H. Pinto, *Phys. Rev. B* **35**, 6956 (1987); T. Matsumoto, T. Shimizu, Y. Yamada, and K. Yoshimura, *J. Magn. Magn. Mater.* **104-107**, 647 (1992).

- ⁵K. Kojima, H. Yabuta, and T. Iihara, *J. Magn. Magn. Mater.* **104-107**, 653 (1992).
- ⁶I.V. Sampathkumaran, N. Nambudripad, S.K. Dhar, R. Vijayaraghavan, and R. Kuentzler, *Phys. Rev. B* **35**, 2035 (1987).
- ⁷T.S. Altshuler, M.S. Bresler, M. Schlott, B. Eischner, and H. Gratz, *Z. Phys. B* **99**, 57 (1995).
- ⁸C. Rettori, D. Davidov, A. Grayewskey, and W.M. Walsh, *Phys. Rev. B* **11**, 4450 (1975).
- ⁹D. Davidov, C. Rettori, and V. Zevin, *Solid State Commun.* **16**, 247 (1975).
- ¹⁰C. Rettori, D. Rao, S. Oseroff, R.D. Zysler, M. Tovar, Z. Fisk, S-W. Cheong, S. Schultz, and D.C. Vier, *Phys. Rev. B* **44**, 826 (1991).
- ¹¹R.D. Zysler, M. Tovar, C. Rettori, D. Rao, H. Shore, S.B. Oseroff, D.C. Vier, S. Schultz, Z. Fisk, and S-W. Cheong, *Phys. Rev. B* **44**, 9467 (1991); F. Mehran and K.W.H. Stevens, *Phys. Rep.* **85**, 123 (1982).
- ¹²A. Severing, H. Gratz, B.D. Rainford, and K. Yoshimura, *Physica B* **163**, 409 (1990).
- ¹³J.L. Sarrao, C.L. Benton, Z. Fisk, J.M. Lawrence, D. Mandrus, and J.D. Thompson, *Physica B* **223&224**, 366 (1996).
- ¹⁴R. Bachmann, F.J. DiSalvo, T.H. Geballe, R.L. Greene, R.H. Howard, C.N. King, H.C. Kivisch, K.N. Lee, R.H. Schwall, H.V. Thomas, and R.B. Zubek, *Rev. Sci. Instrum.* **43**, 205 (1972).
- ¹⁵G. Feher and A.F. Kip, *Phys. Rev.* **98**, 337 (1955); F.J. Dyson, *Phys. Rev.* **98**, 349 (1955).
- ¹⁶N. Pillmayr, L. Bauer, and K. Yoshimura, *J. Magn. Magn. Mater.* **104-107**, 639 (1992).
- ¹⁷M. Peter, D. Shaltiel, J.H. Wernick, H.J. Williams, J.B. Mock, and R.C. Sherwood, *Phys. Rev.* **126**, 1395 (1962).
- ¹⁸K. Yosida, *Phys. Rev.* **106**, 893 (1957).
- ¹⁹J. Koringa, *Physica* **16**, 601 (1950).
- ²⁰C. Rettori, H.M. Kim, H.P. Chock, and D. Davidov, *Phys. Rev. B* **10**, 1826 (1974).
- ²¹D. Davidov, K. Maki, R. Orbach, C. Rettori, and H.P. Chock, *Solid State Commun.* **12**, 621 (1973).
- ²²A. Abragam and B. Bleaney, *EPR of Transition Ions* (Clarendon, Oxford, 1970).
- ²³T. Moriya, *J. Phys. Soc. Jpn.* **18**, 516 (1963).
- ²⁴A. Narath, *Phys. Rev.* **163**, 232 (1967).
- ²⁵D. Davidov, A. Chelkowski, C. Rettori, R. Orbach, and M.B. Maple, *Phys. Rev. B* **7**, 1029 (1973).
- ²⁶G.I. Barberis, D. Davidov, J.P. Donoso, C. Rettori, J.R. Suassuna, and H.D. Dokter, *Phys. Rev. B* **19**, 5495 (1979).
- ²⁷D. Davidov, R. Orbach, C. Rettori, D. Shaltiel, L.J. Tao, and B. Ricks, *Phys. Lett.* **35A**, 339 (1971).
- ²⁸A. Narath and H.T. Weaver, *Phys. Rev.* **175**, 373 (1968).
- ²⁹R.W. Shaw and W.W. Warren, *Phys. Rev. B* **3**, 1562 (1971).
- ³⁰G.I. Barberis, D. Davidov, C. Rettori, J.P. Donoso, I. Torriani, and H.G.G. Gandra, *Phys. Rev. Lett.* **45**, 1996 (1980).
- ³¹H. Schaeffer and B. Eischner, *Z. Phys. Condens. Matter B* **53**, 109 (1983).
- ³²H.G. Gandra, S. Schultz, S.B. Oseroff, Z. Fisk, and J.L. Smith, *Phys. Rev. Lett.* **55**, 2719 (1985).
- ³³H.G. Gandra, M.J. Pontes, S. Schultz, and S.B. Oseroff, *Solid State Commun.* **64**, 859 (1987).



PII: S0038-1098(97)00318-9

ESR OF Gd³⁺ IN LuInCu₄ INTERMETALLIC COMPOUNDP.G. Pagliuso,^a C. Rettori,^a S.B. Oseroff,^{a,t} J. Sarrao,^b Z. Fisk,^b A. Cornelius^c and M.F. Hundley^c^aInstituto de Física "Gleb Wataghin", UNICAMP, 13083-970, Campinas-SP, Brazil^bNational High Magnetic Field Laboratory, Florida State University, Tallahassee, FL 32306, U.S.A.
^cLos Alamos National Laboratories, Los Alamos, NM 87545, U.S.A.

(Received 21 May 1997; accepted 19 June 1997 by C.E.T. Gonçalves da Silva)

Electron spin resonance (ESR) experiments of paramagnetic ions in metallic compounds have been used to investigate the interaction between conduction-electron (c-e) and paramagnetic ions. The Gd³⁺ Korringa rate and g-shift measured in ESR, the susceptibility and specific heat data of LuInCu₄, allowed us to extract the exchange parameters between the Gd³⁺ local moments and the c-e in this compound. These parameters were found to be c-e wave-vector dependent. © 1997 Published by Elsevier Science Ltd

1. INTRODUCTION

Many rare-earth intermetallic compounds present interesting physical properties that can be studied by means of Electron Spin Resonance (ESR) experiments. In a simple metallic host, the exchange parameters between the local magnetic moments and the conduction-electrons (c-e), the electron-electron (e-e) exchange enhancement and the type of c-e at the Fermi level can be obtained from these experiments. LuInCu₄ is an intermetallic compound with a cubic AuBe₃ (C15b, F43m)-type of structure [1]. In our previous work [2], the isostructural compounds RInCu₄ (R = Yb, Y) were also investigated at low temperatures by means of ESR. The Yb-based compound is an intermediate valence (IV) f-ion system. This system has been intensively studied by a variety of techniques [3-5]. ESR in IV compounds require that the obtained results be compared with those of a reference compound. In this work we present low temperature ESR of Gd³⁺ in LuInCu₄, another reference compound of the YbInCu₄ IV compound. Also, susceptibility and specific heat measurements are given. The results allowed us to confirm the assumption made in our previous work [2], that the exchange parameter ratio, $(J_p^2(q))/J_p^2(0)$, may be the same for isostructural compounds.

2. EXPERIMENTAL DETAILS

Single crystals of Lu_{1-x}Gd_xInCu₄ ($0.0002 \leq x \leq 0.002$ nominal) were grown from a flux of excess InCu by the

method described elsewhere [6]. The crystals were of cubic-like shape with typical sizes of $4 \times 3 \times 1$ mm³. For the high temperature ESR measurements, powdered crystals were used in order to increase the ESR signal to noise ratio. The ESR experiments were carried out in a Varian E-line X-band spectrometer, using a liquid-helium tail dewar (1.7-4.15 K) and a helium gas flux (7-100 K) adapted to a room-temperature TE₁₀₂ cavity. The susceptibility measurements were made in a Quantum Design d.c. SQUID magnetometer. Specific heat measurements were performed in a small-mass calorimeter system that employs a quasi-adiabatic thermal relaxation technique [7]. Samples employed here ranged in mass from 45 mg to 145 mg.

3. EXPERIMENTAL RESULTS

Figure 1 shows the ESR powder spectra of Gd³⁺ ($\approx 0.03\%$) in LuInCu₄ measured at $T = 1.6$ K. Typical Dysonian lineshapes [8] with $A/B \approx 2.2(2)$ were observed. This type of lineshape is characteristic of localized magnetic moments in a metallic lattice with a skin depth smaller than the size of the sample particles. The g-value and linewidth were obtained using the fitting of the resonance to the appropriate admixture of absorption and dispersion [9]. The solid line is the best fit to the observed resonance.

Figure 2 gives the temperature dependence of the linewidth for the LuInCu₄ compound. The linear dependence of the linewidth was fitted to the expression $\Delta H = a + bT$. Within the accuracy of the measurements, the g-values were found to be temperature-independent.

^tCurrent address: Department of Physics, San Diego State University, San Diego, CA 92182, U.S.A.

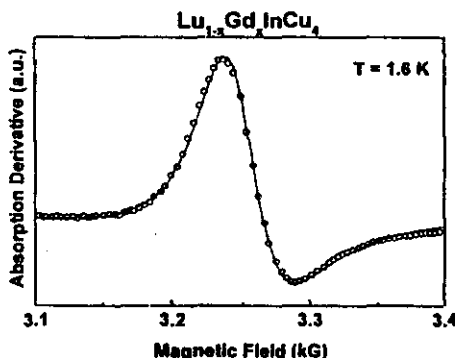


Fig. 1. ESR powder spectra of (a) 0.03% of Gd³⁺ in LuInCu₄. The solid line is the best fit to the observed resonance using the appropriate admixture of absorption and dispersion.

The a , b and g values were, within our experimental error and used concentration, independent of Gd-concentration. In single crystals the Gd³⁺ resonance did not show crystal field features, i.e. fine structure and/or anisotropic linewidth.

Figure 3 shows the temperature dependence of the magnetic susceptibility, $\chi(T)$, for Lu_{1-x}Gd_xInCu₄ ($x = 0.0002(2)$). The Gd concentration was estimated from the low temperature tail ($T \leq 40$ K) of $\chi(T)$, assuming a Curie-Weiss law for Gd³⁺. From the high temperature, we have estimated a temperature-independent contribution (Pauli susceptibility) of $0.027(3) \times 10^{-3}$ emu/FU, which is similar to our previous measurements in YInCu₄ [2].

Figure 4 presents the specific-heat of LuInCu₄ at temperature between $2 \text{ K} \leq T \leq 20 \text{ K}$. The low temperature ($2 \leq T \leq 7 \text{ K}$) C/T data increase linearly with T^2 (see inset in Fig. 4). The fitting parameters obtained from these data are $\gamma = 2.03(3) \text{ mJ mol-K}^{-2}$ and $\beta = 0.41(2) \text{ mJ mol-K}^{-4}$. The Debye temperature, $\theta_D = 305(5) \text{ K}$, is also obtained.

Table 1 summarizes the experimental parameters obtained in the present work for LuInCu₄.

4. ANALYSIS AND DISCUSSION

In the simplest treatment of the exchange interaction, J_{fs} s.s., between a localized 4f electron spin (S) on a solute atom (Gd³⁺) and the free c-e's spin (s) of the host metal, the ESR g-shift (Knight shift) [10] and the thermal broadening of the linewidth (Korringa rate) [11], when "bottleneck" and "dynamic" effects are not present [12], can be written as

$$\Delta g = J_B \eta(E_F), \quad (1)$$

and

$$\frac{d(\Delta H)}{dT} = \frac{\pi k}{g \mu_B} J_B^2 \eta^2(E_F), \quad (2)$$

where J_B is the effective exchange interaction between the Gd³⁺ local moment and the c-e in the absence of c-e momentum transfer [13], $\eta(E_F)$ the "bare" density of states for one spin direction at the Fermi surface, k the Boltzmann constant, μ_B the Bohr magneton and g the Gd³⁺ g-value.

Equations (1) and (2) are used in the analysis of ESR data for highly diluted rare-earth magnetic moments in

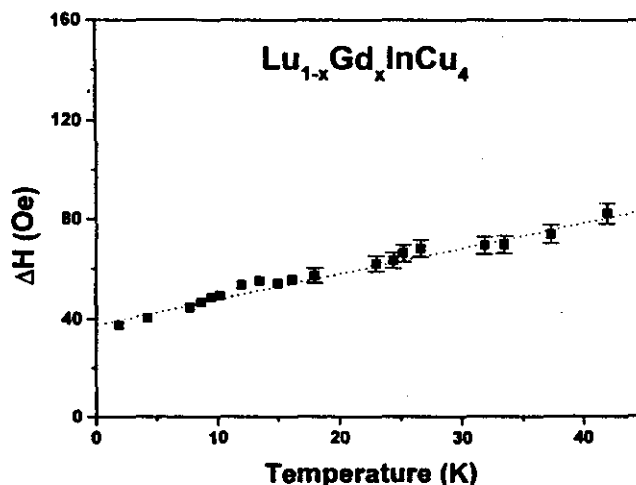


Fig. 2. Temperature dependence of the ESR linewidth for 0.03% of Gd³⁺ in LuInCu₄. The dashed line is the best fit to $\Delta H = a + bT$.

Table 1. Experimental parameters for Gd : LuInCu₄

	<i>g</i>	<i>a</i> Oe	<i>b</i> Oe K ⁻¹	<i>c</i> %	γ mJ/mol·K ²	β mJ/mol·K ⁴
Lu(Gd)InCu ₄	2.003(2)	41(2)	0.9(1)	≈ 0.2	2.03(3)	0.41(2)

intermetallic compounds with appreciable residual resistivity, i.e. large c-e spin-flip scattering. In our case the ESR parameters are found to be independent of the concentration [12]. Hence, it is expected that the following relation would hold:

$$\frac{d(\Delta H)}{dT} = \frac{\pi k}{g\mu_B} (\Delta g)^2. \quad (3)$$

Using the *g*-value of Gd³⁺ in insulators as 1.993(2) [14], $(\pi k/g\mu_B) = 2.34 \times 10^4$ Oe K⁻¹, the measured *g*-shifts and the thermal broadening of the linewidth, *b*, for the Gd³⁺ resonance in LuInCu₄ we found that using $\Delta g \approx 0.010(4)$ in equation (3), a thermal broadening $b \approx 2.4(8)$ Oe K⁻¹ is obtained. That value is larger than the measured one, $b \approx 0.9(1)$ Oe K⁻¹. Therefore, we conclude that the approximations made in equations (1) and (2) are not valid for this compound and conduction electron-electron correlations [15, 16] and *q*-dependent exchange interaction, *J_f(q)* [13], must be considered in the analysis of our ESR data. *J_f(q)* is the Fourier transform of the spatially varying exchange. In our analysis we will only consider the contribution from a single c-e band, because the measured thermal broadening of the linewidth was found to be much smaller than that expected for the measured *g*-shift [17, 18].

As mentioned above, the electronic contribution to the heat capacity for the LuInCu₄ compound yields to $\gamma = 2.03(6)$ mJ mol⁻¹ K⁻². Assuming a free c-e gas model for LuInCu₄, $\gamma = (2/3)\pi^2 k^2 \eta(E_F)$, we calculate a density of states at the Fermi level, $\eta(E_F) = 0.42(2)$ states eV⁻¹ mol-spin. For this density of states, one would expect an electronic spin susceptibility, $\chi_e = 2\mu_B^2 \eta(E_F)$, of $\approx 0.027 \times 10^{-3}$ emu/FU. This value is of the order of the "background" susceptibility (corrected for the core-diamagnetism) measured at high temperatures for this compound (see Fig. 3). Hence, one can assume that electron-electron correlations are not important in LuInCu₄. Taking into account only the wave-vector dependence of the exchange interaction, *J_f(q)* [13], in equations (1) and (2) the exchange parameters should be replaced by *J_f(0)* and $\langle J_f^2(q) \rangle$, respectively. At the Gd³⁺ site the *g*-shift probes the c-e polarization (*q* = 0) and the Korringa rate the c-e momentum transfer ($0 \leq q \leq 2k_F$) averaged over the Fermi surface [13]. Using $\eta(E_F) = 0.42(2)$ states eV⁻¹ mol-spin, $\Delta g = 0.010(4)$ and $b = 0.9(1)$ Oe K⁻¹, we found the exchange parameters between the Gd³⁺ local moments and the c-e in LuInCu₄ to be, *J_f(0)* = 24(6) meV and $\langle J_f^2(q) \rangle^{1/2} = 15(4)$ meV. Table 2 gives the extracted parameters for LuInCu₄.

The exchange parameter *J_f(0)* is found to be positive. Hence, we conclude that the exchange interaction with

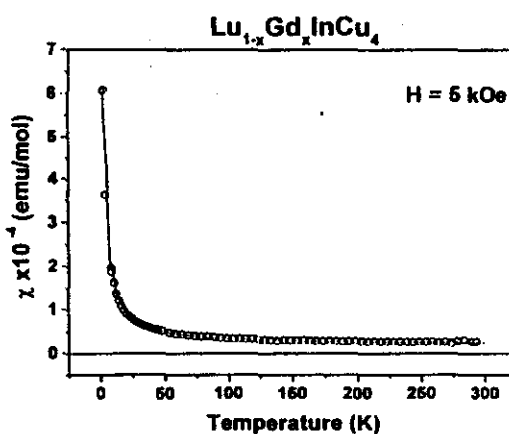


Fig. 3. Magnetic susceptibility as a function of temperature measured at 5 kOe for 0.02% of Gd³⁺ in LuInCu₄. The solid line is the best fit to $\chi = \chi_0 + C/(T - \theta)$ with $\chi_0 = 0.027(3) \times 10^{-3}$ emu mol⁻¹, the Curie constant $C = 0.00189$ emu.K mol⁻¹ and $\theta = -0.1(1)$ K.

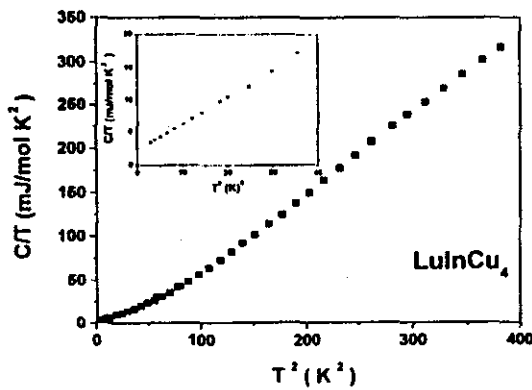


Fig. 4. Specific heat (C/T) as a function of T^2 for LuInCu₄. The inset shows the low temperature T^2 dependence of C/T . The solid line in the inset is the best fit to $C/T = \gamma + \beta T^2$, with $\gamma = 2.03(3)$ mJ mol⁻¹ K⁻² and $\beta = 0.41(2)$ mJ mol⁻¹ K⁻⁴.

Table 2. Extracted parameters for Gd : LuInCu₄

	$\eta(E_F)$ states/eV mol-spin	θ_p K	$J_{f\beta}(0)$ meV	$\langle J_{f\beta}^2(q) \rangle^{1/2}$ meV
Lu(Gd)InCu ₄	0.42(2)	~305	24(6)	15(4)

the c-e is of atomic-like for Gd³⁺ [13]. The values of $J_{f\beta}(0)$ and $\langle J_{f\beta}^2(q) \rangle$ lead to the ratio $\langle J_{f\beta}^2(q) \rangle / J_{f\beta}(0) \approx 0.39(18)$ for LuInCu₄. This value is close to those extracted for this ratio in the isostructural compounds RInCu₄ (R = Y, Yb) [2]. The same behavior was found for the $\langle J_{f\beta}^2(q) \rangle / J_{f\beta}(0)$ ratio in the Kondo lattice compound YbAgCu₄ and its reference compounds RAgCu₄ (R = Y, Lu) [19]. Thus, these results suggest that this ratio may be the same for isostructural compounds.

5. CONCLUSIONS

The ESR data presented for Gd³⁺ in LuInCu₄ show a g-shift and a Korringa rate characteristic of localized magnetic moment diluted in a simple metallic host. The results allowed us to extract the exchange parameters between the c-e and Gd³⁺. The exchange interaction is found to be wave-vector dependent. The $\langle J_{f\beta}^2(q) \rangle / J_{f\beta}(0)$ ratio for LuInCu₄ is nearly the same as those found for the isomorphous compounds RInCu₄ (R = Y, Yb). Negligible electron-electron exchange interaction was found in LuInCu₄.

Acknowledgements—This work was supported by FAPESP grant No 95/4721-4, São Paulo-SP-Brazil and NSF-INT No 9602829, No 9016241 and No 9501529.

REFERENCES'

- Kojima, K., Nakai, Y., Suzuki, T., Asano, H., Izumi, F., Fujita, T. and Hihara, T., *J. Phys. Soc. Jpn.*, **59**, 1990, 792.
- Rettori, C., Oseroff, S.B., Rao, D., Pagliuso, P.G., Barberis, G.E., Sarrao, J., Fisk, Z. and Hundley, M., *Phys. Rev.*, **B55**, 1997, 1016.
- Feiner, I., Nowik, I., Vaknin, D., Potzel, U., Moser, J., Kalvius, G.M., Wortmann, G., Schneidewind, G., Hilscher, G., Gratz, E., Schmitzer, C., Pillmayr, N., Prasad, K.G., deWaard, D. and Pinto, H., *Phys. Rev.*, **B35**, 1987, 6956; Matsumoto, T., Shimizu, T., Yamada, Y. and Yoshimura, K., *J. Mag. Mag. Mat.*, **104-107**, 1992, 647.
- Kojima, K., Yabuta, H. and Hihara, T., *J. Mag. Mag. Mat.*, **104-107**, 1992, 653.
- Sampathkumar, E.V., Nambudripad, N., Dhar, S.K., Vijayaraghavan, R. and Kuentzler, R., *Phys. Rev.*, **B35**, 1987, 2035.
- Sarrao, J.L., Benton, C.L., Fisk, Z., Lawrence, J.M., Mandrus, D. and Thompson, J.D., Accepted in *Physica B*.
- Bachmann, R., DiSalvo, F.J., Geballe, T.H., Greene, R.I., Howard, R.E., King, C.N., Kivisch, H.C., Lee, K.N., Schwall, R.E., Thomas, H.V. and Zubek, R.B., *Rev. Sci. Instrum.*, **43**, 1972, 205.
- Fehler, G. and Kip, A.F., *Phys. Rev.*, **98**, 1955, 337; Dyson, F.J., *Phys. Rev.*, **98**, 1955, 349.
- Pake, G.E. and Purcell, E.M., *Phys. Rev.*, **74**, 1948, 1184.
- Yosida, K., *Phys. Rev.*, **106**, 1957, 893.
- Korringa, J., *Physica*, **16**, 1950, 601.
- Rettori, C., Kim, H.M., Chock, E.P. and Davidov, D., *Phys. Rev.*, **B10**, 1974, 1826.
- Davidov, D., Maki, K., Orbach, R., Rettori, C. and Chock, E.P., *Solid State Commun.*, **12**, 1973, 621.
- Abragam, A. and Bleaney, B., *EPR of Transition Ions*, Clarendon Press, Oxford, 1970.
- Moriya, T., *J. Phys. Soc. Jpn.*, **18**, 1963, 516.
- Narath, A., *Phys. Rev.*, **163**, 1967, 232.
- Davidov, D., Chelkowski, A., Rettori, C., Orbach, R. and Maple, M.B., *Phys. Rev.*, **B7**, 1973, 1029.
- Barberis, G.E., Davidov, D., Donoso, J.P., Rettori, C., Suassuna, J.F. and Dokter, H.D., *Phys. Rev.*, **B19**, 1979, 5495.
- Pagliuso, P.G., Rettori, C., Oseroff, S.B., Sarrao, J., Fisk, Z., Cornelius, A. and Hundley, M.F., *Phys. Rev. B*, **56**, (in press).

Seção 2.4

2.4 Estudos de RPE de Gd^{3+} no
composto Tipo Rede de Kondo
 YbAgCu_4 e seus compostos de
referência $(\text{Y}, \text{Lu})\text{AgCu}_4$

2.4) Estudos de RPE de Gd³⁺ no composto Tipo Rede de Kondo YbAgCu₄ e seus compostos de referência (Y, Lu)AgCu₄.

PHYSICAL REVIEW B

VOLUME 56, NUMBER 14

1 OCTOBER 1997-II

ESR of Gd³⁺ in the Kondo-lattice compound YbAgCu₄ and its reference compounds RAgCu₄ (R=Y,Lu)

P. G. Pagliuso and C. Rettori

Instituto de Física "Gleb Wataghin," UNICAMP, 13083-970, Campinas-SP, Brazil

S. B. Oseroff

San Diego State University, San Diego, California 92182

J. Sarrao and Z. Fisk

National High Magnetic Field Laboratory, Florida State University, Tallahassee, Florida 32306

A. Cornelius and M. F. Hundley

Los Alamos National Laboratories, Los Alamos, New Mexico 87545

(Received 14 March 1997)

Low-temperature ($T < 30$ K) electron-spin-resonance (ESR) experiments of Gd³⁺ diluted in the Kondo-lattice compound YbAgCu₄ and its reference compounds YAgCu₄ and LuAgCu₄ are interpreted in terms of an enhanced density of states at the Fermi level for the Yb-based compound. The results of susceptibility and ESR (Korringa rate and γ -shift) measurements show negligible electron-electron exchange enhancement for all the studied compounds. The exchange interaction between the Gd³⁺ local moment and the conduction electrons (c-e) is c-e wave vector dependent in all three compounds. [S0163-1829(97)01038-2]

I. INTRODUCTION

Hybridization between localized f -electron and conduction-electron (c-e) states have motivated experimentalists and theoreticians to study the phenomena involving strong electronic correlations.¹ The Ce- and Yb-based compounds are well suited for these studies. The 4f shell of Ce and Yb may contribute with an electron and a hole, respectively, to the conduction band, simplifying the theoretical analysis. The YbAgCu₄ compound of cubic AuBe₃ (C15b, F43m)-type structure,² is particularly appropriate because it has the following Kondo-type properties: (i) a relatively large linear coefficient of specific heat, $\gamma \sim 240$ mJ/mol K^{2,3,4} (ii) a temperature-dependent electrical resistivity characteristic of a Kondo-lattice system,⁵ and (iii)

a temperature-dependent magnetic susceptibility with a maximum at ~ 35 K,³ that can be described by the Bethe-Annan solution of the Crugblin-Schrieffer Hamiltonian.^{3,6,7} The relatively weak interaction between the Yb magnetic moments⁸ makes electron-spin resonance (ESR) of diluted Gd³⁺ in YbAgCu₄ suitable to study the electronic properties of this compound. For comparison, the ESR of Gd³⁺ in the reference compounds of YAgCu₄ and LuAgCu₄ were measured. Complimentary susceptibility and specific-heat experiments were also performed.

In a recent paper we have studied the ESR of Gd³⁺ in the intermediate valence phase ($T \leq T_v \sim 50$ K) of YbInCu₄ and its reference compound YInCu₄.⁸ Those results were interpreted in terms of an enhanced density of states at the Fermi level for the Yb-based compound. The aim of this work is to

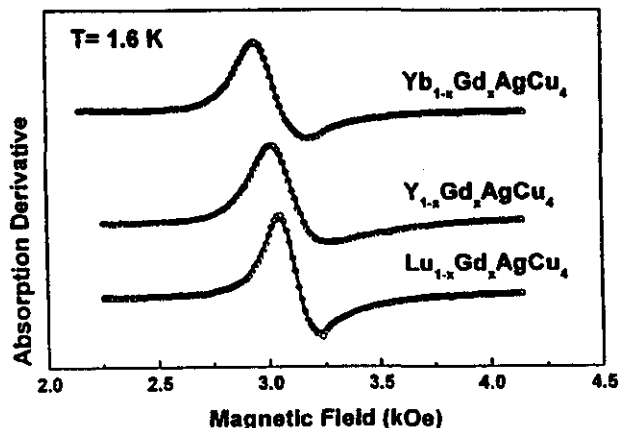


FIG. 1. Low temperature, $T = 1.6$ K, ESR powder spectra for (a) 0.9(2)% of Gd³⁺ in YbAgCu₄, (b) 0.22(2)% of Gd³⁺ in YAgCu₄, and (c) 0.16(2)% of Gd³⁺ in LuAgCu₄. The solid lines are the best fit of the resonance to a Dyson line shape.

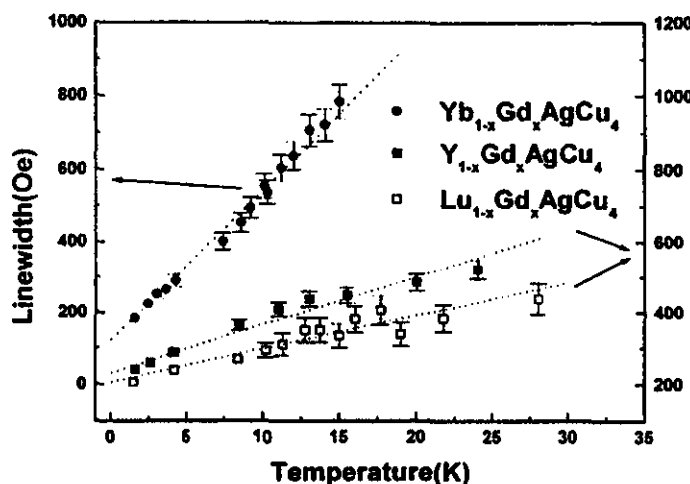


FIG. 2. Temperature dependence of the ESR linewidth for 0.9(2)% of Gd³⁺ in YbAgCu₄, 0.22(2)% of Gd³⁺ in YAgCu₄, and 0.16(2)% of Gd³⁺ in LuAgCu₄. The dashed lines are the best fit to $\Delta H = a + bT$. a and b are given in Table I.

study, also via ESR of Gd³⁺ impurities, the electronic properties of the Kondo-lattice compound YbAgCu₄ and compare it with the intermediate valence compound YbInCu₄.

II. EXPERIMENT

Single crystals of $R_{1-x}Gd_xAgCu_4$ ($R = Yb, Y, Lu$; $0.0008 \leq x \leq 0.009$ nominal) were grown from a flux of excess AgCu by the method described elsewhere.⁹ The crystals were of cubiclike shape with typical sizes of $4 \times 3 \times 1$ mm³. The room-temperature lattice parameters were measured in x-ray powder-diffraction experiments. The ESR experiments have been carried out in a Varian E-line X-band spectrometer, using a liquid-helium tail dewar (1.6–4.15 K) and a helium gas flux (7–30 K) adapted to a room-temperature TE₁₀₂ cavity. For the high-temperature ESR measurements, powdered crystals were used in order to increase the ESR signal-to-noise ratio. The susceptibility measurements have been taken in a Quantum Design dc superconducting quantum interference device magnetometer. Specific-heat measurements were performed in a small-mass calorimeter system that employs a quasiadiabatic thermal relaxation technique.¹⁰ Undoped samples have been used for these measurements and the masses ranged from 45 to 145 mg.

III. EXPERIMENTAL RESULTS

Figure 1 shows the ESR powder spectra of Gd³⁺ diluted in YbAgCu₄, YAgCu₄, and LuAgCu₄ measured at $T = 1.6$ K. Typical Dysonian line shapes¹¹ with $A/B \approx 2.2(2)$ were observed. These line shapes are characteristic of localized magnetic moments in a metallic host with a skin depth

smaller than the size of the sample particles. The g value and linewidth were obtained from the fitting of the resonances to the appropriate admixture of absorption and dispersion.¹² The solid lines, in Fig. 1, are the best fit to the observed resonances.

Figure 2 gives the temperature dependence of the linewidth for the three compounds. The linear dependence of the linewidth was fitted to the expression $\Delta H = a + bT$. Within the accuracy of the measurements, the g values have been found to be temperature independent. The a , b , and g parameters were, within our experimental error and used concentrations, independent of the Gd concentration. Their values are shown in Table I. In single crystals the Gd³⁺ resonance did not show crystal-field features, i.e., fine structure and/or anisotropic linewidth.

Figure 3 shows the magnetic susceptibility, corrected for the compound core diamagnetism, for some of the samples used in our ESR experiments. From the low-temperature tails ($T < 20$ K) the Gd concentrations were estimated and their values are given in Table I. For $T > 20$ K, the temperature dependence of the susceptibility of the $Yb_{1-x}Gd_xAgCu_4$ samples presents similar features to that found in undoped YbAgCu₄.³

Figure 4 shows the specific heat for the $RAgCu_4$ ($R = Yb, Y, Lu$) crystals in the temperature range of $2 K < T < 20$ K. The low-temperature C/T data increase linearly with T^2 as seen in the inset of Fig. 4. The fitting parameters, γ and β , obtained from these data are given in Table I. Notice that our values for γ and β in YbAgCu₄ are significantly different from those found by others.^{3,4} This probably has to do with the high purity of our crystals.⁹ The density of states,

TABLE I. Experimental parameters for Gd: $RAgCu_4$ ($R = Yb, Y, Lu$).

	a Å	a Oe	b Oe/K	c %	γ mJ/mol K ²	β mJ/mol K ⁴
Yb(Gd)AgCu ₄	7.08(1)	2.17(1)	123(15)	0.17(2)	207(6)	0.63(6)
Y(Gd)AgCu ₄	7.20(1)	2.10(1)	227(9)	0.22(2)	11.4(2)	0.46(2)
Lu(Gd)AgCu ₄	7.10(1)	2.09(1)	180(12)	0.16(2)	10.0(2)	0.68(2)

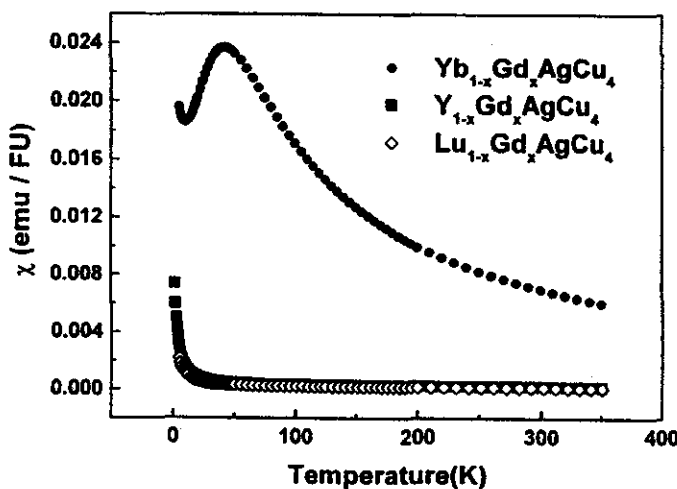


FIG. 3. Temperature dependence of the magnetic susceptibility, measured at 5 kOe, for 0.17% of Gd³⁺ in YbAgCu₄, 0.22% of Gd³⁺ in YAgCu₄, and 0.16% of Gd³⁺ in LuAgCu₄.

$\eta(E_F)$, and the Debye temperatures, θ_D , extracted from these parameters are given in Table II.

Table I summarizes the experimental parameters obtained in this work for the $R\text{AgCu}_4$ ($R = \text{Yb}, \text{Y}, \text{Lu}$) compounds.

IV. ANALYSIS AND DISCUSSION

The exchange interaction, $J_{\text{fx}}S \cdot s$, between a localized 4f electron spin (S) on a solute atom (Gd³⁺) and the free c-c's spin (s) of the host metal, results in a g shift (Knight shift)¹³ and in a thermal line broadening (Korringa relaxation)¹⁴ of the ESR spectra. Conduction electron-electron exchange enhancement^{15,16} and q -dependent exchange interaction, $J_{\text{fx}}(q)$,¹⁷ are often used in the analysis of the ESR data.⁸ $J_{\text{fx}}(q)$ is the Fourier transform of the spatially varying exchange coupling. In this case, and when "bottleneck" and "dynamic" effects are not present, the g shift (Δg) and Korringa rate (b) can be written as¹⁸

$$\Delta g = J_{\text{fx}}(0) \frac{\eta(E_F)}{1 - \alpha} \quad (1)$$

and

$$b = \frac{d(\Delta H)}{dT} = \frac{\pi k}{g \mu_B} \langle J_{\text{fx}}^2(q) \rangle \eta^2(E_F) \frac{K(\alpha)}{(1 - \alpha)^2} \quad (2)$$

where $J_{\text{fx}}(0)$ and $\langle J_{\text{fx}}^2(q) \rangle$ are the effective exchange parameters between the Gd³⁺ local moment and the c-c in the presence of c-c momentum transfer.¹⁷ Under this assumption the Gd³⁺ g shift probes the c-c polarization ($q=0$) and the Korringa rate the c-c momentum transfer ($0 \leq q \leq 2k_F$) averaged over the Fermi surface.¹⁷ $(1 - \alpha)^{-1}$ and $K(\alpha)$ are the Stoner and the Korringa enhancement factors, respectively, due to the electron-electron (c-c) exchange interaction.^{8,19,20} $\eta(E_F)$ is the "bare" density of states for one spin direction at the Fermi level, k is the Boltzmann constant, μ_B is the Bohr magneton, and g is the Gd³⁺ g value.

Equations (1) and (2) are appropriated for the analysis of ESR data of highly diluted rare earths in metallic hosts with appreciable c-c spin-flip scattering, i.e., *unbottleneck* regime. We found in this work that the ESR parameters do not de-

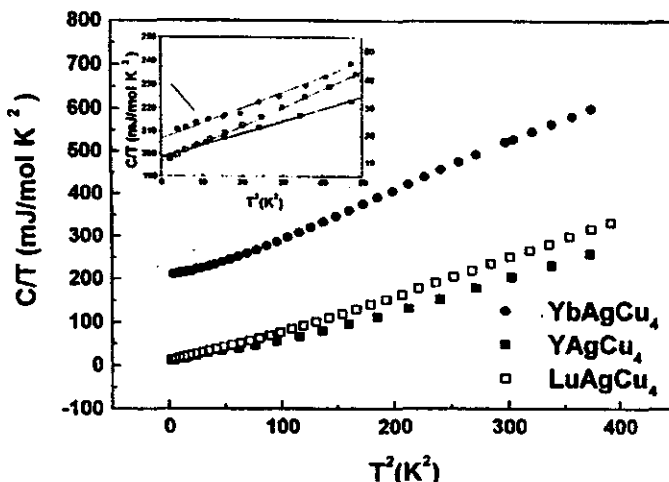


FIG. 4. Specific heat (C/T) as a function of T^2 for $R\text{AgCu}_4$ ($R = \text{Yb}, \text{Y}, \text{Lu}$) compounds. The inset shows the low-temperature T^2 dependence of C/T . The solid line is the best fit to $C/T = \gamma + \beta T^2$. γ and β are given in Table I.

TABLE II. Extracted parameters for Gd:R₂AgCu₄ (R = Yb, Y, Lu).

	$\eta(E_F)$ states/eV mol spin	θ_D K	$J_{fs}(0)$ meV	$\langle J_{fs}^2(q) \rangle^{1/2}$ meV	$K(\alpha)$	α
Yb(Gd)AgCu ₄	44(2)	~264	4.0(3)	0.9(2)	0.9(4)	0.1(4)
Y(Gd)AgCu ₄	2.42(4)	~294	44(5)	11(1)	~1	~0
Lu(Gd)AgCu ₄	2.12(4)	~257	45(5)	10(1)	~1	~0

pend on the Gd³⁺ concentration. Hence, it is expected that the following relation would hold:^{8,18}

$$b = \frac{d(\Delta H)}{dT} = \frac{\pi k}{g \mu_B} \frac{\langle J_{fs}^2(q) \rangle}{J_{fs}(0)} (\Delta g)^2 K(\alpha). \quad (3)$$

In our analysis the contribution from different c-c bands can be neglected, because the measured thermal broadening of the linewidths is much smaller than that expected from the measured *g* shifts.^{21,22}

The electronic contribution to the heat capacity of these compounds yields to the γ values shown in Table I. In a free c-c gas model $\gamma = (2/3) \pi^2 k^2 \eta(E_F)$. Thus, the density of states at the Fermi level, $\eta(E_F)$, can be estimated for the Y- and Lu-based samples (see Table II). From the density of states, the electronic spin susceptibility, $\chi_e = 2\mu_B^2 \eta(E_F)$, can be evaluated. The values calculated are 0.15×10^{-3} and 0.13×10^{-3} cmu/FU for the Y- and Lu-based, respectively. These results are in good agreement with their susceptibility measured at high temperatures (Pauli susceptibility), once corrected for the core diamagnetism (see Fig. 3). Hence, one can assume that c-c exchange enhancement is not important in these compounds, i.e., $\alpha \approx 0$ and $K(\alpha) \approx 1$.^{19,20}

The exchange parameters between the Gd³⁺ local moment and the c-c in R₂AgCu₄ (R = Y, Lu) were estimated using Eq. (3), where we used the *g* value of Gd³⁺ in insulators as a reference, 1.993(2),²³ $\pi k/g \mu_B = 2.34 \times 10^4$ Oe/K, and the values of Δg , *b*, and $\eta(E_F)$ listed in Tables I and II. Table II summarizes the obtained values. Notice that the ratio, $\langle J_{fs}^2(q) \rangle^{1/2}/J_{fs}(0)$, is nearly the same for these isomorphous compounds.

For the analysis of the Gd³⁺ ESR data in YbAgCu₄, we assume that the ratio, $\langle J_{fs}^2(q) \rangle/J_{fs}(0) \approx 0.056(4)$, is the same for YbAgCu₄ and R₂AgCu₄ (R = Y, Lu) compounds. Using for YbAgCu₄ $\Delta g = 0.18(1)$ and $b = 42(2)$ Oe/K from Table I, we calculated $K(\alpha) \approx 0.9(4)$ from Eq. (3). From Refs. 19 and 20 this value corresponds to $\alpha \approx 0.1(4)$, i.e., for YbAgCu₄, the c-c exchange enhancement is also negligible. There is still not a model that includes the c-c exchange interaction for the analysis of the ESR, magnetic susceptibility, and specific-heat data in Kondo-lattice systems.²⁴ Hence, at the moment it is not possible to compare the Stoner factor obtained from ESR and that from transport measurements.²⁵ Thus, the best we can do is to use $\eta(E_F) = 43(2)$ states/eV mol spin, $\alpha \approx 0.1(4)$ (see Table II), and Eqs. (1) and (2) to estimate the exchange parameters, $J_{fs}(0)$ and $\langle J_{fs}^2(q) \rangle^{1/2}$, between Gd³⁺ and the c-c in YbAgCu₄. Those values are given in Table II.

The exchange parameters, $J_{fs}(0)$ and $\langle J_{fs}^2(q) \rangle^{1/2}$ calculated for YbAgCu₄, are both about ten times smaller than

their respective values for the Y- and Lu-based compounds. This may suggest a much higher c-c localization for the Yb than for the Y- and Lu-based compounds. That is consistent with the large density of states associated with a "narrow" 4f band at the Fermi level of the Kondo-lattice compound YbAgCu₄. But a smaller positive exchange parameter, $J_{fs}(0)$, may also suggest a larger covalent (interband mixing) contribution to the exchange parameter in the Yb-based compound.^{17,26} However, due to the oversimplified model used to extract the density of states, $\eta(E_F)$, the values for $J_{fs}(0)$ and $\langle J_{fs}^2(q) \rangle^{1/2}$ obtained for YbAgCu₄ should be taken with extra caution. Collective effects may enhance the density of states,²⁷ $\eta(E_F)$. Thus, our values represent just a lower limit for the exchange parameters.

V. CONCLUSIONS

The large density of states at the Fermi level for the Kondo-lattice compound YbAgCu₄, characteristic of highly correlated electron systems, results in a larger *g* shift and Korringa rate of the Gd³⁺ resonance when compared with the corresponding values of its reference compounds R₂AgCu₄ (R = Y, Lu). The exchange interaction between the localized magnetic moment of Gd³⁺ and the c-c is wave-vector dependent, $J_{fs}(q)$, for all three isomorphous compounds. The exchange parameter, $J_{fs}(0)$, is found to be positive for all of them. As YbAgCu₄ is a Kondo-lattice system, an antiferromagnetic exchange interaction is expected between the localized magnetic moment of Yb³⁺ and the c-c. Hence, we conclude that the exchange interaction with the c-c is atomiclike for Gd³⁺ and covalentlike for Yb³⁺.¹⁷

There is an interesting observation to be made from the results of our previous measurements in the intermediate-valent compound YbInCu₄ (Ref. 8) and the present measurements in the Kondo-lattice compound YbAgCu₄. Both compounds belong to the class of highly correlated electron systems with relatively large γ values, 50(5) and 207(6) mJ/mol K² for YbInCu₄ and YbAgCu₄, respectively. For YbInCu₄ our results suggested a large electron-electron exchange interaction. Instead, for YbAgCu₄ this interaction, within the accuracy of our experiments, seems to be negligible. If so Coqblin-Schrieffer's model for magnetic impurities dissolved in a free c-c metal,^{6,7} could be a good description for the magnetic susceptibility, $\chi(T)$, of YbAgCu₄.³

Finally, as in our earlier work,⁸ the present results show that ESR experiments of Gd³⁺ diluted in metallic hosts with large electronic effective masses may be used to probe the high density of states at the Fermi level of these compounds. However, we should mention that ESR failed to observe this

property in other strongly correlated electron systems.²⁸⁻³¹ Therefore, a model that takes into account the large electronic effective mass, c-c localization, impurity perturbation of the local density of states, and c-c interactions is needed for a realistic analysis of the ESR results.

ACKNOWLEDGMENTS

This work was supported by a FAPESP Grant No. 95/4721-4, São Paulo-SP-Brazil and NSF-DMR Grant Nos. 9117212, 9016241, and 9501529.

-
- ¹See, *Valence Fluctuation in Solids*, edited by L. M. Falicov, W. Hanke, and M. B. Maple (North-Holland, Amsterdam, 1981); *Valence Instabilities*, edited by P. Wachter and H. Boppert (North-Holland, Amsterdam, 1982); *Valence Fluctuation*, edited by E. Müller-Hartmann, B. Roden, and D. Wohleben (North-Holland, Amsterdam, 1984); *Valence Fluctuations*, edited by G. E. Barberis, M. B. Maple, Z. Fisk, H. Zirngiebl, and J. D. Thompson, Phys. Rev. B **35**, 1914 (1987).
- ²K. Kojima, Y. Nakai, T. Suzuki, H. Asano, H. Izumi, T. Fujita, and T. Hihara, J. Phys. Soc. Jpn. **59**, 792 (1990).
- ³C. Rossel, K. N. Yang, M. B. Maple, Z. Fisk, H. Zirngiebl, and J. D. Thompson, Phys. Rev. B **35**, 1914 (1987).
- ⁴Z. Fisk and M. B. Maple, J. Alloys Compd. **183**, 303 (1992).
- ⁵N. Pilimayr, H. Bauer, and K. Yoshimura, J. Magn. Magn. Mater. **104-107**, 639 (1992).
- ⁶V. T. Rajan, Phys. Rev. Lett. **51**, 308 (1983).
- ⁷H. Coqblin and J. R. Schrieffer, Phys. Rev. **185**, 847 (1963).
- ⁸C. Rettori, S. B. Oseroff, D. Rao, P. G. Pagliuso, G. E. Barberis, J. Sarrao, Z. Fisk, and M. Hundley, Phys. Rev. B **55**, 1016 (1997).
- ⁹J. L. Sarrao, C. L. Benton, Z. Fisk, J. M. Lawrence, D. Mandrus, and J. D. Thompson, Physica B **223-224**, 366 (1996); J. L. Sarrao, C. D. Immer, C. L. Benton, Z. Fisk, J. M. Lawrence, M. Mandrus, and J. D. Thompson, Phys. Rev. B **54**, 12207 (1996).
- ¹⁰R. Bachmann, H. J. DiSalvo, T. H. Geballe, R. L. Greene, R. H. Howard, C. N. King, H. C. Kibisch, K. N. Lee, R. E. Schwall, H. V. Thomas, and R. B. Zubek, Rev. Sci. Instrum. **43**, 205 (1972).
- ¹¹G. Feher and A. F. Kip, Phys. Rev. **98**, 337 (1955); H. J. Dyson, *ibid.* **98**, 349 (1955).
- ¹²G. E. Pake and E. M. Purcell, Phys. Rev. **74**, 1184 (1948).
- ¹³K. Yosida, Phys. Rev. **106**, 893 (1957).
- ¹⁴J. Korringa, Physica (Amsterdam) **16**, 601 (1950).
- ¹⁵T. Moriya, J. Phys. Soc. Jpn. **18**, 516 (1963).
- ¹⁶A. Narath, Phys. Rev. **163**, 232 (1967).
- ¹⁷D. Davidov, K. Maki, R. Orbach, C. Rettori, and E. P. Chock, Solid State Commun. **12**, 621 (1973).
- ¹⁸D. Davidov, R. Orbach, C. Rettori, D. Shaltiel, L. J. Tao, and B. Ricks, Phys. Lett. **35A**, 339 (1971); C. Rettori, H. M. Kim, E. P. Chock, and D. Davidov, Phys. Rev. B **10**, 1826 (1974).
- ¹⁹A. Narath and H. T. Weaver, Phys. Rev. **175**, 373 (1968).
- ²⁰R. W. Shaw and W. W. Warren, Phys. Rev. B **3**, 1562 (1971).
- ²¹D. Davidov, A. Chelkowski, C. Rettori, R. Orbach, and M. B. Maple, Phys. Rev. B **7**, 1029 (1973).
- ²²G. E. Barberis, D. Davidov, J. P. Donoso, C. Rettori, J. I. Suassuna, and H. D. Dokter, Phys. Rev. B **19**, 5495 (1979).
- ²³A. Abragam and B. Bleaney, *EPR of Transition Ions* (Clarendon, Oxford, 1970).
- ²⁴P. Schlottmann, in *Theory of Heavy Fermion and Valence Fluctuation*, edited by T. Kasuya and T. Sano (Springer-Verlag, Berlin, 1985), p. 68.
- ²⁵N. Tsujii, J. Ilc, K. Yoshimura, K. Kosuge, H. Michor, K. Kreiner, and G. Hilscher, Phys. Rev. B **55**, 1032 (1997).
- ²⁶R. H. Wilson, A. J. Freeman, and S. Koide, Phys. Rev. B **186**, 625 (1969).
- ²⁷M. A. Continentino, Phys. Rev. B **47**, 11587 (1993).
- ²⁸G. E. Barberis, D. Davidov, C. Rettori, J. P. Donoso, I. Torriani, and F. C. G. Gandra, Phys. Rev. Lett. **45**, 1966 (1980).
- ²⁹H. Schaeffer and B. Bischner, Z. Phys. B **53**, 109 (1983).
- ³⁰H. G. Gandra, S. Schultz, S. B. Oseroff, Z. Fisk, and J. L. Smith, Phys. Rev. Lett. **55**, 2719 (1985).
- ³¹H. G. Gandra, M. J. Pontes, S. Schultz, and S. B. Oseroff, Solid State Commun. **64**, 859 (1987).

Seção 2.5

2.5 Estudos de RPE de Gd³⁺ e Nd³⁺ no composto LuInA₄ (A = Ni, Cu) - (submetido para Phys. Rev. B em 04/01/1999 e resubmetido em 03/05/1999)

2.5) Estudos de RPE de Gd³⁺ e Nd³⁺ no composto LuInA₄ (A = Ni, Cu) - (submetido para Phys. Rev. B em 04-01-1999).

ESR of Gd³⁺ and Nd³⁺ in LuInA₄ (A = Cu, Ni)

P.G. Pagliuso and C. Rettori

*Instituto de Física "Gleb Wataghin", UNICAMP, 13083-970,
Campinas-SP, Brazil.*

J.L. Sarrao, A. Cornelius and M.F. Hundley

Los Alamos National Laboratory, Los Alamos, New Mexico 87545, U.S.A.

Z. Fisk

*National High Magnetic Field Laboratory, Florida State University,
Tallahassee, FL 32306, U.S.A.*

S.B. Oseroff

San Diego State University, San Diego, CA 92182, U.S.A.

Abstract

Low temperature (1.6 K \lesssim T \lesssim 60 K) data of Electron Spin Resonance for Gd³⁺ and Nd³⁺ diluted in LuInA₄ (A = Cu, Ni) compounds are presented. The results are interpreted in terms of a density of states at the Fermi level built up of a single s-band for the Cu-based system and a multiple (s and d) bands for the Ni-based system. The susceptibility and specific heat data show negligible electron-electron exchange enhancement for both compounds. For the Cu-based system the exchange interaction between the rare-earth (Gd³⁺ and Nd³⁺) local moment and the conduction electrons depends on the conduction electron wave-vector.

76.30.Kg, 78.30.-v, 71.20.b, 71.20.Lp

Typeset using REVTEX

I. INTRODUCTION

Electron spin resonance (ESR) of rare-earths (RE) impurities in metallic hosts has been widely used to study: *i*) the exchange interaction between the impurity localized magnetic moment and the conduction-electrons, *ii*) band structures effects of the host metal, *iii*) crystal field effects, *iv*) hyperfine interactions, *v*) highly correlated electron systems, and *vi*) superconductivity of the host metal.¹

The exchange interaction experienced by a RE ion impurity in transition metals^{2,3} and intermetallic compounds^{1,4} varies in sign and magnitude depending on the transition metal ion.¹ Because of the stability of the Gd³⁺ and Nd³⁺ ions 4f shell, the negative exchange integral is not associated with a covalent mixing mechanism.⁵ It has been suggested that a negative effective exchange for RE impurities in some d-band compounds is due to the lack of orthogonality between the 4f and d-orbitals of the neighbor sites.^{5,6} The purpose of this work is to show that ESR of Gd³⁺ and Nd³⁺ in the LuInA₄ (A = Cu,Ni) compounds can provide a means to probe the band structure of these systems. We showed that the ESR data of Gd³⁺ in LuInCu₄⁷ and YInCu₄⁸ could be explained in terms of a single s electronic band contribution to the density of states at the Fermi level. Alternatively, we will show here that the ESR data of Gd³⁺ and Nd³⁺ in LuInNi₄ cannot be explained with a single band. We propose that the contribution of s and d electronic bands to the density of states at the Fermi level is required to explain the data.

II. EXPERIMENT

Single crystals of Lu_{1-x}RE_xInA₄ (RE = Gd,Nd; A= Cu,Ni; 0.0005 ≤ x ≤ 0.005 nominal) of cubic AuBe₅ (C15b, F43m)-type structure⁹ were grown from a flux of excess InCu by the method described elsewhere.¹⁰ The crystals were of cubic-like shape with typical sizes of 4x3 x1 mm³. The ESR experiments were carried out in a Varian E-line and a Bruker ELEXSYS X-band spectrometers, using a liquid-helium tail dewar (1.6 K - 4.15 K) and

a helium gas flux (4 K - 60 K) adapted to a room temperature TE₁₀₂ cavity. Dysonian lineshapes¹¹ with A/B ≈ 2.2(2) were always observed. These lineshapes are characteristic of localized magnetic moments in a metallic host with a skin depth smaller than the size of the samples. In order to increase the ESR signal to noise ratio, powdered crystals were used in most of the ESR measurements. Experiments conducted in single crystals did not show any anisotropy which could be attributed to crystal field effects. Susceptibility measurements were made in a Quantum Design dc SQUID magnetometer. Specific heat measurements were performed in a small-mass calorimeter system that employs a quasi-adiabatic thermal relaxation technique.¹² Samples used here ranged from 50 mg to 150 mg.

III. EXPERIMENTAL RESULTS

Figure 1 shows the specific-heat for the LuInNi₄ compound in the temperature range of 2 K \lesssim T \lesssim 20 K. In the low temperature region, C/T increases linearly with T² as seen in the inset of Figure 1. The fitting parameters, γ and β , obtained from these data are given in Table I. The Debye temperature, θ_D , is given in Table II.

Figure 2 gives the magnetic susceptibility data for some of the Lu_{1-x}RE_xInNi₄ (RE = Gd,Nd) crystals used in ESR experiments, corrected for the compound core-diamagnetism. Using the effective magnetic moments, $\mu_{eff} = 7.94 \mu_B$ and $3.62 \mu_B$ for Gd³⁺ and Nd³⁺ respectively, the Gd and Nd concentrations were estimated and their values are given in Table I. Also, the concentration of the Gd³⁺ natural impurities in LuInNi₄ was estimated and is given in Table I.

Figures 3 and 4 show the ESR powder spectra for $\sim 0.2\%$ of Gd³⁺ and $\sim 0.05\%$ of Nd³⁺ diluted in LuInA₄(A= Cu,Ni) at T = 1.6 K, respectively. The g-values and linewidths were obtained from the fitting of the resonances to the appropriate admixture of absorption and dispersion lorentzian derivatives.¹³ The solid lines are the best fit to the observed resonances and the extracted ESR parameters are presented in Table I. The inset of Figure 4 shows the Nd³⁺ resonances corresponding to the various Nd isotopes and also the Gd³⁺ natural

impurities resonance. The *g*-value for the ¹⁴⁰Nd (*I* = 0) isotope is close to the *g*-value of a Γ_6 Kramers doublet ground state (*g* = 2.667). This indicates that the RE are in a site of cubic symmetry.¹⁴ Table I gives the hyperfine constants ¹⁴³A and ¹⁴⁵A corresponding for the ¹⁴³Nd (*I* = 7/2) and ¹⁴⁵Nd (*I* = 7/2) isotopes, extracted from the measured spectra using the Breit-Rabi formula.¹⁴

Figures 5 and 6 show the temperature dependence of the linewidth for the ~ 0.2 % of Gd³⁺ and ~0.05 % of Nd³⁺ diluted in LuInA₄ (A= Cu,Ni), respectively. The linear dependence of the linewidth was fitted to the expression $\Delta H = a + bT$. Within the accuracy of the measurements, the *g*-values are found to be temperature independent. The *b* and *g* parameters are independent of the Gd and Nd concentration. The values are presented in Table I.

IV. ANALYSIS AND DISCUSSION

Figure 1 shows the electronic contribution to the heat capacity in LuInNi₄. A Sommerfeld coefficient, $\gamma = 19(1)$ mJ/mol-K², was obtained from it. In a free c-e gas model, this coefficient is given by $\gamma = (2/3)\pi^2k^2\eta(E_F)$. Then, for LuInNi₄, we calculate the density of states at the Fermi level $\eta(E_F) = 3.9(1)$ states/eV mol-spin. From this density of states, we estimate an electronic spin susceptibility, $\chi_e = 2\mu_B^2\eta(E_F)$, of $\approx 0.31 \times 10^{-3}$ emu/mol. This value is in good agreement with the susceptibility (corrected for the core-diamagnetism) measured at high temperatures (see dashed line in Figure 2). Thus, as in LuInCu₄,⁷ the Stoner'S factor is negligible. Therefore, we conclude that electron-electron exchange enhancement is not important in LuInNi₄. The exchange interaction, $J_{f,s}$ S.s, between a localized 4*f* electron spin (S) on the RE ion impurities and the c-e's spin (s) of the host metal causes a *g*-shift (Knight shift)¹⁵ and a linear thermal broadening of the ESR lines (Korringa rate).¹⁶ Allowing for a *q*-dependent exchange interaction, $J_{f,s}(q)$,^{8,17} but in the absence of conduction electron-electron exchange enhancement,^{18,19} bottleneck, and dynamic effects, the *g*-shift (Δg) and Korringa rate (*b*) can be written as:²⁰

$$\Delta g = g_i \frac{g_J - 1}{g_J} J_{fs}(0) \eta(E_F), \quad (1)$$

and

$$b = \frac{d(\Delta H)}{dT} = \frac{\pi k}{g_i \mu_B} \left(g_i \frac{g_J - 1}{g_J} \right)^2 \langle J_{fs}^2(q) \rangle \eta^2(E_F), \quad (2)$$

where g_i is the ionic g -factor measured in insulators ($g_i = 1.993^{21}$ for Gd³⁺ and $g_i = 2.63^{22}$ for Nd³⁺), g_J is the Lande g -factor ($g_J = 2$ for Gd³⁺ and $g_J = 8/11$ for Nd³⁺). $J_{fs}(0)$ and $\langle J_{fs}^2(q) \rangle$ are the effective exchange parameters between the RE³⁺ local moment and the conduction-electrons in the presence of conduction-electron momentum transfer.¹⁷ The g -shift measures the conduction-electrons polarization ($q = 0$) and the Korringa rate the conduction-electron momentum transfer ($0 \leq q \leq 2k_F$), averaged over the Fermi surface.¹⁷ Finally, $\eta(E_F)$ is the "bare" density of states for one spin direction at the Fermi surface, k is the Boltzman constant, and μ_B is the Bohr magneton.

In the analysis of the ESR data for Gd³⁺ and Nd³⁺ in LuInCu₄ the contribution from different conduction-electron bands can be neglected because the measured Korringa rates are much smaller than those expected from the measured g -shifts (see Eq. 4 below).^{23,24} Besides, Δg and b were found to be concentration independent i.e., the RE³⁺ spin system is *unbottleneck* in LuInCu₄. Thus, by taking into consideration the q -dependence of the exchange interaction only, Eqs. 1 and 2 may be combined to give:^{8,19}

$$\frac{b}{(\Delta g)^2} = \frac{\pi k}{g_i \mu_B} \frac{\langle J_{fs}^2(q) \rangle}{J_{fs}^2(0)}. \quad (3)$$

In the case of the absence of a q -dependence of the exchange interaction, Eq. 3 reduces to

$$\frac{b}{(\Delta g)^2} = \frac{\pi k}{g_i \mu_B}. \quad (4)$$

From the experimental values given in Table I, we observe that Eq. 4 does not hold for LuInCu₄. Therefore, a q -dependent exchange interaction must be included. Using in Eqs. 1 and 2 the g -factors (g_i and g_J) for Gd³⁺ and Nd³⁺, $\pi k/g_i \mu_B$, and the values of Δg , b , and $\eta(E_F)$ given in Tables I and II, the exchange parameters between the local moment and the

conduction-electrons for Gd³⁺ and Nd³⁺ in LuInCu₄ were estimated. Table II summarizes these parameters. Notice that the ratio, $\langle J_{fs}^2(\mathbf{q}) \rangle^{1/2} / J_{fs}(0)$, is different for each RE³⁺. That suggest a different wave-vector dependence of the exchange interaction for each RE³⁺ in LuInCu₄.

To attempt to explain the ESR data of the Gd³⁺ and Nd³⁺ in LuInNi₄ we propose that contributions from *s* and *d* conduction-electron bands are relevant. The justification for this assertion are: *i*) the measured Korringa rates are much larger than those expected from the measured *g*-shifts (see Eq. 4 and Table I),^{24,25} and *ii*) the *g*-shifts are negative for both Gd³⁺ and Nd³⁺ (see Figures 3 and 4). Notice that in the case of a single band model, due to the $g_J = 8/11$ value for Nd³⁺, the *g*-shifts for Gd³⁺ and Nd³⁺ are of opposite sign (see Eq. 1). In a two, *s* and *d*, band framework, Eqs. 1 and 2 can be re-written as:²⁵

$$\Delta g = g_i \frac{g_J - 1}{g_J} (J_{fs}(0) \eta_s(E_F) + J_{fd}(0) \eta_d(E_F)), \quad (5)$$

and

$$b = \frac{d(\Delta H)}{dT} = \frac{\pi k}{g_i \mu_B} \left(g_i \frac{g_J - 1}{g_J} \right)^2 \left(\langle J_{fs}^2(\mathbf{q}) \rangle \eta_s^2(E_F) + F_d \langle J_{fd}^2(\mathbf{q}) \rangle \eta_d^2(E_F) \right), \quad (6)$$

where F_d is the reduction core polarization factor, which depends of the orbital degeneracy of the *d*-band at the Fermi Level.²⁶ For LuInNi₄ *bottleneck* and *dynamic* effects are not taken into account because the *g*-shifts and Korringa rates are RE concentration independent, and no temperature dependence of the *g*-shift was measured. In the absence of a band structure calculation for LuInNi₄, we argue that its band structure will be similar to that of the isomorphous compound LuInCu₄.²⁷ Besides, we have not seen any magnetism (ESR and Magnetization) that could be associated to Ni²⁺ (3d⁸) in LuInNi₄. Then, we assume that the contribution of the *s*-band is the same in both compounds. The density of states associated to the Sommerfeld coefficient derived above may be written as $\eta_{tot}(E_F) = \eta_s(E_F) + \eta_d(E_F)$. Thus, we can extract the contribution of the *d*-electrons to the density of states at the Fermi level in LuInNi₄. Using $\eta_s(E_F) = 0.42(2)$ states/eV-1mol-spin,⁷ one finds $\eta_d(E_F) = 3.48(12)$ states/eV-1mol-spin. As found for isomorphous compounds,^{7,8,28} we may expect

the ratio $\langle J_{fs}^2(q) \rangle^{1/2} / J_{fs}(0)$ to be the same in the Cu and Ni-based compounds. To the best of our knowledge there is no calculation that take into consideration the q-dependence of exchange interaction between localized spins and *d*-conduction electrons. So, we take J_{fd} to be q-independent ($\langle J_{fd}^2(q) \rangle^{1/2} = J_{fd}(0) = J_{fd}$). If crystal field splitting of the *d* electronic levels (e_g , t_{2g}) at the Fermi level are not included, the F_d factor in Eq. 6 may be shown to be 1/5.²⁶ Having made those assumptions we derived the values for the parameters, $\langle J_{fs}^2(q) \rangle^{1/2}$, $J_{fs}(0)$, and J_{fd} , for Gd³⁺ and Nd³⁺ in LuInNi₄ listed in Table II. Notice that the Gd³⁺ exchange parameters with the *s*-conduction electrons, $J_{fs}(0)$ and $\langle J_{fs}^2(q) \rangle^{1/2}$, are comparable to those found in the isomorphous compounds REInCu₄ (RE = Y, Lu).^{7,8} Therefore, we feel confident about the assumption that the *s*-conduction electrons contribution to the density of states at the Fermi level are about the same in these isomorphous compounds. Nevertheless, this assumption may underestimate $\eta_s(E_F)$, and in turn, overestimates $\eta_d(E_F)$. Therefore, more precisely, the values extracted for the exchange parameters in LuInNi₄ are an upper limit for the exchange with the *s*-electrons and a lower limit for the exchange with the *d*-electrons.

V. CONCLUSIONS

The ESR data of Gd³⁺ and Nd³⁺ in LuInCu₄ are reasonably well described within a framework of: *i*) a single *s*-band model with no electron-electron exchange enhancement, and *ii*) a wave-vector dependent exchange interaction between the 4*f* localized magnetic moment and the conduction-electrons, $J_{fs}(q)$. On the other hand, for the LuInNi₄ compound a two band model, *s* and *d*, with no electron-electron exchange enhancement can explain the ESR results. The *d*-electron band may be thought to be associated with the incomplete Ni electronic 3*d* shell.

It is interesting to note that for the Cu-based compounds, our results show that the q-dependence of the exchange interaction, $J_{fs}(q)$, is RE-dependent. The Nd³⁺ exchange parameters are systematically larger than those of Gd³⁺. That is probably caused by the larger

Nd³⁺ 4f shell radius. Again, the values given for the exchange parameters $\langle J_{fs}^2(q) \rangle^{1/2}$, $J_{fs}(0)$, and J_{fd} for the Ni-based systems should be taken with care.

VI. ACKNOWLEDGMENTS

This work was supported by FAPESP (SP-Brazil) Grants No 95/4721-4, No 95/6177-0, No 97/03065-1, No 98/614-7, CNPq (Brazil) Grant No 910102/96-1, and NSF-DMR No 9705155, No 9527035, No 9501529, and NSF- INT. 9602928. The work in Los Alamos was performed under the auspices of the U.S. Department of Energy..

REFERENCES

- ¹ R.H. Taylor, Adv. Phys. **24**, 681 (1975).
- ² D. Davidov, R. Orbach, C. Rettori, D. Shaltiel, L.J. Tao, and B. Ricks, Solid State Commun. **10**, 451 (1972); R.A.B. Devine, D. Shaltiel, J.N. Moret, W. Zingg, and M. Peter, Solid State Commun. **11**, 525 (1972).
- ³ G. Koopman, K. Baberschke, and S. Hufner, Phys. Lett. A **50**, 407 (1975).
- ⁴ G.E. Barberis, D. Davidov, J.P. Donoso, F.G. Gandra, C. Rettori, and J.F. Suassuna, Solid State Commun. **28**, 427 (1978).
- ⁵ D. Davidov, R. Orbach, C. Rettori, D. Shaltiel, L.J. Tao, and B. Ricks, Phys. Lett. A **37**, 361 (1971).
- ⁶ G.E. Barberis, D. Davidov, J.P. Donoso, C. Rettori, and J.F. Suassuna, and H.D. Dokter, Phys. Rev. B**19**, 5495 (1979); A. Troper and A.A. Gomes, Phys. Rev. B**34**, 6487 (1986).
- ⁷ P.G. Pagliuso, C. Rettori, S.B. Oseroff, J. Sarrao, Z. Fisk, A. Cornelius, and M.F. Hundley, Solid State Commun. **104**, 223 (1997).
- ⁸ C. Rettori, S.B. Oseroff, D. Rao, P.G. Pagliuso, G.E. Barberis, J. Sarrao, Z. Fisk, and M. Hundley, Phys. Rev. B**55**, 1016 (1997).
- ⁹ K. Kojima, Y. Nakai, T. Suzuki, H. Asano, F. Izumi, T. Fujita, and T. Hihara, J. Phys. Soc. Jpn. **59**, 792 (1990).
- ¹⁰ J.L. Sarrao, C.L. Benton, Z. Fisk, J.M. Lawrence, D. Mandrus, and J.D. Thompson, Physica B**223 - 224**, 366 (1996).
- ¹¹ G. Feher and A.F. Kip, Phys. Rev. **98**, 337 (1955); F.J. Dyson, Phys. Rev. **98**, 349 (1955).
- ¹² R. Bachmann, F.J. DiSalvo, T.H. Geballe, R.L. Greene, R.E. Howard, C.N. King, H.C. Kivisch, K.N. Lee, R.E. Schwall, H.V. Thomas, and R.B. Zubek, Rev. Sci. Instrum. **43**, 205 (1972).

- ¹³ G.E. Pake and E.M. Purcell, Phys. Rev. **74**, 1184 (1948).
- ¹⁴ L.J. Tao, D. Davidov, R. Orbach, and E.P. Chock, Phys. Rev. B **4**, 5 (1971).
- ¹⁵ K. Yosida, Phys. Rev. **106**, 893 (1957).
- ¹⁶ J. Korringa, Physica **16**, 601 (1950).
- ¹⁷ D. Davidov, K. Maki, R. Orbach, C. Rettori, and E.P. Chock, Solid State Commun. **12**, 621 (1973).
- ¹⁸ T. Moriya, J. Phys. Soc. Jpn. **18**, 516 (1963).
- ¹⁹ A. Narath, Phys. Rev. **163**, 232 (1967).
- ²⁰ D. Davidov, R. Orbach, C. Rettori, D. Shaltiel, L.J. Tao, and B. Ricks, Phys. Letters **35A**, 339 (1971); C. Rettori, H.M. Kim, E.P. Chock, and D. Davidov, Phys. Rev. B **10**, 1826 (1974).
- ²¹ A. Abragam and B. Bleaney, *EPR of Transitions Ions* (Clarendon, Oxford, 1970).
- ²² P.G. Pagliuso, C. Rettori, S.B. Oseroff, M. Torelli, G. B. Martins, Z. Fisk, J. Sarrao, M.F. Hundley and A. Cornelius, submitted to Phys. Rev. B.
- ²³ R.W. Shaw and W.W. Warren, Phys. Rev. B **3**, 1562 (1971).
- ²⁴ D. Davidov, A. Chelkowski, C. Rettori, R. Orbach, and M. B. Maple, Phys. Rev. B **7**, 1029 (1973).
- ²⁵ D. Davidov, R. Orbach, C. Rettori, L.J. Tao, and B. Ricks, Phys. Lett. A **40**, 269 (1972).
G.E. Barberis, D. Davidov, J.P. Donoso, C. Rettori, J.F. Suasuna, and H.D. Dokter, Phys. Rev. B **19**, 5495 (1979).
- ²⁶ Y. Yafet and V. Jaccarino, Phys. Rev. **133**, 1630 (1964).
- ²⁷ K. Takegahara and T. Kasuya, J. Phys. Soc. Jpn. **59**, 3299 (1990).

²⁸ P.G. Pagliuso, C. Rettori, S.B. Oseroff, J. Sarrao, Z. Fisk, A. Cornelius, and M.F. Hundley, Phys. Rev. B56, 8933 (1997).

FIGURES

FIG. 1. Specific heat (C/T) as a function of T² for LuInNi₄. The inset shows the low temperature T² dependence of C/T. The dashed line is the best fit to C/T = $\gamma + \beta T^2$. The parameters γ and β are given in Table I.

FIG. 2. Temperature dependence of the measured magnetic susceptibility at 10 kOe, for 0.16(5) % of Gd³⁺ and 0.06(2) % of Nd³⁺ in LuInNi₄, 0.03(2) % of Nd³⁺ in LuInCu₄ and pure LuInNi₄. The dashed line is the calculated Pauli susceptibility χ_0 , with $\eta(E_F) = 3.9(1)$ states/eV mol-spin for LuInNi₄.

FIG. 3. ESR powder spectra of ~ 0.2 % Gd³⁺ in LuInCu₄ and LuInNi₄ at T = 1.6 K. The solid lines are the best fit of the resonance to a Dyson lineshape.

FIG. 4. ESR powder spectra of ~ 0.05 % Nd³⁺ in LuInCu₄ and LuInNi₄ at T = 1.6 K. The solid lines are the best fit of the resonance to a Dyson lineshape. The inset shows the resonances for the various Nd³⁺ isotopes and the resonance of natural impurities of Gd³⁺.

FIG. 5. Temperature dependence of the ESR linewidth for ~ 0.2 % of Gd³⁺ in LuInCu₄ and LuInNi₄. The dashed lines are the best fit to $\Delta H = a + bT$. Values of a and b are given in Table I.

FIG. 6. Temperature dependence of the ESR linewidth for ~ 0.05 % of Nd³⁺ in LuInCu₄ and LuInNi₄. The dashed lines are the best fit to $\Delta H = a + bT$. Values of a and b are given in Table I.

TABLES

TABLE I. Experimental parameters for (Gd,Nd):LuInA₄(A = Cu, Ni)

<i>g</i>	<i>a</i>	<i>b</i>	<i>c</i>	γ	β	¹⁴³ A	¹⁴⁵ A
	Oe	Oe/K	%	$\frac{mJ}{mol \cdot K^4}$	$\frac{mJ}{mol \cdot K^4}$	Oe	Oe
LuInCu ₄				2.03(3) ^a	0.41(2) ^a		
LuInNi ₄				0.009(7) ^b	19(1)	0.46(2)	
Lu(Gd)InCu ₄	2.003(3) ^a	41(2) ^a	0.9(1)	≈ 0.2			
Lu(Gd)InNi ₄	1.980(2)	30(5)	6.0(8)	0.16(5)			
Lu(Nd)InCu ₄	2.582(4)	52(5)	3.5(5)	0.06(5) and ~ 0.005 ^b		215(10)	130(8)
Lu(Nd)InNi ₄	2.61(2)	93(10)	30(6)	0.03(5)			

^asee ref. 7^bGd³⁺ natural impurities concentrationTABLE II. Derived parameters for (Gd,Nd):LuInA₄(A = Cu, Ni)

	$\eta(E_F)$ <small>states eV mol-spin</small>	θ_D K	$J_{fs}(0)$ meV	$\langle J_{fs}^2(q) \rangle^{1/2}$ meV	J_{fd} meV
LuInCu ₄	0.42(2) ^a	≈ 305 ^a			
LuInNi ₄	3.9(1)	≈ 295			
Lu(Gd)InCu ₄			24(6) ^a	15(4) ^a	
Lu(Gd)InNi ₄			37(10)	23(8)	- 8(3)
Lu(Nd)InCu ₄			115(40)	35(8)	
Lu(Nd)InNi ₄			215(70)	65(20)	- 20(8)

^asee ref. 7

TABLES

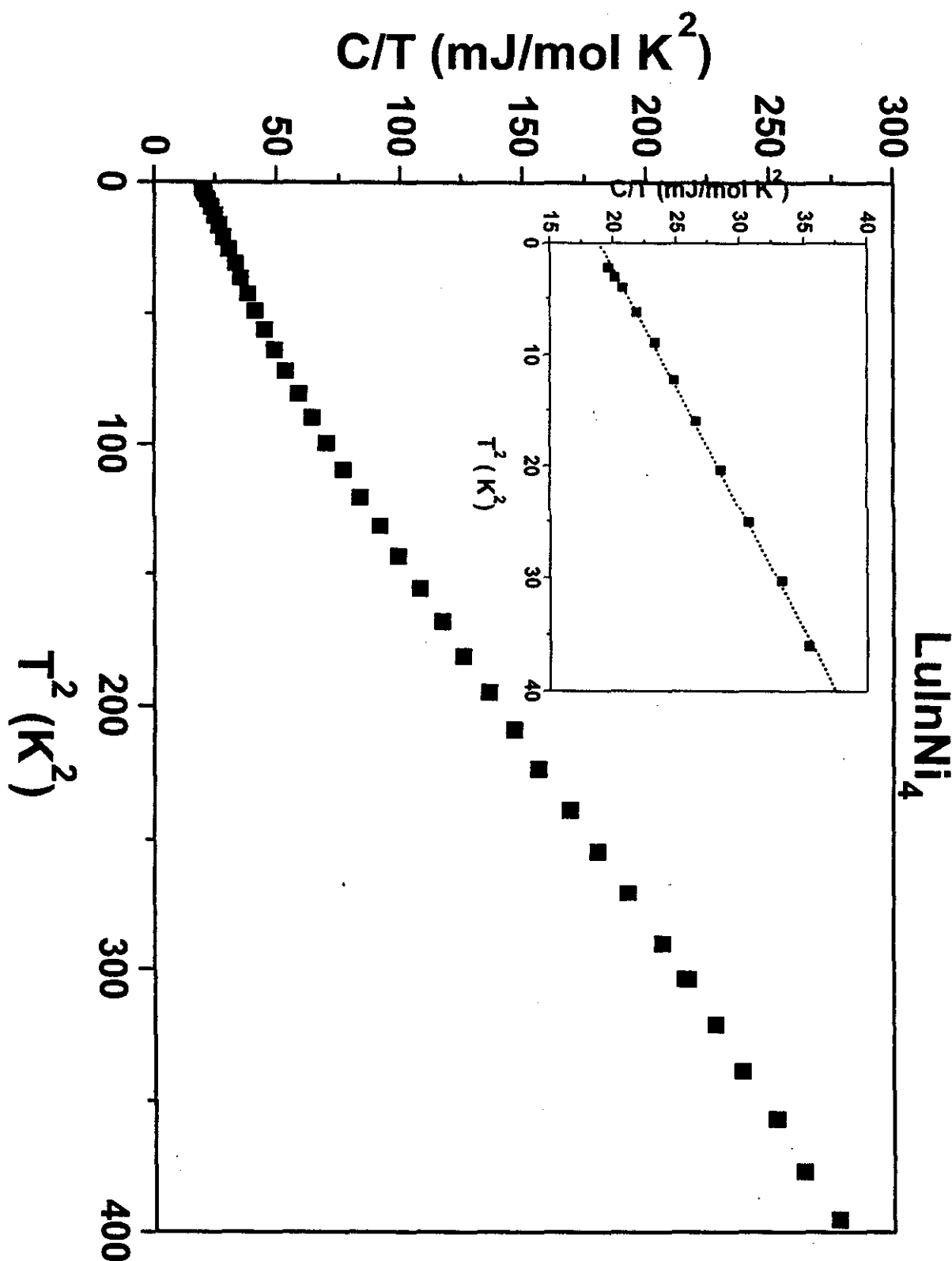
TABLE I. Experimental parameters for (Gd,Nd):LuInA₄(A = Cu, Ni)

<i>g</i>	<i>a</i>	<i>b</i>	<i>c</i>	γ	β	¹⁴³ A	¹⁴⁵ A
	Oe	Oe/K	%	$\frac{\text{mJ}}{\text{mol}\cdot\text{K}^3}$	$\frac{\text{mJ}}{\text{mol}\cdot\text{K}^4}$	Oe	Oe
LuInCu ₄				2.03(3) ^a	0.41(2) ^a		
LuInNi ₄				0.009(7) ^b	19(1)	0.46(2)	
Lu(Gd)InCu ₄	2.003(3) ^a	41(2) ^a	0.9(1)	≈ 0.2			
Lu(Gd)InNi ₄	1.980(2)	30(5)	6.0(8)	0.16(5)			
Lu(Nd)InCu ₄	2.582(4)	52(5)	3.5(5)	0.06(5) and ~ 0.005 ^b		215(10)	130(8)
Lu(Nd)InNi ₄	2.61(2)	93(10)	30(6)	0.03(5)			

^asee ref. 7^bGd³⁺ natural impurities concentrationTABLE II. Derived parameters for (Gd,Nd):LuInA₄(A = Cu, Ni)

	$\eta(E_F)$	θ_D	$J_{fs}(0)$	$< J_{fs}^2(\mathbf{q}) >^{1/2}$	J_{fd}
	$\frac{\text{states}}{\text{eV mol-spin}}$	K	meV	meV	meV
LuInCu ₄	0.42(2) ^a	≈ 305 ^a			
LuInNi ₄	3.9(1)	≈ 295			
Lu(Gd)InCu ₄			24(6) ^a	15(4) ^a	
Lu(Gd)InNi ₄			37(10)	23(8)	- 8(3)
Lu(Nd)InCu ₄			115(40)	35(8)	
Lu(Nd)InNi ₄			215(70)	65(20)	- 20(8)

^asee ref. 7



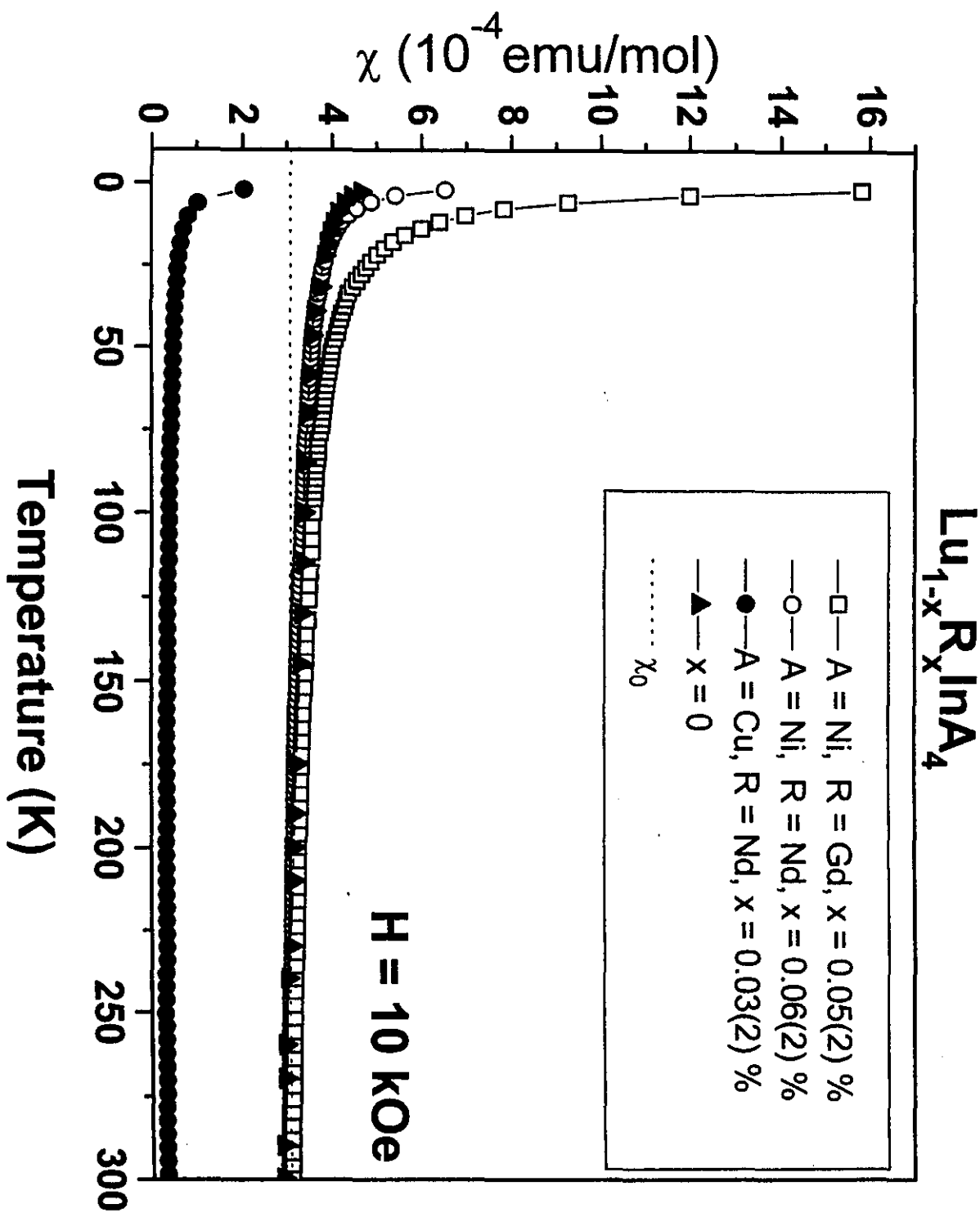


Figura 2

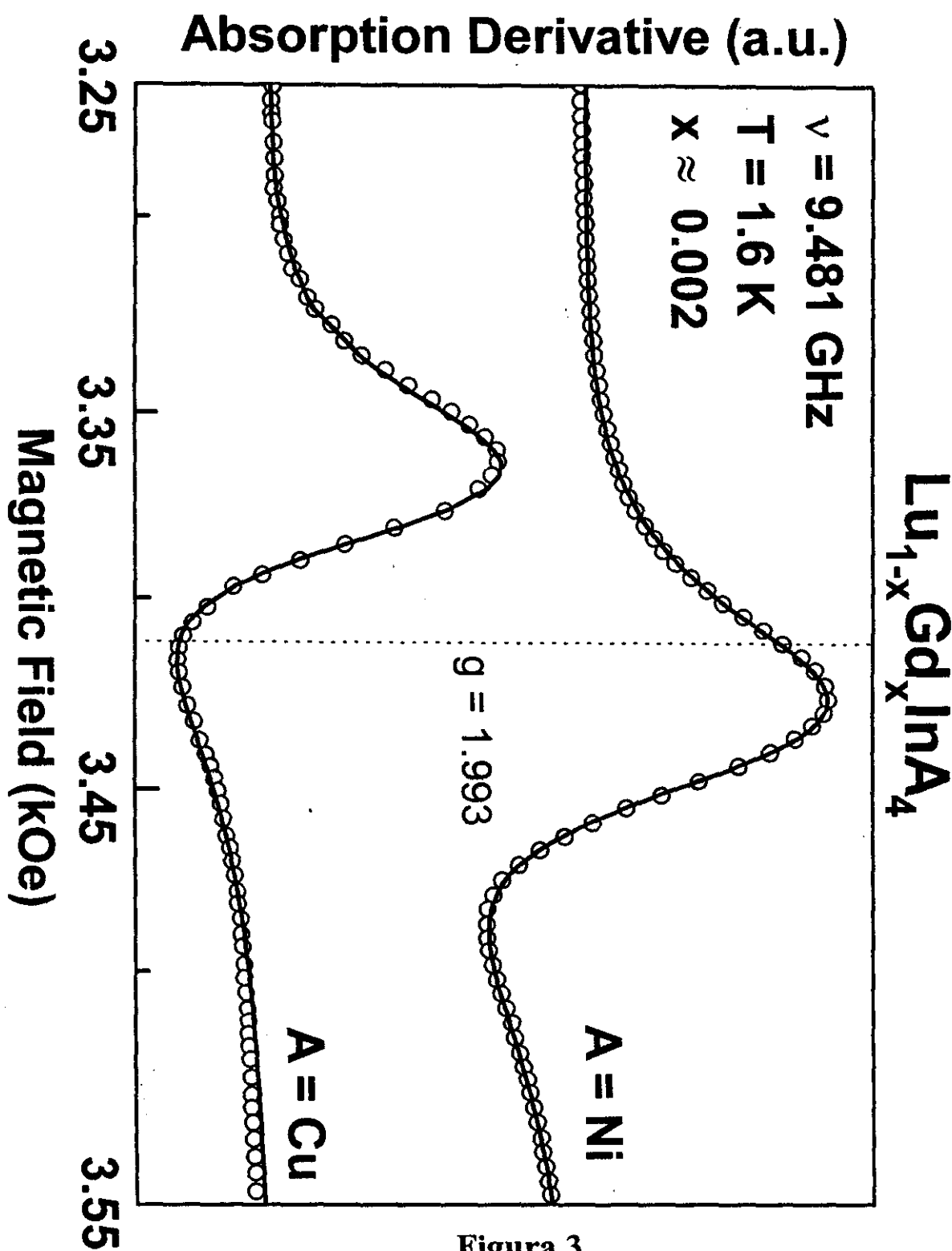


Figura 3

Absorption Derivative (a.u.)

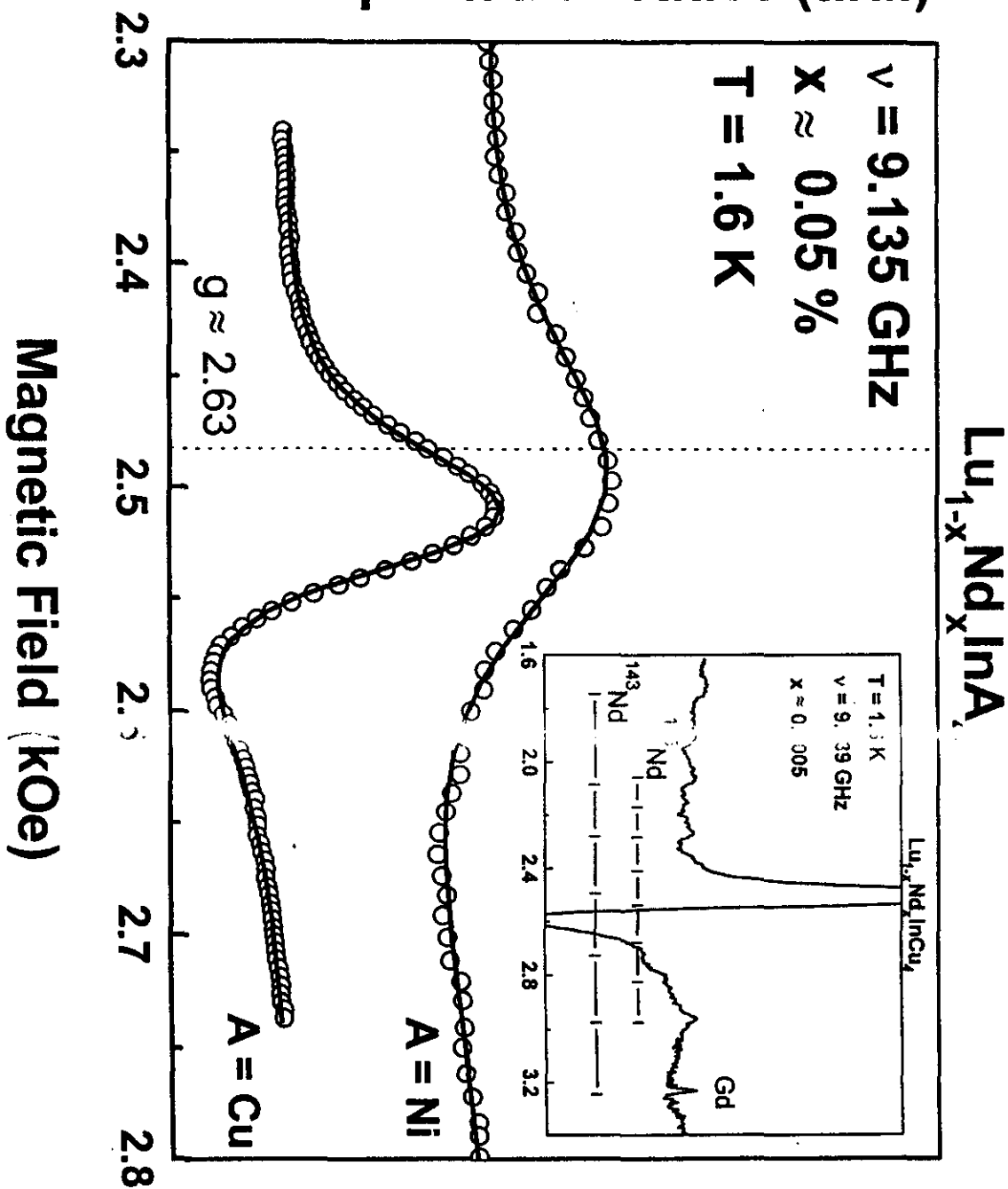


Figura 4

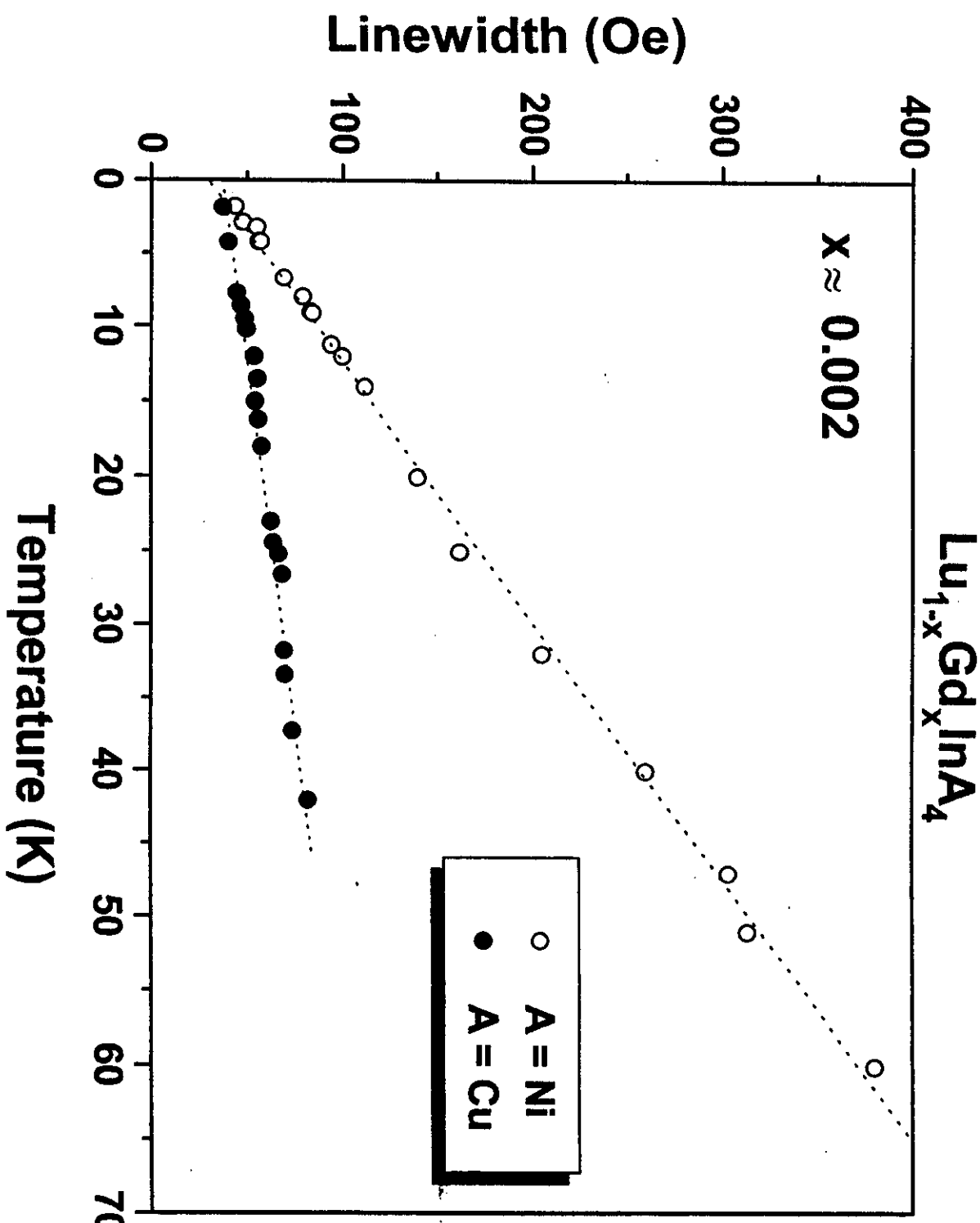


Figura 5

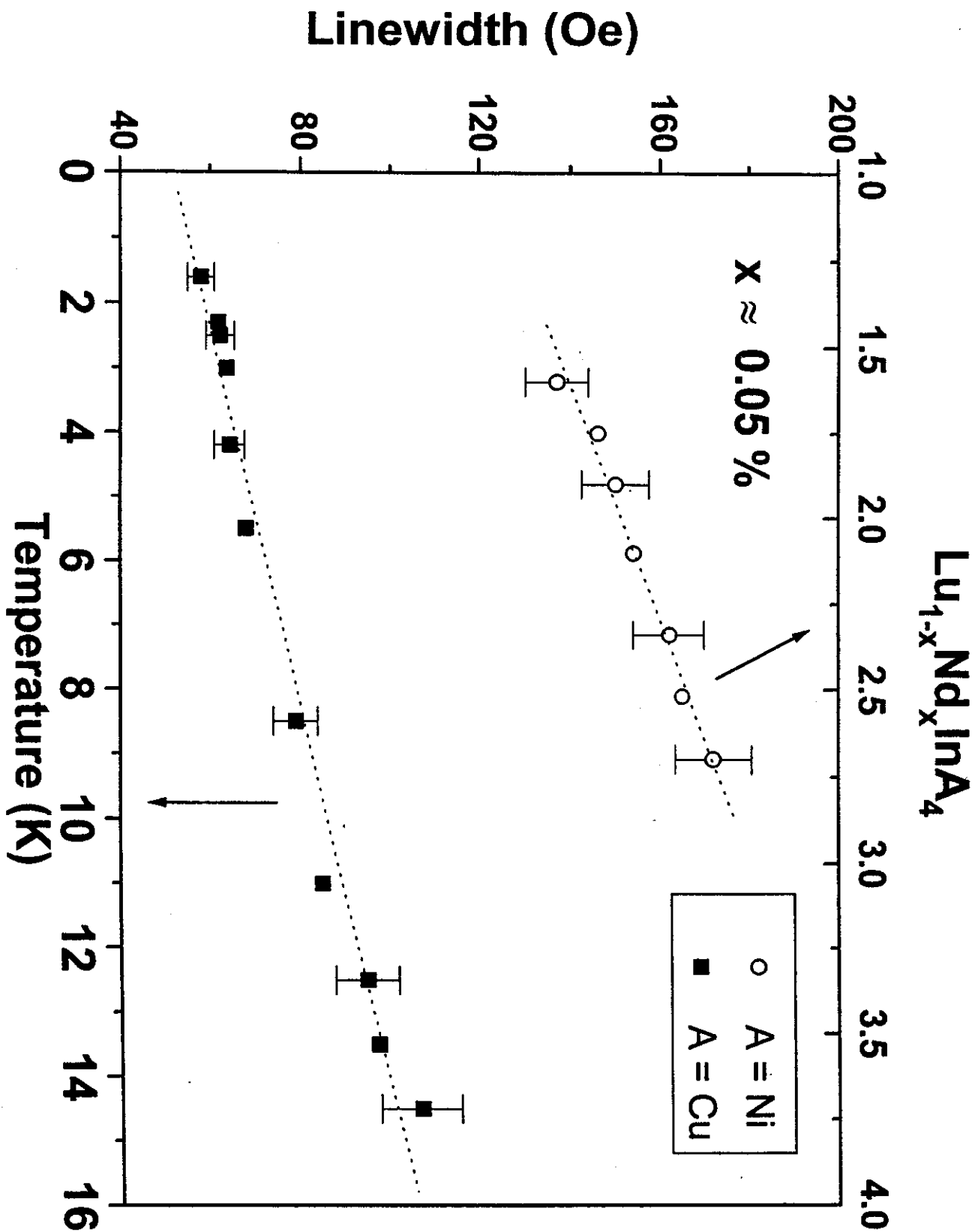


Figura 6

Seção 2.6

2.6 Estudos de Efeitos de Campo
Cristalino no composto
semicondutor de gap pequeno
Yb_{1-x}Pt - (aceito para publicação na
Phys. Rev. B em 07/04//1999)

2.6) Estudos de Efeitos de Campo Cristalino no composto semicondutor de gap pequeno YBiPt (artigo aceito para publicação na Phys. Rev. B em 07/04/1999).

Crystal field study in rare-earth doped semiconducting YBiPt.

P.G. Pagliuso and C. Rettori

Instituto de Física "Gleb Wataghin", UNICAMP, 13083-970, Campinas-SP, Brazil.

M. E. Torelli, G.B. Martins, and Z. Fisk

NIIMFL, Florida State University, Tallahassee, FL 32306, U.S.A.

J. L. Sarrao and M.F. Hundley

Los Alamos National Laboratories, Los Alamos, New Mexico 87545, U.S.A.

S.B. Oseroff

San Diego State University, San Diego, CA 92182, U.S.A.

Abstract

Electron spin resonance (ESR) and magnetic susceptibility experiments in the rare-earth ($R = Nd$, Er , and Yb) doped cubic semiconducting $YBiPt$, allow estimates of the fourth (A_4) and sixth (A_6) order crystal field parameters for this compound. It is found that these parameters are of the same order for all the R studied. On the other hand, no crystal field effects were found for the Gd^{3+} doped single crystal system. Consistent with the small gap semiconducting character of the $YBiPt$ intermetallic compound, a Dysonian ESR lineshape with no g-shift and Korringa broadening was observed.
76.30.Kg, 76.30.-v, 71.20.Ip, 76.90.+d

Typeset using REVTeX

I. INTRODUCTION

The series of intermetallic compounds $RBiPt$ (R = rare earths Nd-Lu) have recently attracted great attention due to their interesting properties.¹ Most of these materials are narrow gap semiconductors ($\Delta = 0.1 - 0.01$ eV) with a gradual evolution towards semi-metallic behavior as R is varied through the rare-earth series.² $YbBiPt$ is the heavy fermion system with the largest linear specific heat coefficient, $\gamma = 8$ J/mole K.² The $RBiPt$ series forms in the cubic $AgAsMg$ structure which can be viewed as three face-centered sublattices placed at $(0, 0, 0)$, $(1/4, 1/4, 1/4)$, and $(3/4, 3/4, 3/4)$. In this series, the rare-earths order antiferromagnetically (T_N) below 9 K and present negative paramagnetic temperatures $|\theta| \lesssim 44$ K.^{2,3} The systematic change from semiconducting, for the light R , to metallic compounds, for the heavier R , is attributed to the decrease in the unit cell volume as the R series is traversed.^{2,3} Hence, it is expected that the strength of the crystal field potential plays an important role on the physical properties of these materials. The $YBiPt$ compound belongs to this family and shows a semiconducting behavior with a lattice parameter close to that of the Tb-based compound, i.e., near the middle of the R series.^{2,3}

This work aims to study the crystal field effects (CFE) in the $Y_{1-x}R_xBiPt$ ($R = Nd, Gd, Er, Yb$, and $0.002 \lesssim x \lesssim 0.10$) compounds. By means of ESR and magnetic susceptibility experiments, it was possible to estimate the fourth (A_4) and sixth (A_6) order cubic crystal field parameters (CFP) in the $Y_{1-x}R_xBiPt$ ($R = Nd, Er, Yb$, and $0.002 \lesssim x \lesssim 0.10$) systems. We found that the overall crystal field splitting is of the order of 100 - 200 K, of the same magnitude as the semiconducting gap (Δ) of these materials. In a previous report on ESR of Er^{3+} in $YBiPt$, we extracted the CFP from the analysis of the ESR spectra of the $Er^{3+} \Gamma_8^{(3)}$ ground state.⁴ The CFP reported are in agreement with the values obtained in this work.

II. EXPERIMENT

Single crystalline samples of the $Y_{1-x}R_xBiPt$ ($R = Nd, Gd, Er, Yb$, and $0.002 \lesssim x \lesssim 0.10$) compounds were grown from the melt in Bi flux as described previously.² Typical crystal sizes were $2x2x2$ mm³. The structure and phase purity were checked by x-ray powder diffraction and the crystals orientation determined by the usual Laue method. The ESR experiments were carried out in conventional Varian and Bruker ESR spectrometers using a TE₁₀₂ room temperature cavity. The sample temperature was varied using a helium gas flux temperature controller and a quartz tail dewar for liquid helium bath experiments. To increase the ESR signal to noise ratio, the temperature dependence of the spectra was taken in powdered samples. In order to look for anisotropic effects, single crystalline samples were used. Magnetization measurements have been taken in a Quantum Design dc SQUID MPMS-5 magnetometer. Specific heat measurements were performed in a small-mass calorimeter system that employs a quasi-adiabatic thermal relaxation technique.⁵ Samples employed ranged in mass from 50 mg to 150 mg.

III. RESULTS AND ANALYSIS

Figure 1 shows the temperature dependence of the specific heat of YBiPt. A linear fit of the data to C/T vs T^2 yields a very small Sommerfeld coefficient ($\gamma \lesssim 0.1$ mJ/mole K). Therefore, the electronic contribution to the heat capacity in this compound is negligible, i.e., the density of states at the Fermi level is very small.

Figure 2 shows the temperature dependence of the susceptibility of $Y_{1-x}Gd_xBiPt$ ($x = 0.002$, nominal concentration and $x = 0$) single crystals measured at $H = 0.5$ T. The data, for the Gd-doped samples, corrected for the core diamagnetism, was fitted to a Curie-Weiss law. Assuming $7.94 \mu_B/Gd$, the Gd concentration was estimated to be $\approx 0.21\%$, close to the nominal value.

Figure 3 shows the Gd^{3+} ESR powder spectra observed in $Y_{1-x}Gd_xBiPt$ at $T = 280$ K and

$T = 7$ K for $x \approx 0.002$. The resonance shows the usual Dysonian-lineshape,⁶ characteristic of metallic particles of dimensions larger than the skin depth. The continuous lines in Figure 3 are the best fit of the experimental spectra to a lorentzian admixture of absorption and dispersion derivatives.⁷ From these fits, the linewidth ΔH , and g -value of the resonances are obtained. Several samples of Gd concentrations, between 0.2% to 0.5%, were measured. The temperature dependence of the Gd^{3+} ESR linewidth was fitted to the formula, $\Delta H = a + b T$. Within the accuracy of the measurements, b and the g -value were found to be concentration independent. The residual linewidth, a , increases with the concentration of Gd. The g -value was found to be temperature independent in all cases. Table I gives the experimental parameters obtained for the most diluted samples.

The very small value found for $b \lesssim 0.05$ Oe/K and a g -value close to those in insulators ($g = 1.993(5)$) indicates that the Gd^{3+} localized magnetic moment is basically not coupled to the conduction electrons.⁸ This is expected because *i*) electronic structure calculations for $YBiPt$ show a gap of about 0.08 eV at the Fermi level³ and *ii*) from the specific heat measurements (see Figure 1) a very small density of states at the Fermi level is derived ($\eta(E_F) \lesssim 0.02$ states/eV mol spin).

ESR experiments in single crystals of $Y_{1-x}Gd_xBiPt$ did not show CFE at any temperature, neither a splitting of the line nor a linewidth anisotropy. Since the measured linewidth at 1.6 K was found to be $\Delta H \approx 40$ Oe, an upper limit for the fourth-order CFP, $|b_4|$, can be estimated, $\lesssim 1$ Oe. That is consistent with the trends already observed in low carrier density metallic pnictides⁹ and narrow gap semiconductors,¹⁰ where the b and b_4 parameters are small.

Figure 4 presents the Nd^{3+} ESR powder spectra observed in $Y_{1-x}Nd_xBiPt$ at $T = 4.2$ K for $x \approx 0.002$. The spectra show a main line corresponding to the $^{140}Nd^{3+}$ ($I = 0$) isotope and the hyperfine lines due to the $^{143}Nd^{3+}$ ($I = 7/2$) and $^{145}Nd^{3+}$ ($I = 7/2$) isotopes. The small line seen at 3400 Oe is associated to natural impurities of Gd^{3+} , probably present in Y. The positions of the hyperfines satellites were determined experimentally by taking the second derivative of the spectra. Table I gives the hyperfine constants $A(^{143}Nd)$ and

$A(^{145}\text{Nd})$ corresponding to the ^{143}Nd and ^{145}Nd isotopes as extracted from the observed spectra using the Breit-Rabi formula.¹¹ The g-value and hyperfine constants given in Table I indicate that the Nd^{3+} ion is in a cubic site environment and that its ground state is a Γ_6 Kramers doublet.¹² These results were found to be concentration independent in the range $0.002 \lesssim x \lesssim 0.10$. Thus, we may neglect the exchange coupling between the rare-earths in the analysis of the susceptibility data. Within the accuracy of our measurements the linewidth and g-value were temperature independent. That is consistent with the ESR results obtained for Gd^{3+} in YBiPt.

It is reasonable to assume that the cubic CFP, A_4 and A_6 , at the R site in $Y_{1-x}R_xBiPt$ ($R = \text{Yb}, \text{Nd}, \text{Er}$) would not be strongly affected by the R impurities. Therefore, the ratio A_4/A_6 should remain basically the same for all R. The analysis of ESR data for the Er^{3+} in YBiPt,⁴ show a $\Gamma_8^{(3)}$ ground state with Lea, Leask, and Wolf (LLW)¹³ parameters, $x = 0.271$ and $W = -0.17$ K. Taking into account the ratios $\langle r^4 \rangle / \langle r^6 \rangle$ for Er^{3+} , Yb^{3+} and Nd^{3+} ,¹⁴ values of $x \approx 0.69$ for Yb^{3+} and $x \approx 0.30$ for Nd^{3+} in YBiPt are obtained. From which a Γ_6 for Nd^{3+} and a Γ_7 for Yb^{3+} as ground states are predicted. The Γ_6 ground state for Nd^{3+} is consistent with ESR data reported here (see Figure 4).

Figures 5 and 6 show the temperature and field dependence of the inverse magnetic susceptibility, $\chi^{-1}(T, H = 1 \text{ T}, 5 \text{ T}) - \chi_{\infty}^{-1}$, for the $Y_{0.9}Yb_{0.1}BiPt$ and $Y_{0.9}Nd_{0.1}BiPt$ single crystals. χ_{∞}^{-1} is the free ion value of the inverse susceptibility shown in the insets of these figures. Assuming the nominal concentration for the Yb^{3+} and Nd^{3+} doped samples, the expected high temperature limit of the Curie law is obtained, $\mu_{eff} = 4.5(2) \mu_B$ and $\mu_{eff} = 3.65(20) \mu_B$ for Yb^{3+} and Nd^{3+} , respectively. The solid lines are the best fit to the data using the Hamiltonian

$$\vec{H} = B_4 [O_4^0 + 5O_4^4] + B_6 [O_6^0 - 21O_6^4] + g_J \mu_B \vec{H} \cdot \vec{J} \quad (1)$$

that includes the cubic crystal field and Zeeman terms. The B_n and O_n^m are the fourth and sixth order CFP and Stevens equivalent operators, respectively. $B_n = A_n \langle r^n \rangle \theta_n$, g_J is the Landé factor and μ_B is the Bohr magneton.¹³ Diagonalizing numerically the Hamiltonian

we get the eigenvalues E_n and corresponding eigenfunctions that can be written as

$$|\phi_n\rangle = \sum_{M=-J}^J C_M^n |JM\rangle \quad (2)$$

where the $|JM\rangle$ expand the manifold of angular momentum J . Hence, the magnetic susceptibility is given by

$$\chi = \frac{g_J \mu_B \sum_n \exp(-\frac{E_n}{kT}) \sum_{M=-J}^J |C_M^n|^2 M}{H \cdot \sum_n \exp(-\frac{E_n}{kT})}. \quad (3)$$

Defining the LLW parameters x and W by the equations

$$B_4 F(4) = Wx \quad (4)$$

$$B_6 F(6) = W(1 - |x|) \quad (5)$$

where $F(4)$ and $F(6)$ are scaling parameters appropriate for each J value, we perform a least squares fitting of the susceptibility leaving x and W as adjustable parameters. The fittings for Yb³⁺ in YBiPt lead to the LLW parameters, $x = -0.61(5)$ and $W = -3.9(4)$. These parameters predict a Γ_7 ground state, a Γ_8 first excited state at 6(2) K, and a Γ_6 second excited state at 88(10) K (see Figure 5). We did not observe the ESR line expected for the Kramer doublet Γ_7 ground state for Yb³⁺. A possible explanation for it is that the YbBiPt is a heavy fermion with a semi-metallic conductivity, thus the large coupling with conduction band should induce a large Korring-like relaxation, even for rather low density of states in the Yb-doped YBiPt sample. Also, the proximity of the anisotropic Γ_8 first excited state at 6(2) K may contribute to a strong broadening of the resonance line. For Nd³⁺ in YBiPt, the fits lead to the LLW parameters, $x = 0.15(5)$ and $W = 2.0(5)$. From which a Γ_6 ground state, a Γ_8 first excited state at 53(10) K, and a Γ_6 second excited state at 190(30) K are expected (see Figure 6). The A_4 and A_6 CFP and crystal field overall splitting, Δ_{cc} , for Yb³⁺, Nd³⁺ and Er³⁺ in YBiPt, are given in Table II. For comparison, the A_4 and A_6 CFP estimated from the level scheme for PrBiPt¹⁶ and YbBiPt¹⁷ are also given.

IV. DISCUSSION

The fine structure in the ESR spectrum of the S-state ion Gd^{3+} is believed to be associated with the admixture of excited crystal-field-split configurational states into the ground S-state mainly via spin-orbit coupling.⁹ Although it is not a general rule, in many materials it has been found that the Gd^{3+} fourth-order CFP b_4 is negative in insulators¹¹ and semiconductors of appreciable gap,¹⁵ but positive in metals.⁹ Whereas, for materials of low carriers density this parameter was found to be very small.⁹ Therefore, it could be expected that in the narrow gap semiconductor YBiPt $|b_4|$ would be small and the CFE of Gd^{3+} in YBiPt could be masked by the resonance residual linewidth. But, we showed above, that the A_4 and A_6 CFP obtained for the non S-state ions, Er^{3+} , Nd^{3+} , and Yb^{3+} in YBiPt are of the same order of magnitude as those reported for rare-earths in other cubic materials, where CFE were observed in the ESR spectra of Gd^{3+} .¹⁸⁻²¹ It suggests that CFE should be present in the ESR of Gd^{3+} doped YBiPt, specially when considering the relative small Gd^{3+} ESR residual linewidth (≈ 40 Oe). Thus, the absence of CFE in the ESR spectrum of Gd^{3+} in YBiPt is yet not understood. Thus, a mechanism that may explain the observed "quenching" of CFE for the S-state ion Gd^{3+} in small gap semiconductors and semimetals with low carrier density is still missing.

The A_4 and A_6 CFP found here for YBiPt are consistent with those obtained from specific heat and susceptibility measurements in PrBiPt ¹⁶ and neutron diffraction experiments in YbBiPt (see Table II).¹⁷ Notice that the level scheme shown in Figure 6 is very close to that obtained for YbBiPt .¹⁷ The small differences are probably associated to the different lattice parameter and to the metallic character of YbBiPt . Notice that the splitting of the quartet, claim in ref. 17, was not observed in any of our compounds. The sign and order of magnitude of the A_4 CFP is in agreement with that obtained from a point charge model (PCM) assuming a tetrahedron of $-e$ charges sited at the Pt first near neighbors (see Table II). But, the A_6 CFP turns out to be positive, contrary to the experimental value given in Table II. Besides, the addition of an octahedron of negative charges at the position of the

Bi next near neighbors, increases the positive value of A_4 and A_6 . It is generally accepted that for cubic crystal fields, due to the absence of second order terms, the first nearest neighbors constitute the main contribution to the CFP. Therefore, corrections to the PCM as, screening, size effects, and covalency, are needed to be included to improve the calculated values of the CFP using a simple PCM.

V. CONCLUSIONS

The CFP A_4 and A_6 in $Y_{1-x}R_xBiPt$, for the non S-state ions, $R = Nd^{3+}$, Er^{3+} , and Yb^{3+} , were determined from ESR and magnetic susceptibility experiments. The obtained values were found to be in reasonable agreement with those measured by others in $PrBiPt$ ¹⁶ and $YbBiPt$.¹⁷ However, the PCM only accounts for the sign and value of the A_4 CFP. Surprisingly, CFE were not observed in the ESR spectrum of Gd^{3+} in $YBiPt$. An upper limit of about 1 Oe for the $|b_4|$ parameter is estimated from the residual ESR linewidth. That result and those from others⁹ suggests that a small $|b_4|$ value is characteristic for narrow gap semiconductors and semimetals of low carrier densities.

VI. ACKNOWLEDGMENTS

This work was supported by FAPESP (SP-Brazil) Grants No 95/4721-4, No 95/6177-0, No 97/03065-1, No 98/614-7, CNPq (Brazil) Grant No 910102/96-1, and NSF-DMR No 9705155, No 9016241, No 9501529, and NSF- INT. 9602928.

REFERENCES

- ¹ Z. Fisk, P.C. Canfield, W.P. Beyermann, J.D. Thompson, M.F. Hundley, H.R. Ott, E. Felder, M.B. Maple, M.A. Lopez de la Torre, P. Visani, and C.L. Seaman, Phys. Rev. Lett. **67**, 3310 (1991).
- ² P.C. Canfield, J.D. Thompson, W.P. Beyermann, A. Lacerda, M.F. Hundley, E. Peterson, and Z. Fisk, J. Appl. Phys. **70**, 5800 (1991); M.F. Hundley, J.D. Thompson, P.C. Canfield and Z. Fisk, Phys. Rev. B **56**, 8098 (1997).
- ³ O. Eriksson, J.M. Wills, and A.M. Boring, J. of Alloy and Compounds **185**, 145 (1992).
- ⁴ G.B. Martins, D. Rao, G.E. Barberis, C. Rettori, R.J. Duro, J. Sarrao, Z. Fisk, S. Oseroff, and J.D. Thompson, Phys. Rev. B **52**, 15062 (1995).
- ⁵ R. Bachmann, F.J. DiSalvo, T.H. Geballe, R.L. Greene, R.E. Howard, C.N. King, H.C. Kivisch, K.N. Lee, R.E. Schwall, H.V. Thomas, and R.B. Zubeck, Rev. Sci. Instrum. **43**, 205 (1972).
- ⁶ G. Feher and A.F. Kip, Phys. Rev. **98**, 337 (1955); F.J. Dyson, *ibid.* **98**, 349 (1955).
- ⁷ G.E. Pake and E.M. Purcell, Phys. Rev. **74**, 1184 (1948).
- ⁸ D. Davidov *et al.*, Phys. Rev. B **5**, 1711 (1972); C. Rettori *et al.*, *ibid.* B **7**, 1 (1973).
- ⁹ G.E. Barberis, D. Davidov, C. Rettori, and J.F. Suassuna, Phys. Rev. B **19**, 2385 (1979).
- ¹⁰ R.N. Mesquita, G.E. Barberis, C. Rettori, M.S. Torikachvili, and M.B. Maple, Solid State Commun. **74**, 1047 (1990).
- ¹¹ L.J. Tao, D. Davidov, R. Orbach, and E.P. Chock, Phys. Rev. B **4**, 5 (1971).
- ¹² A. Abragam and B. Bleaney, Electron Paramagnetic Resonance of Transition Ions. Clarendon Press-Oxford, (1970).
- ¹³ K.R. Lea, M.J.M. Leask, and W.P. Wolf, J. Phys. Chem. Solids **22**, 1381 (1962); M.T.

Hutchings, Solid State Physics, 16, 227 (1964).

¹⁴ A.J. Freeman and R.E. Watson, Phys. Rev. B 127, 6 (1962).

¹⁵ M. Bartkowski, D.J. Northcott, J.M. Park, A.H. Reddoch, and F.T. Hedgcock Solid State Commun. 56, 659 (1985).

¹⁶ H. Suzuki, M. Kasaya, T. Miyazaki, Y. Nemoto, and T. Goto, J. Phys. Soc. Japan 66, 2566 (1997).

¹⁷ R.A. Robinson, M. Kohgi, T. Osakabe, F. Trouw, J.W. Lynn, P.C. Canfield, J.D. Thompson, Z. Fisk, and W.P. Beyermann, Phys. Rev. Letters 75, 1194 (1995).

¹⁸ R.J. Birgeneau, E. Bucher, J. P. Maita, L. Passel and K. C. Turberfield, Phys. Rev. B, 8, 5345 (1973).

¹⁹ P. Urban, D. Davidov, B. Elschner, and G. Sperlich, Phys. Rev. B, 12, 12 (1975).

²⁰ P. Urban and D. Seipler, J. Phys. F: Metal Phys., Vol 7, 1598 (1977).

²¹ C. Rettori, R. Levin and D. Davidov, J. Phys. F: Metal Phys., Vol 5, 2379 (1975)

FIGURES

FIG. 1. Specific heat (C/T) as a function of T^2 for YBiPt. The inset shows the low temperature T^2 dependence of C/T. The solid line is the best fit to $C/T = \gamma + \beta T^2$, with $\gamma \lesssim 0.1$ mJ/mol-K² and $\beta = 0.79(7)$ mJ/mol-K⁴.

FIG. 2. Temperature dependence of the susceptibility of $Y_{1-x}Gd_x BiPt$ ($x \approx 0.002$, nominal concentration and $x = 0$) single crystals measured at $H = 0.5$ T.

FIG. 3. ESR spectra of Gd^{3+} in $Y_{1-x}Gd_x BiPt$ ($x \approx 0.0021$) at $T = 7$ K and $T = 280$ K. The thermal broadening of the linewidth was found to be $b \lesssim 0.05$ Oe/K and $g = 1.993(4)$.

FIG. 4. ESR spectra of Nd^{3+} in $Y_{1-x}Gd_x BiPt$ ($x \approx 0.0020$) at $T = 4.2$ K. The resonance Gd^{3+} natural impurities is also indicated. The vertical lines show the positions of the various hyperfines satellites appropriate for the ^{143}Nd and ^{145}Nd isotopes.

FIG. 5. Temperature and field dependence of the inverse magnetic susceptibility, $\chi^{-1}(T, H = 1$ T, 5 T) - χ_{∞}^{-1} for the $Y_{0.9}Yb_{0.1}BiPt$ single crystal. χ_{∞}^{-1} is the free Yb^{3+} ion value of the inverse susceptibility shown in the inset. The solid lines are the best fit to the data of the calculated susceptibility including the Zeeman and LLW cubic crystal field terms in the Hamiltonian. The Yb^{3+} crystal field splitted ground state multiplet ($J = 7/2$) is shown.

FIG. 6. Temperature and field dependence of the inverse magnetic susceptibility, $\chi^{-1}(T, H = 1$ T, 5 T) - χ_{∞}^{-1} for the $Y_{0.9}Nd_{0.1}BiPt$ single crystal. χ_{∞}^{-1} is free Nd^{3+} ion value of the inverse susceptibility shown in the inset. The solid lines are the best fit to the data of the calculated susceptibility including the Zeeman and LLW cubic crystal field terms in the Hamiltonian. The Nd^{3+} crystal field splitted ground state multiplet ($J = 9/2$) is shown.

TABLES

TABLE I. Experimental parameters for R:YBiPt

	<i>g</i>	<i>a</i>	<i>b</i>	^{143}A	^{145}A	<i>W</i>	<i>x</i>
		Oe	Oe/K	Oe	Oe	K	
Gd:YBiPt	1.993(4)	40(3)	$\lesssim 0.05$				
Nd:YBiPt	2.63(1)	70(5)	$\lesssim 0.1$	213(5)	133(5)	2.0(5)	0.15(5)
Yb:YBiPt						-3.9(7)	-0.61(8)
Er:YBiPt						$\approx -0.17^{\circ}$	$\approx 0.271^{\circ}$
PrBiPt						$\approx -1.79^{\circ}$	$\approx -0.20^{\circ}$
YbBiPt						$\approx -3.5^{\circ}$	$\approx -0.60^{\circ}$

*see refs. 4, 16, 17.

TABLE II. Extracted parameters for R:YBiPt

	A_4 K per a_0^{-4}	A_6 K per a_0^{-6}	$A_4(\text{PCM})$ K per a_0^{-4}	$A_6(\text{PCM})$ K per a_0^{-6}	Δ_{cc} K
PrBiPt	$\approx -3^{\circ}$	$\approx -1.2^{\circ}$	-11.60	0.11	$\approx 210^{\circ}$
Nd:YBiPt	-7(4)	-1.4(8)	-11.93	0.11	190(30)
Er:YBiPt	≈ -15	≈ -1	-13.24	0.13	85(20) ^a
Yb:YBiPt	-24(8)	-2.6(9)	-13.50	0.13	88(10)
YbBiPt	$\approx -21^{\circ}$	$\approx -2.4^{\circ}$	-13.50	0.13	$\approx 70^{\circ}$

*see refs. 4, 16, 17.

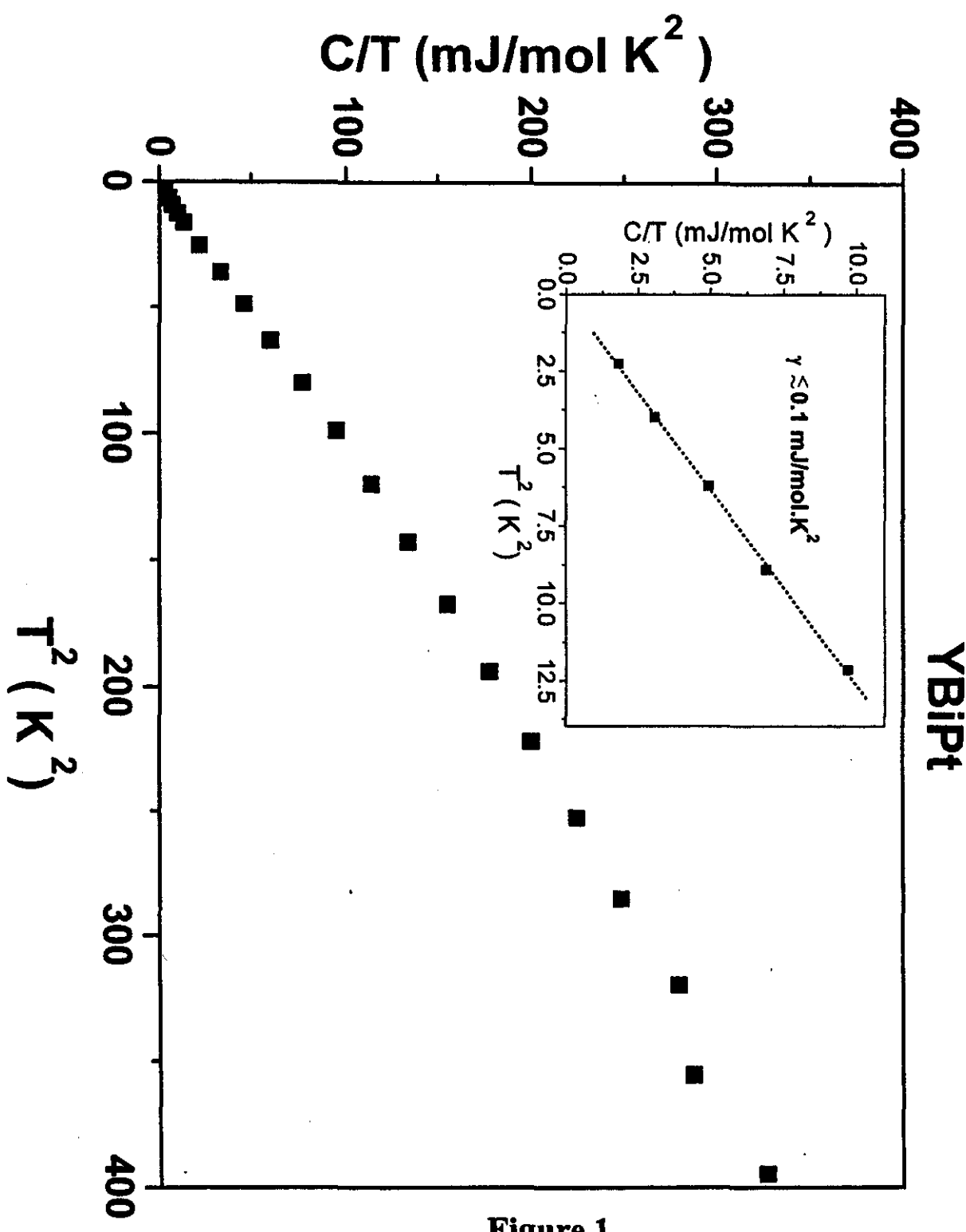


Figure 1

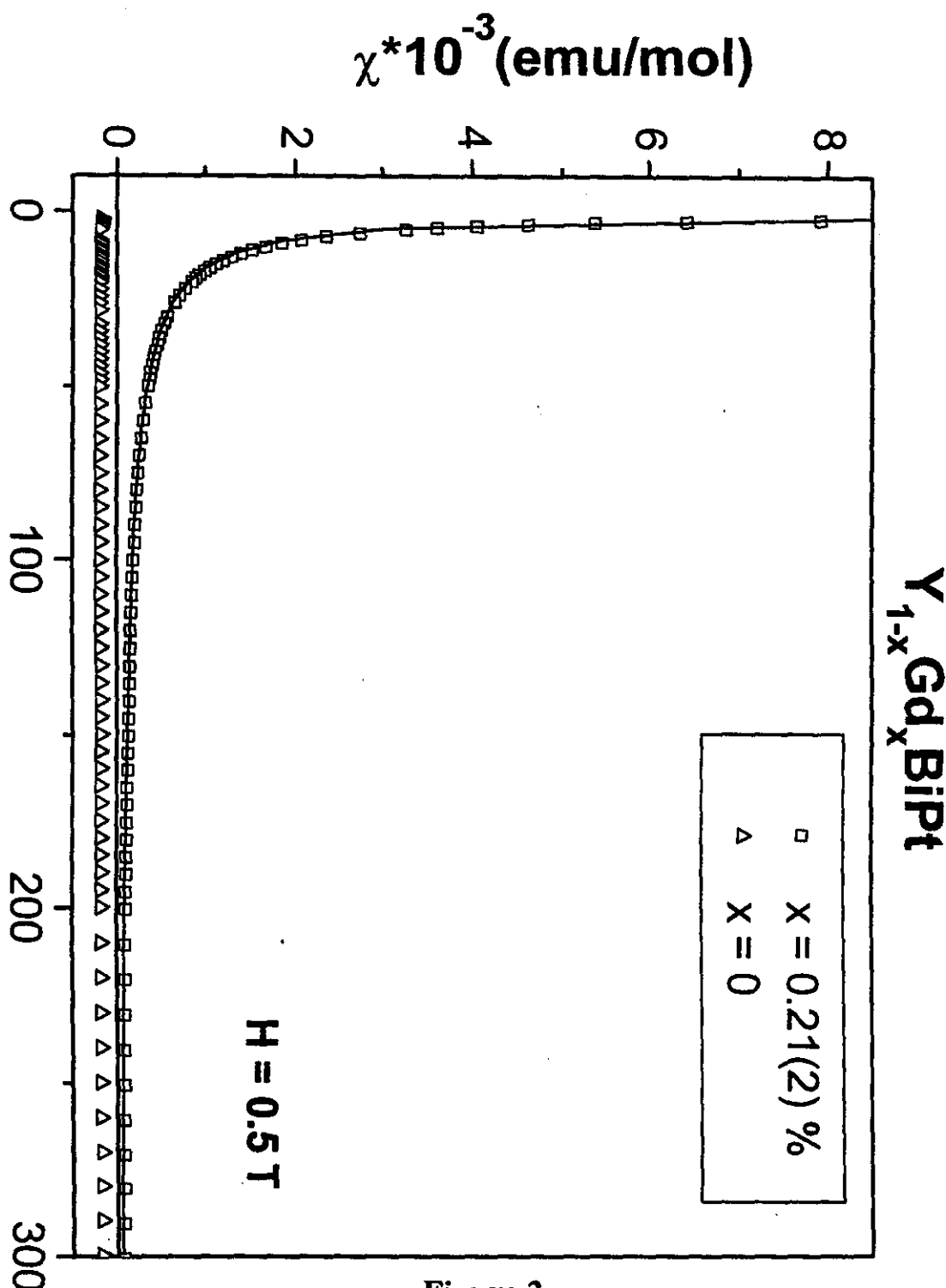
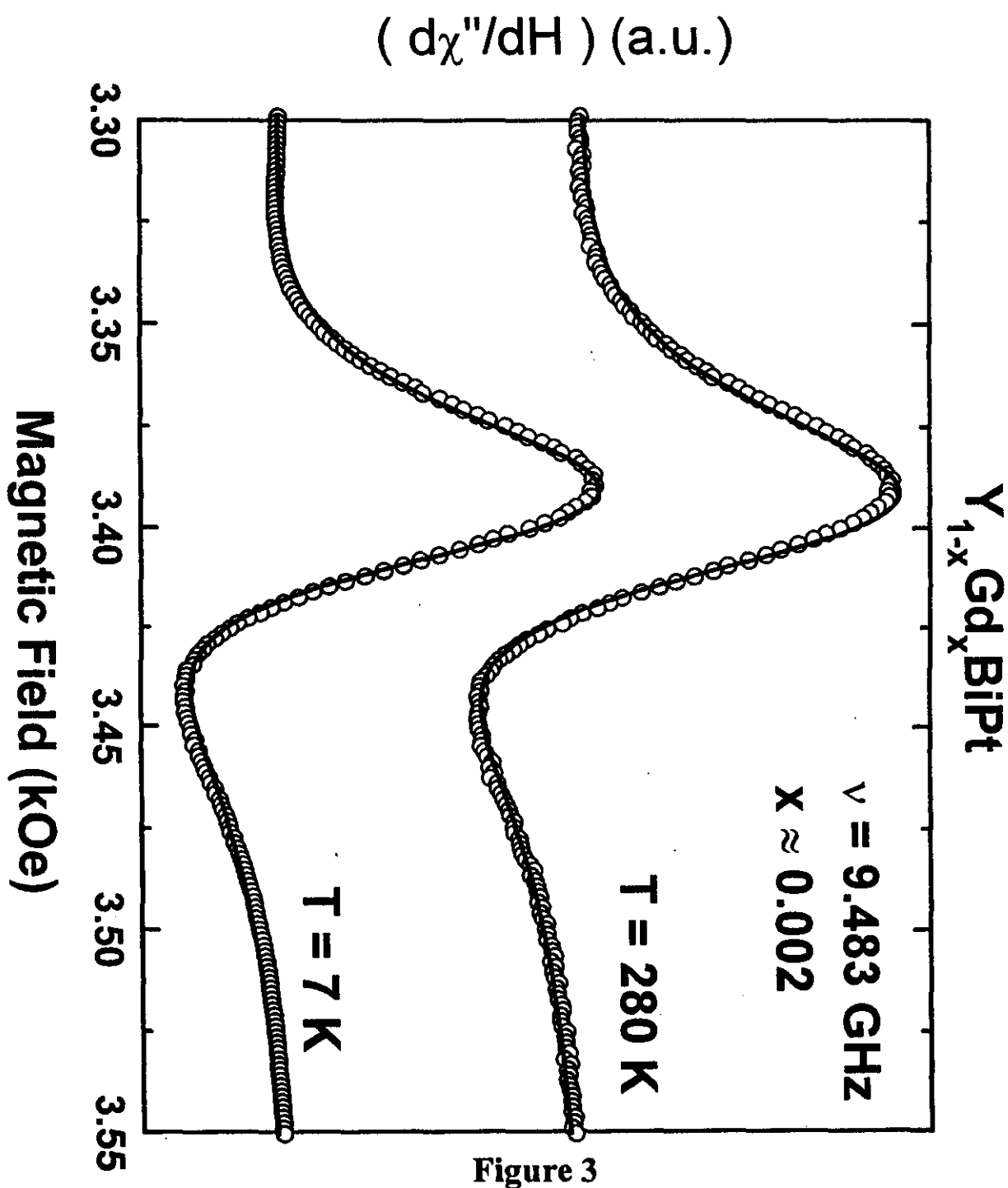


Figure 2



Absorption Derivative (a.u.)

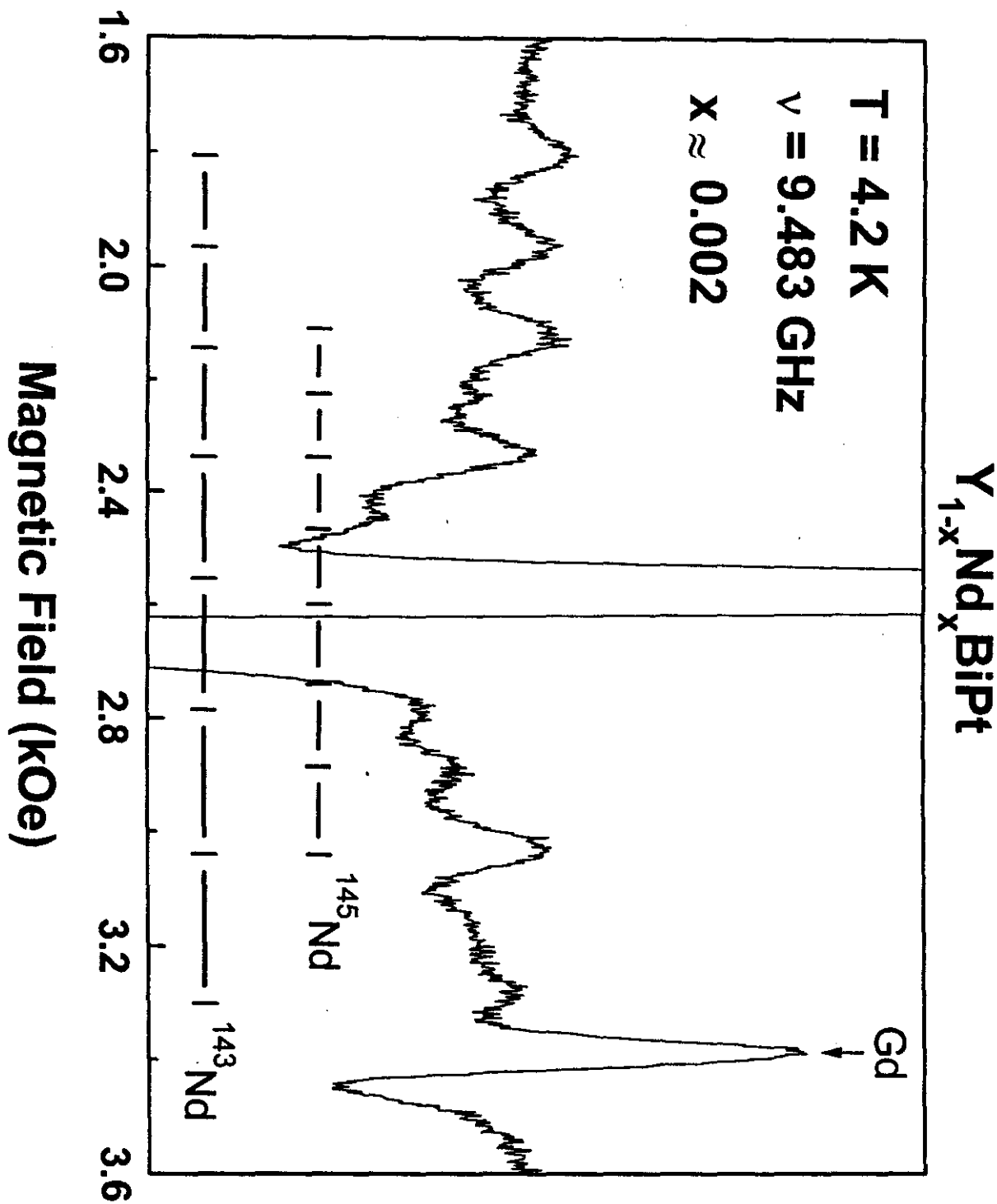


Figure 4

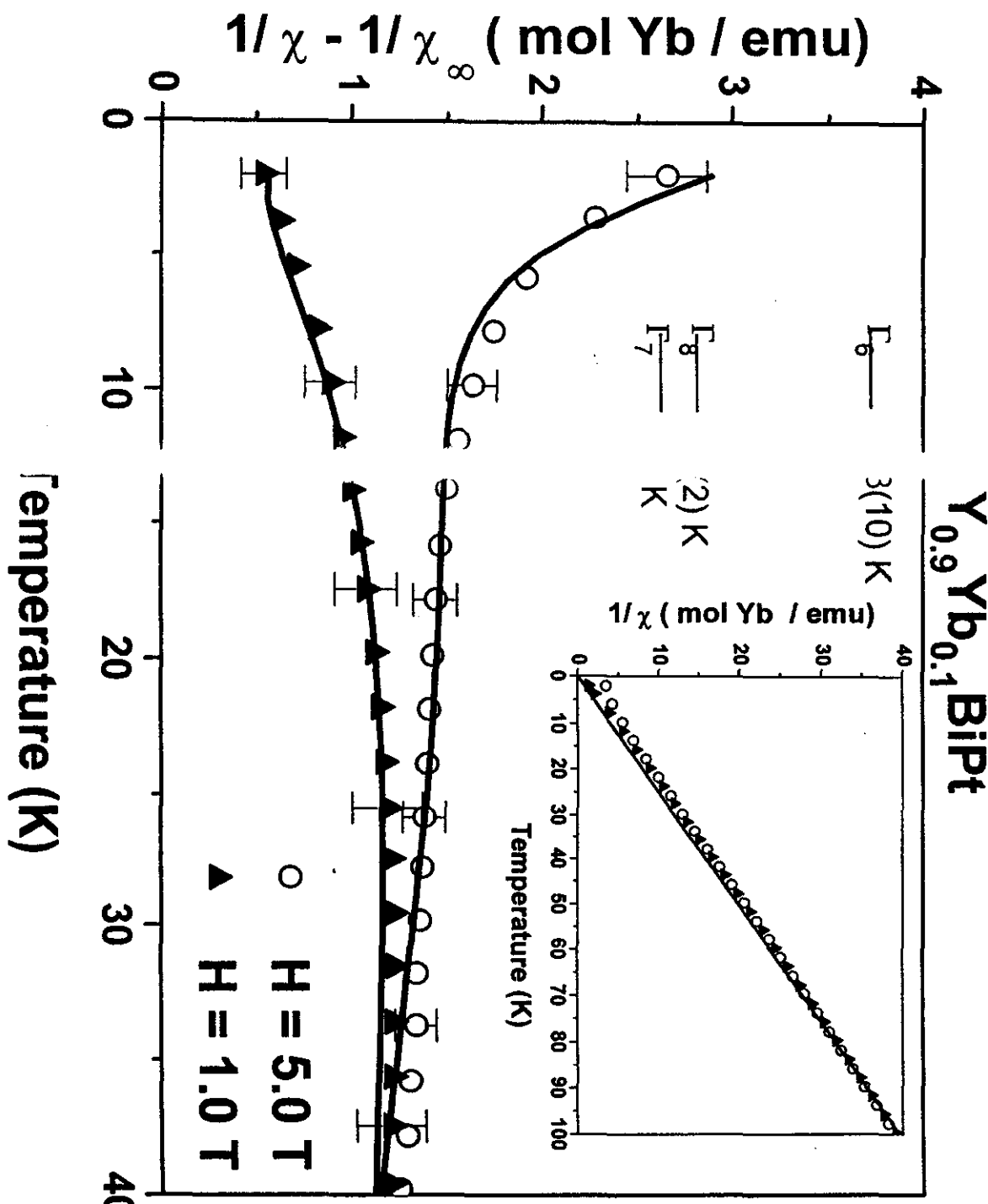


Figure 5

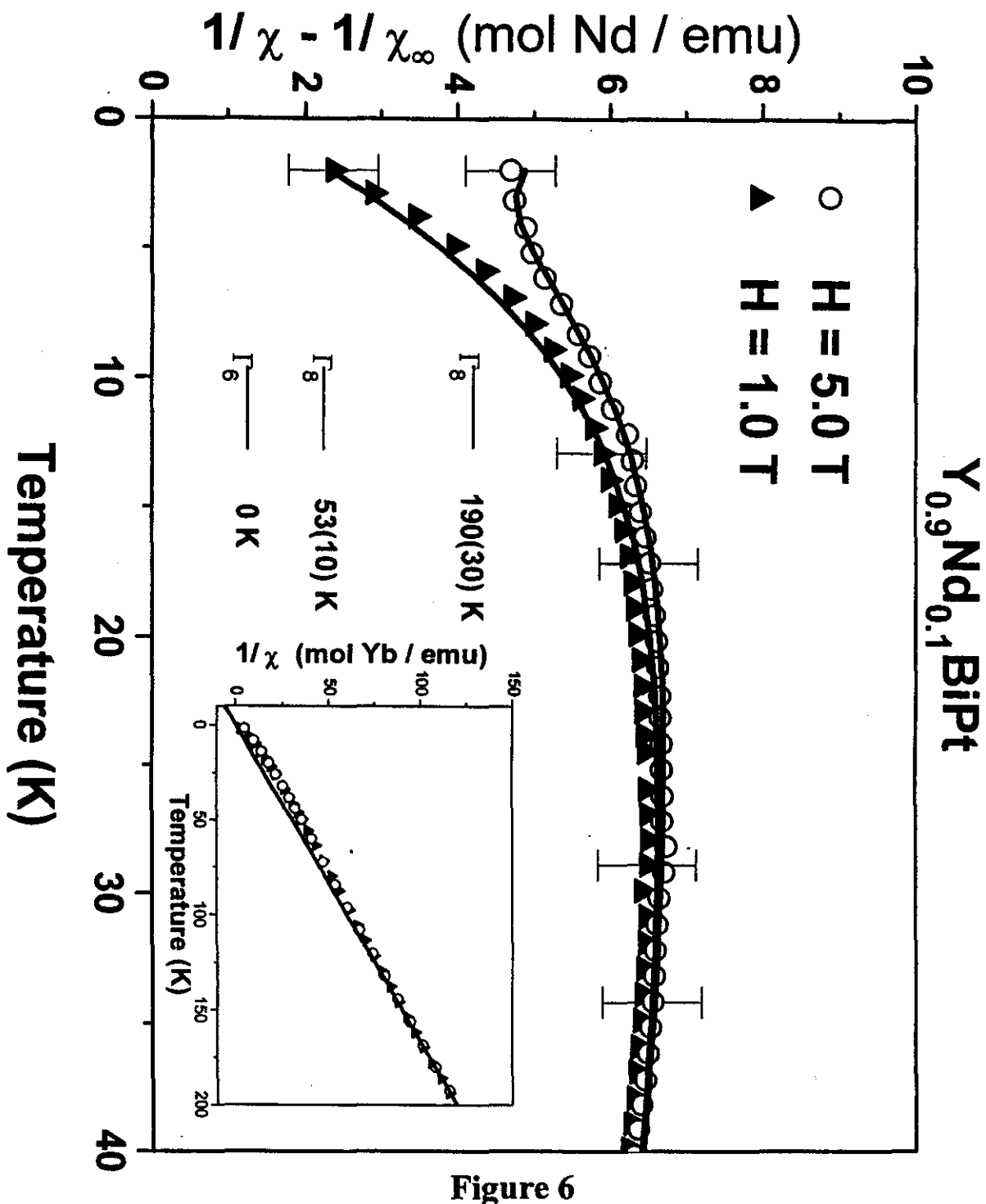


Figure 6

Seção 2.7

2.7 Efeitos de Inomogeneidade nas Propriedades Magnéticas dos compostos $R_{1-x}A_xMnO_3$ ($R = La, Pr$; $A = Ca, Sr$)

2.7) Efeitos de Inhomogeneidade nas Propriedades Magnéticas dos compostos R_{1-x}A_xMnO₃ (R = La, Pr; A = Ca, Sr).

Proceedings of the Fifth International Workshop on
Non-Crystalline Solids

NON-CRYSTALLINE AND NANOSCALE MATERIALS

Editors

J. Rivas & M.A. López-Quintela

World Scientific

EFFECT OF INHOMOGENEITIES IN THE MAGNETIC PROPERTIES OF $R_{1-x}A_xMnO_3$ ($R = La, Pr$; $A = Ca, Sr$)

E. Granado, P.G. Pagliuso, J.A. Sanjurjo, G. Rettori, and S.B. Oseroff*

*Instituto de Física "Gleb Wataghin", UNICAMP, 13083-970,
Campinas-SP, Brazil*

M.T. Causa, A. Butera, A. Canciro, and M. Tovar
Centro Atómico Bariloche and Instituto Balseiro, 8400 S.C. Bariloche, Argentina

J.J. Neumeier and K.J. McClellan

Los Alamos National Laboratory, Los Alamos, New Mexico 87545, USA

S.-W. Cheong

AT & T Bell Laboratories, Murray Hill, New Jersey 07974, USA

Y. Tokura

Department of Physics, University of Tokyo 113, Japan

R. Sanchez and J. Rivas

*Departamento de Física Aplicada, Universidad de Santiago, E-15706,
Santiago de Compostella, España*

S. Schultz

University of California San Diego, CA 92093, USA

We present a systematic Electron Spin Resonance (ESR) and magnetization study of the $R_{1-x}A_xMnO_3$ ($R = La, Pr$; $A = Ca, Sr$) perovskites, up to 1100 K. Special care was taken in the data obtained in the region of T immediately above the ferromagnetic ordering temperature ($T_c \lesssim T \lesssim 1.2T_c$). In this interval of T , for most samples, the resonance line broadens, distorts, and splits into several lines. In conjunction with it, small hysteresis loops, and a susceptibility which is field and T dependent are measured. The origin of these findings are associated to non-stoichiometric samples due to inhomogeneities, probably, result of a non-random distribution of vacancies, defects, and oxygen content. It is shown that these features are easily observed by ESR. We also discuss the possible origin of the T dependence of the ESR linewidth for all the region of T measured.

1 Introduction

Metal-insulator (MI) and ferromagnetic-paramagnetic (FM-PM) transitions of the $La_{1-x}A_xMnO_3$ ($A = Ca, Sr, Pb, Ba$; $0.15 \lesssim x \lesssim 0.5$) perovskites are known since 1950.¹ Their properties are, at least qualitatively, explained by a model of exchange interaction, termed double exchange (DE).² Large magnetoresistance,

106

and recently "colossal magnetoresistance" (CMR) effects, were reported in a variety of thin films and bulk samples of these materials.³ That makes them extremely attractive for potential commercial magnetic sensing applications.⁴ As a result, renewed experimental and theoretical attention has been paid to these compounds. It has been argued that DE alone can not explain the large resistivity drop between the PM and FM phase.⁵ Polaron effects, either *lattice*,^{5,6} enhanced by strong Jahn-Teller electron-phonon coupling, or *magnetic*⁷ were invoked to allow for carriers localization at the MI transition. Evidences for *lattice*⁸ and *magnetic*⁷ polarons at the MI transition have been reported in neutron diffraction experiments and transport measurements.

In this work we present Electron Spin Resonance (ESR) and magnetization (M) measurements up to 1100 K. Mechanisms that may explain the T dependence of the ESR linewidth are discussed. Detailed low-field magnetic measurements and ESR near the MI transition for $La_{0.78}Ca_{0.22}MnO_3$, $La_{0.83}Sr_{0.17}MnO_3$, $La_{0.70}Sr_{0.30}MnO_3$ and $Pr_{0.625}Sr_{0.375}MnO_3$ single crystals, and their powders are presented. Also, a ceramic sample of $La_{2/3}Ca_{1/3}MnO_3$ was studied in great detail. We will show that ESR is an extremely sensitive and useful technique to study the sample quality of these compounds. It will become clear that extreme care need to be taken before one can associate the data to particular models, or to ascribe a particular feature to entities such as *spin-clusters*,⁹ *magnetic-spin polarons*,⁷ *lattice polarons*,^{5,6,8} etc.

2 Experimental Details

Single crystals of $La_{0.78}Ca_{0.22}MnO_3$, $La_{0.83}Sr_{0.17}MnO_3$, and $La_{0.70}Sr_{0.30}MnO_3$ were grown by the optical floating zone method. Typical rotation rates for both, the seed crystal and the feed rod, were ~ 50 rpm. The crystals were grown at a rate of ~ 6 mm/h. The $Pr_{0.625}Sr_{0.375}MnO_3$ single crystal was also grown by the floating zone method, using a lamp-image furnace.¹⁰ The ceramic sample of $La_{2/3}Ca_{1/3}MnO_3$ was prepared as described in Ref. 9. The structure and phase purity were checked by x-ray powder diffraction and the crystals orientation determined by the conventional Laue method. These measurements do not indicated the presence of spurious phases or any evidence that would suggest that the samples were inhomogeneous. ESR measurements were performed in very small crystals, less than 1mg, or powders of small and well dispersed particles, $\sim 10 \mu m$. Special care was taken to avoid overloading the cavity, a current problem when working with ferromagnetic materials.¹¹ M measurements have been done in a Quantum Design dc SQUID magnetometer. To minimize possible T drifts,^{12,13} the M measurements at constant T were taken only after 3-8 hrs. of being stable at the target T. The T dependence of

M was taken increasing T after zero field cooling (ZFC).

3 Results and Discussions

The transport properties of the single crystals and ceramics show the general behavior expected for a CMR system. The high T susceptibility data, $\chi^{-1}(T)$, for $La_{2/3}Ca_{1/3}MnO_3$ is shown in Fig. 1. A departure from a simple Curie-Weiss law is observed below $T \approx 2T_c$. Similar behavior was found for the other systems studied. M measurements in a $La_{0.78}Ca_{0.22}MnO_3$ single crystal, of ~10 mg, (from where small pieces were taken to perform the ESR measurements) are shown in Fig. 2. For $T \gtrsim 245$ K the system is paramagnetic with a field independent susceptibility, $\chi^{-1}(T)$. Assuming a Curie-Weiss behavior, we

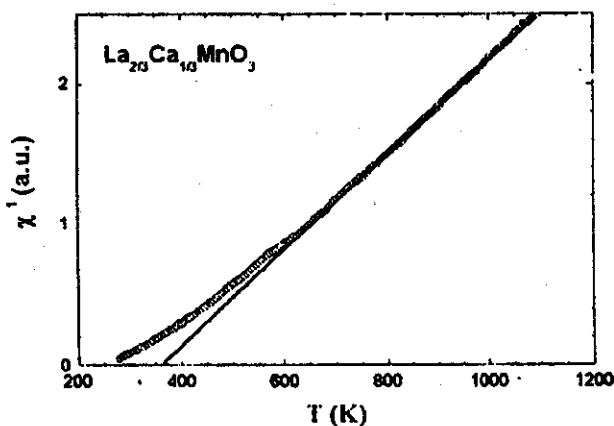


Figure 1: $\chi^{-1}(T)$, as a function of T for a ceramic sample of $La_{2/3}Ca_{1/3}MnO_3$ ($T_c \approx 270$ K). The solid line represent the best fit to a Curie-Weiss law for $T \geq 700$ K.

extract $\sim 7.3 \mu_B$ for $245 K \lesssim T \lesssim 270$ K, in agreement with published data,¹⁴ but larger than the value of $3.78 \mu_B$ expected for $x \approx 0.22$. For $T \gtrsim T_c$, and in the T interval between 210 K and 245 K, M is found to be H and T dependent, $\chi^{-1}(H,T)$. The transition temperature, $T_c = 195(5)$ K, was defined at the maximum of $\partial M / \partial T$. The resistivity, for $H = 0$ T, shows a MI transition at $T \approx T_c$, and above 240 K a thermally activated behavior with an activation energy of $E_a \approx 93$ meV. At $T = 205$ K and $H = 5$ T we measured large, approximately

108

-98% resistivity change. The ESR linewidth (ΔH_{pp}) for $La_{2/3}Ca_{1/3}MnO_3$ as a function of T is given in Fig. 3. A linear increase of ΔH_{pp} is observed for $T_c + \Delta T_c \lesssim T \lesssim 2T_c$ for all the compounds measured. Also, a reduction in the slope is found for $T \gtrsim 2T_c$, as seen in Fig. 3. As it will be shown below for $La_{0.70}Sr_{0.30}MnO_3$, a single resonance line is observed in all the region of T measured, including $T \lesssim T_c$. Instead, for the rest of the samples, as T_c

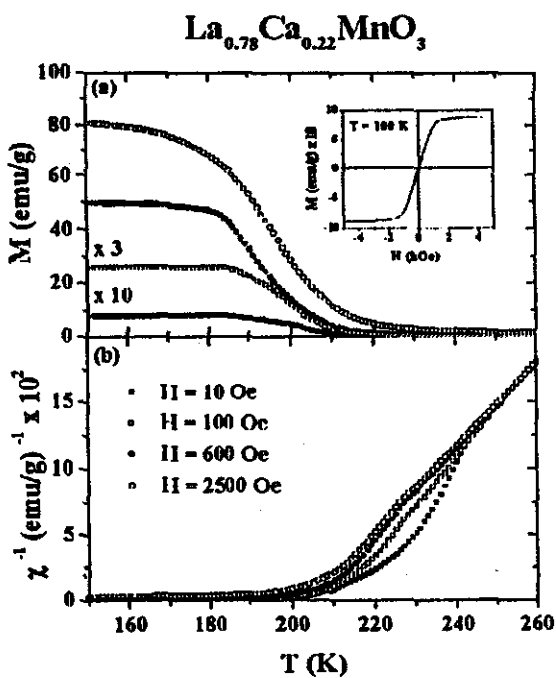


Figure 2: T and H dependence of M and the χ^{-1} for a ~ 10 mg single crystal of $La_{0.78}Ca_{0.22}MnO_3$ ($T_c = 195(5)$ K). The inset shows M vs H at $T = 100$ K.

is approached from above and at $T \approx T_c + \Delta T_c$, the resonance line becomes broader, distorts, and in most cases splits into several components. Finally, at T below T_c all the lines collapsed into a single and broader one, shifted

from $g = 2.0$. The spread of T_c (ΔT_c), where such behavior is found, depends on the compound. It was found to be larger for the $La_{0.78}Ca_{0.22}MnO_3$ ($T_c = 195(5)$ K) single crystal, where the resonance line starts to get broader at $T \approx T_c + 50$ K, as shown in Fig. 4. ΔT_c is reduced to just 5 - 20 K in the other compounds. For $La_{0.70}Sr_{0.30}MnO_3$ only a small broadening, of about 20 % of the minimum linewidth $\Delta H_{pp} \approx 150$ Oe at $T \approx 380$ K, is observed at $T \ll T_c$. Already Bhagat and coworkers have reported that an increase in the linewidth below T_c could be an indication of some magnetic inhomogeneity in

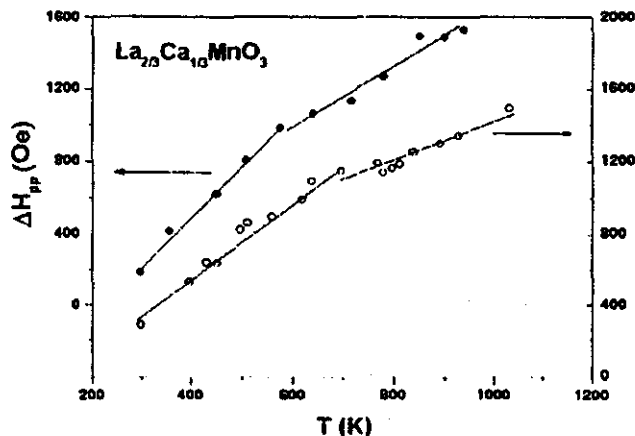


Figure 3: ESR linewidth as function of T for two ceramic samples of $La_{2/3}Ca_{1/3}MnO_3$ measured at 9 GHz.

the sample, and that the sample that shows a single resonance line below T_c , could be associated to an homogeneous sample.¹⁵ In the region of T where a departure from a single resonance line is observed, small hysteresis loops appear in the magnetization. The hysteresis loops, shown in Fig. 4, were obtained after subtracting a straight line passing through the origin with the high field slope of $M(H,T)$ vs H . For $T \rightarrow T_c$, the remnant, M_r , and saturation, M_s , magnetization of these loops increases several orders of magnitude, whereas the coercive field, H_c , remains almost constant at about 20 Oe. The magnetic field was swept between +200 Oe and -200 Oe. No differences between ZFC and FC experiments were detected within the accuracy of our measurements. We should notice that the resonance line starts to broaden and distort at different

110

T for distinct pieces taken from the whole crystal used for the M measurements. The M measurements were made with samples 100 to 1000 times larger than those used for ESR, due to the different sensitivity of both techniques. In Fig. 4 the resonance lines obtained at similar T , are also shown. For the much higher sensitivity of ESR, a sample of ~ 1 mg was used, cut from the ~ 10 mg crystal used for the M measurements. The resonance lines shown in the insets were obtained in a much smaller sample, less than $100 \mu g$, of the same main crystal.

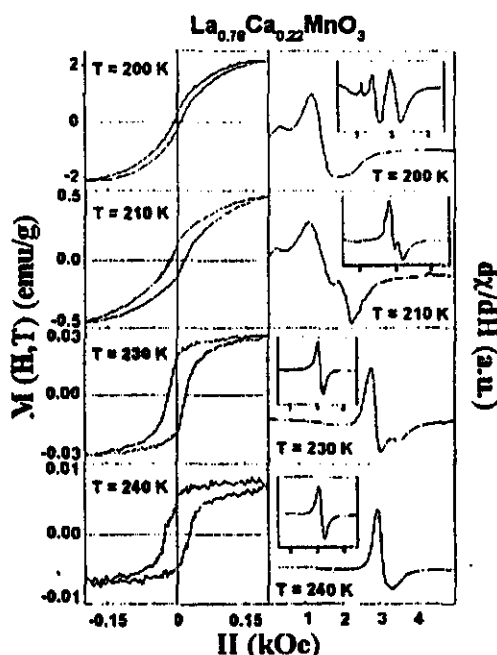


Figure 4: Left: Hysteresis loops for a ~ 10 mg single crystal of $La_{0.78}Ca_{0.22}MnO_3$ ($T_c = 195(5)$ K), after subtracting a straight line passing through the origin with the high field slope of $M(H,T)$ vs H . Right: ESR lines obtained at similar T , measured in a ~ 1 mg piece cut from the main crystal. The insets give the resonance of a $\sim 100 \mu g$ piece cut from different region of the main crystal.

It is interesting to notice that the line for the 1 mg sample start to distort at a T similar to the T' where the loops are first observed. Instead, the smaller piece shows a departure from a lorentzian line at a lower T , a clear indication

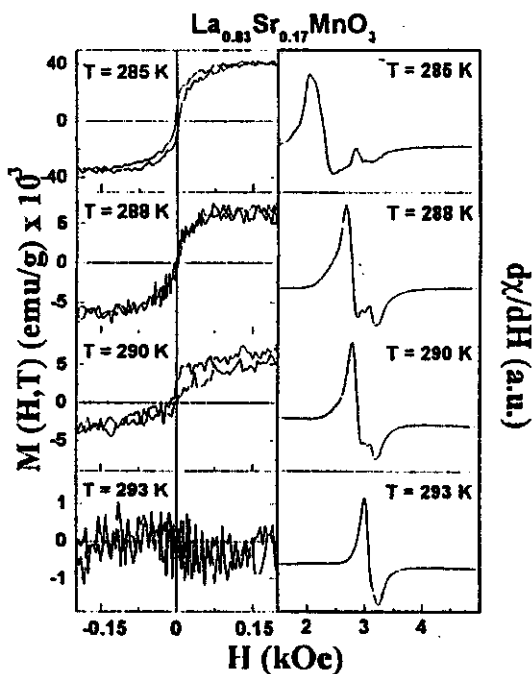


Figure 5: Similar data than in Fig. 4 is given for a $La_{0.83}Sr_{0.17}MnO_3$ crystal ($T_c \approx 280 \text{ K}$).

that this particular sample is highly inhomogeneous. Loops similar to those found in the $La_{0.78}Ca_{0.22}MnO_3$ single crystal, but with smaller coercive fields, were observed in the $La_{0.83}Sr_{0.17}MnO_3$ crystal ($T_c = 284(2) \text{ K}$) between 285 K and 290 K, as shown in Fig. 5. Resonance lines for the same T , taken in a piece of $\sim 0.1 \text{ mg}$ cut from the same crystal, are also shown. Similar data were obtained for a $Pr_{0.825}Sr_{0.375}MnO_3$ crystal ($T_c = 304(1) \text{ K}$) for $303 \text{ K} \leq T \leq 307 \text{ K}$, and in a ceramic sample of $La_{2/3}Ca_{1/3}MnO_3$ ($T_c = 270(2) \text{ K}$) between 275 K and 280 K. Instead, for $La_{0.70}Sr_{0.30}MnO_3$ ($T_c = 366(1) \text{ K}$) crystal, loops with much smaller H_c were only observed at T immediately above T_c . In that case a single resonance line was observed above and below T_c . Fig. 6 shows the ESR line for several T and a typical M vs H curve, just above T_c , for $La_{0.70}Sr_{0.30}MnO_3$. The change from a lorentzian to a dysonian-like resonance line shape, seen in Fig. 6 as we go through T_c , may result from the increase

of the conductivity, σ , and permeability, μ , at the MI and PM-FM transitions at T_c . The linear increase of the linewidth with T up to $\sim 2T_c$ was associated recently by us and other authors to a one-phonon process.⁹ This mechanism,

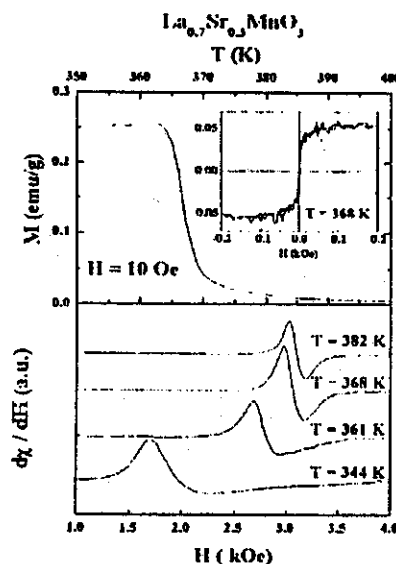


Figure 6: M data for a $La_{0.70}Sr_{0.30}MnO_3$ single crystal (~ 5 mg) measured at 10 Oe in the region of $T_c \approx 366$ K. The inset shows a typical M vs H curve, just above T_c . For $La_{0.70}Sr_{0.30}MnO_3$ loops with small H_c were observed only immediately above T_c . ESR lines measured for a ~ 100 μg single crystal are presented at T close to T_c . Notice, that in this case only a single resonance line is observed. The change from a lorentzian to a dysonian resonance line shape, is the result of the MI-transition at the ordering temperature.

first proposed by Huber and Sheera,¹⁶ suggests that the linewidth cannot be accounted only by spin-spin interactions. The expression that accounts for the linewidth can be written as $\Delta H_{pp} = K(T)/\chi' T$, where $K(T)$ contains the T dependence of ΔH_{pp} . We also suggested that the slow down could be related to the fact that the Debye T in these systems is of the order of $2T_c$. On the other hand, Shengelaya et al.¹⁷ suggested that the linear increase may be associated to a strong bottleneck between the Mn^{4+} and the Mn^{3+} . The slow down in the relaxation rate, observed above $\sim 2T_c$, was explained by those authors as a result of an opening of the bottleneck due to a more effective relaxation of the

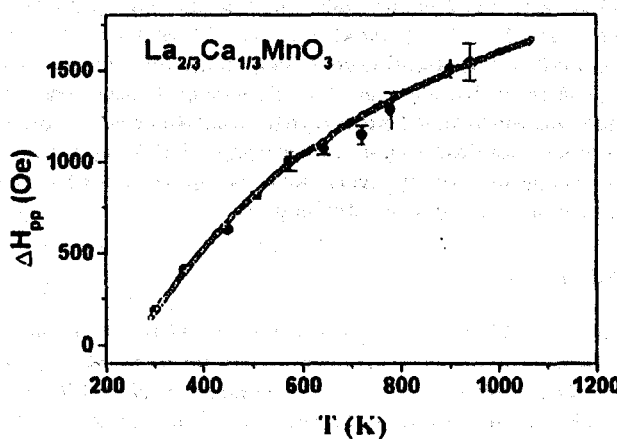


Figure 7: The solid circles correspond to the linewidth as function of T for a sample of ceramic $La_{2/3}Ca_{1/3}MnO_3$ measured at 9 GHz. The open circles correspond to the best fit using $\Delta H_{pp} \sim K/\chi T$ ($K \approx 7200$ Oe K), with the data for χ measured on a sample of the same batch than the one used for ESR.

spin system to the lattice as T increases. The last argument was based in the fact that Mn^{3+} , contrary to Mn^{4+} , is a strong Jahn-Teller ion. However, our more recent and extended data in T show that, within the experimental error, the linewidth for $T \gtrsim T_c + \Delta T_c$, where the anomalies described above are first noticed, can be simply explained by a spin-spin interaction mechanism. That is:

$$\Delta H_{pp} = \frac{K}{\chi T} \quad (1)$$

In Fig. 7 we fit the data of ΔH_{pp} vs T for a sample of $La_{2/3}Ca_{1/3}MnO_3$ to expression (1). The χ data taken for a sample of the same ceramic bulk was used in Eq. 1. As it can be seen the agreement is excellent for $K \approx 7200$ Oe K, independent of T . Further support for it is that similar measurements made in $La_2Mn_2O_7$,¹⁸ a compound that only has Mn^{4+} , a smaller T_c , and a similar Debye T , presents similar M and ESR features.¹⁹ That is, a departure from a Curie-Weiss law of χ^{-1} and a reduction on the slope of ΔH_{pp} at $\sim 2T_c$. The origin of the features found above T_c , that is, broadening, splitting, distortion

of the ESR line, and the associated hysteresis loops are clear evidence of the existence of small FM regions at $T \gtrsim T_c$. Their existence depend not only of the compound but within different regions of the same sample. That support the picture that a distribution of T_c is present in these systems.

These data show that ESR is a very sensitive tool to learn about the quality of the sample. Besides, it should be stressed that these types of measurements are very simple and require very small samples, less than one mg, orders of magnitude smaller than other techniques.

4 Conclusions

In summary, we show that careful studies must be made on the quality of the sample, before the measured properties can be ascribed to a compound and are not the result of extrinsic factors. The large spread of T_c is probably due to the presence of a non-random distribution of vacancies, defects, and/or oxygen content, that differs from the nominal concentration.

Acknowledgments

This work was supported by FAPESP Grants No 95/4721-1 and 96/12585-6, São Paulo-SP-Brazil, NSF-DMR No 9705155, and NSF-INT 9602928.

*Permanent address, Department of Physics, San Diego State University, San Diego, Ca. 92182, U.S.A.

References

1. G.M. Jonker and J.H. van Santen, *Physica (Utrecht)* **16**, 337 (1950).
2. C. Zener, *Phys. Rev.* **82**, 403 (1951); P.W. Anderson and H. Hasegawa, *Phys. Rev. B* **100**, 675 (1955); P.G. de Gennes, *Phys. Rev.* **118**, 141 (1960); K. Kubo and A. Ohata, *J. Phys. Soc. Jpn* **33**, 21 (1972).
3. J. Volger, *Physica (Utrecht)* **2**, 49 (1954); R. von Helmolt et al., *Phys. Rev. Lett.* **71**, 2331 (1993); H.L. Ju et al., *Appl. Phys. Lett.* **65**, 2108 (1994); K. Cahira et al., *Appl. Phys. Lett.* **63**, 1990 (1993); R. Mahendiran et al., *Appl. Phys. Lett.* **66**, 233 (1995).
4. A. Asamitsu et al., *Nature (London)* **373**, 407 (1995); Y. Tomioka et al., *Phys. Rev. Lett.* **74**, 5108 (1995); H. Kuwahara et al., *Science* **272**, 80 (1996); R.D. Sanchez et al., *Appl. Phys. Lett.* **68**, 134 (1996).
5. A.J. Millis, P.B. Littlewood, and B.I. Shraiman, *Phys. Rev. Lett.* **74**, 5144 (1995); A.J. Millis, *Phys. Rev. B* **53**, 8434 (1996). A.J. Millis, B.I. Shraiman, and R. Mueller, *Phys. Rev. Lett.* **77**, 175 (1996).

6. H. Roder, J. Zang, and A.R. Bishop, *Phys. Rev. Lett.* **76**, 1356 (1996); Y.X. Jia et al., *Phys. Rev. B* **52**, 9147 (1996).
7. R.M. Kusters, D.A. Singleton, R. McGreevey, and W. Hayes, *Physica (Amsterdam)* **155B**, 362 (1982); R. von Helmolt, J. Wecker, B. Holzapfel, L. Schultz, and K. Samwer, *Phys. Rev. Lett.* **71**, 2331 (1993); J.M.D. Coey, M. Viret, L. Ranno, and K. Ounadjeda, *Phys. Rev. Lett.* **75**, 3910 (1995); M.F. Hundley, M. Hawley, R.H. Hefner, Q.X. Jia, J.J. Neumeier, J. Tesmer, J.D. Thompson, and X.D. Wu, *Appl. Phys. Lett.* **67**, 860 (1995); J.M. De Teresa, M.R. Ibarra, P.A. Algarabel, C. Ritter, G. Marquina, J. Blasco, J. Garcia, A. del Moral, and Z. Arnold, *Nature (London)* **386**, 256 (1997).
8. S.J.L. Billinge, R.G. DiFrancesco, G.H. Kwei, J.J. Neumeier, and J.D. Thompson, *Phys. Rev. Lett.* **77**, 715 (1996); Y. Yamada, O. Hino, S. Nohdo, and R. Kanao, *Phys. Rev. Lett.* **77**, 901 (1996); G. Zhao, K. Conder, H. Keller, and K. A. Müller, *Nature (London)* **381**, 676 (1996).
9. S.B. Oseroff, M. Torikachvili, J. Singley, S. Ali, A.-W. Cheong and S. Schultz, *Phys. Rev. B* **53**, 6521 (1996); C. Rettori, D. Rao, J. Singley, D. Kidwell, S.B. Oseroff, M.T. Causa, J.J. Neumeier, K.J. McClellan, S.-W. Cheong and S. Schultz, *Phys. Rev. B* **55**, 3085 (1997).
10. A. Urushibara, Y. Moritomo, T. Arima, A. Asamitsu, G. Kido, Y. Tokura, *Phys. Rev. B* **51**, 14103 (1995).
11. M.S. Seehra, *Rev. Sc. Inst.* **39**, 1041 (1968).
12. L.M. Paulius, C.C. Alamanas, and M.B. Maple, *Phys. Rev. B* **47**, 11627 (1993); Y. Kopelevich and S. Mochlecke, *Physica C* **253**, 325 (1995).
13. S. Spagna, D.M. Pratt, R.E. Seger, J. Diederichs, and C. Rettori, *Czech. J. of Phys.* **46**, 2805 (1996).
14. J. Tanaka, H. Nozaki, S. Oriuchi, and M. Tsukioka, *J. Physique Lett.* **44**, L129 (1983).
15. S.E. Loafand, S.M. Bhagat, H.L. Ju, C.G. Xiong, T. Venkatesan, R.L. Greene, *Phys. Rev. B* **52**, 15058 (1995); M. Dominguez, S.E. Loafand, S.M. Bhagat, A.K. Raychaudhuri, H.L. Ju, T. Venkatesan, R.L. Greene, *Solid State Commun.* **97**, 193 (1996).
16. D.L. Huber, and M.S. Seehra, *J. Phys. Chem. Solids* **36**, 723 (1975).
17. A. Shengelaya, Guo-meng Zhao, H. Keller, and K.A. Müller, *Phys. Rev. Lett.* **77**, 5296 (1996).
18. N.P. Raju, J.E. Greidan, and M.A. Subramanian, *Phys. Rev. B* **49**, 1086 (1994); Y. Shimakawa, Y. Kubo, T. Manako, Y.V. Sushko, D.N. Argyriou, and J.D. Jorgensen, *Phys. Rev. B* **55**, 6399 (1997).
19. M.T. Causa et al., *to be published*.

Seção 2.8

2.8 Estudos de RPR e FMR
(Ressonância Ferromagnética) nos
compostos Laminares:
 $\text{La}_{1.2}\text{Sr}_{1.8}\text{Mn}_2\text{O}_7$ - (submetido para
Phys. Rev. B. em 17/02/1999)

**2.8) Estudos de RPR e FMR (Ressonância Ferromagnética) nos compostos Laminares:
 $\text{La}_{1.2}\text{Sr}_{1.8}\text{Mn}_2\text{O}_7$ (submetido para Phys. Rev. B em 17/02).**

EPR and FMR studies in layered manganite: $\text{La}_{1.2}\text{Sr}_{1.8}\text{Mn}_2\text{O}_7$

N. O. Moreno, P. G. Pagliuso, and C. Rettori

Instituto de Física "Gleb Wataghin", UNICAMP, 13083-970, Campinas-SP,

Brazil.

J.S. Gardner, J.L. Sarrao, and J.D. Thompson

Los Alamos National Laboratories, Los Alamos, NM 87545, U.S.A.

A. Garcia-Flores* and S.B. Oseroff

San Diego State University, San Diego, CA 92182, U.S.A.

Abstract

We have performed EPR and dc magnetization measurements on single crystals of $\text{La}_{1.2}\text{Sr}_{1.8}\text{Mn}_2\text{O}_7$. Similar to previous authors, we found an increase in the magnetization, M , near 300 K, a temperature well above $T_C \approx 125$ K. Previously, this high temperature (≈ 300 K) transition has been suggested to be intrinsic to the system. We have observed at these high temperatures the appearance of new ferromagnetic resonance modes, FMR. Within the experimental error the volume of sample required to explain the extra M and the intensity of the FMR modes is the same. Furthermore, the EPR data do not show any feature above T_C that could be associated to short-range order of the $\text{La}_{1.2}\text{Sr}_{1.8}\text{Mn}_2\text{O}_7$ phase. We conclude that the increase in M is due to the presence of extrinsic Rudlesden-Popper (RP) phases and not to intrinsic effects as has been claimed.

pacs 78.30.-j, 75.30.-m, 63.20.-e, 72.10.Di

Typeset using REVTeX

The observation of colossal magnetoresistance, CMR, in the series of Ruddlesden-Popper (RP) phases [1], $\text{A}_{n+1}\text{Mn}_n\text{O}_{3n+1}$, has attracted considerable attention. Most of the work was done in the perovskite manganite, $\text{La}_{1-x}\text{Sr}_x(\text{Ca})\text{MnO}_3$ ($n = \infty$). Recently, the $n = 2$ member, $\text{A}_3\text{Mn}_2\text{O}_7$, has received considerable attention due to their interesting and somewhat unusual properties. The RP phases consist of n layers of perovskite octahedra blocks along the c -axis. The blocks are separated by the insertion of rock-salt layers of A_2O_2 , which lead to a larger c -axis. Moritomo *et al.* [2] observed CMR in the layered $\text{La}_{1.2}\text{Sr}_{1.8}\text{Mn}_2\text{O}_7$ at $T_C \sim 125$ K, that nominally correspond to 40 % of holes. Those authors claimed that the intra-layer exchange interaction was due to double exchange and that intrinsic 2D spin-correlations were present well above the ferromagnetic (FM) transition temperature T_C . Several authors have reported a significant increase of the magnetization, M , at ~ 300 K, in $(\text{La},\text{Sr})_3\text{Mn}_2\text{O}_7$. This feature was associated, in most cases, with 2D spin correlations, and is claimed to be intrinsic to the system. Kimura *et al.* [3] reported on the existence of two intrinsic transitions in $\text{La}_{1.4}\text{Sr}_{1.6}\text{Mn}_2\text{O}_7$. One at ~ 270 K, a temperature below which the system behaves like a 2D-FM metal, and another at ~ 100 K, where 3D ordering is observed due to low-field interplane tunneling. Perring *et al.* [4] suggested the presence of weak antiferromagnetic correlations within the planes coexisting with ferromagnetic fluctuations well above T_C . Zhou *et al.* [5] interpreted the increase of M as an indication of either superparamagnetism clusters or short-range FM ordering. Kelley *et al.* [6] reported on quasi-elastic magnetic scattering well above T_C . Heffner *et al.* [7] did not find evidence of 2D spin ordering or in-plane correlations above T_C in their muon spin relaxation studies. Potter *et al.* [8] observed two transitions, but argued that the high temperature transition was not intrinsic to the $n = 2$ system, and was associated with intergrowths of other RP phases. Finally, we note that the volume fraction, assuming FM order, required to explain the high temperature transition vary from 0.1 % to several percent among the different reports on $(\text{La},\text{Sr})_3\text{Mn}_2\text{O}_7$.

Electron Paramagnetic Resonance, EPR, has proved to be a sensitive technique, capable of examining the presence of small amounts of impurity phases in a variety of systems.

In the high T_C superconductors the presence of 1 μg of the green phase R_2BaCuO_5 , is easily observed. [9] A mass of less than 100 μg is sufficient to see the resonance line in $\text{La}_{0.67}\text{Sr}_{0.33}\text{MnO}_3$. [10] Thus, EPR allows the study of compounds for which it is difficult to obtain homogenized samples of large size. We have used EPR to study the $n = 2$ compounds and have tried to clarify the discrepancies in the interpretation of the data reported in the literature.

We have carried out EPR and dc magnetization measurements on two "high quality single crystals" of $\text{La}_{1.2}\text{Sr}_{1.8}\text{Mn}_2\text{O}_7$. Each presented a different increase of the M at high T , relative to their saturation M below T_C . In order to prepare the crystals polycrystalline materials were synthesized by a solid-state reaction of stoichiometric quantities of MnO_2 , SrCO_3 , and La_2O_3 at temperatures up to 1550 degrees Celsius in air. Polycrystalline material was shown from X-ray diffraction to be free of other members of the Ruddlesden-Popper series (< 3% by volume). The polycrystalline compounds were then used as starting materials for the crystal growth. Crystals of $\text{La}_{1.2}\text{Sr}_{1.8}\text{Mn}_2\text{O}_7$ were melt grown in a flow of O_2 using a floating zone optical image furnace. The resulting boule contained many shiny black crystals that could easily be cleaved away. The EPR experiments were carried out in a Bruker spectrometer at 9.4 GHz in the range of temperature between 100 K and 700 K. The M data were taken in a MPMS-5 Quantum Design SQUID magnetometer between 2 K and 400 K.

Figure 1 shows M vs T for two crystals (1 and 2) of $\text{La}_{1.2}\text{Sr}_{1.8}\text{Mn}_2\text{O}_7$ with $H = 3$ Oe applied parallel to the $[a,b]$ plane. The lower transition occurs at $T_C \sim 125$ K. A sudden increase of M for $T \gg T_C$ is measured for both samples at $T = T_C^*$. The inset displays M vs T for the high T region. The differences in the M between both samples is large in this T range. At ~ 200 K, the M of sample 1 is about one order of magnitude smaller than in sample 2. A small step in the M , centered at ~ 280 K, is seen for sample 1. In sample 2, no less than four steps are observed between ~ 260 K and 320 K. Fig. 2 presents hysteresis loops for both crystals with $T = 270$ K and $H // [a,b]$. The inset shows loops for $H // c$. For clarity, in all cases the paramagnetic contribution of the system has been subtracted. The saturation magnetic moment measured at 20 kOe for both samples in the three directions,

below T_C , is $\sim 3.6(1)\mu_B/\text{Mn}$. The volume of sample required for the increase of the M above T_C can be estimated from the number of Bohr magnetons obtained from the hysteresis loops seen in Fig. 2, normalized by the saturation magnetic moment measured at high field. The volumes obtained are $\lesssim 0.03\%$ and $\sim 0.25\%$ for samples 1 and 2, respectively.

A dysonian resonance line, with $g = 2.0$, is observed for $T \sim T_C^* + 20$ K. Its intensity, I , follows the same T dependence of $\chi_{dc}(T)$, as observed in the perovskites and pyrochlore manganites. [10] Thus, all the Mn ions contribute to the EPR line. At lower T , the appearance of new resonances modes, FMR, are observed. In Fig. 3, the spectra for sample 1 with $H // a$ are given for several T . At ~ 310 K new resonances lines emerge from $g = 2$, which shift to lower field as T decreases and collapse into a single line at ~ 240 K. In the inset of Fig. 3 we present the I vs. T of the EPR line, that remains at $g = 2.0$ down to T_C , and the FMR modes that appear at high T . In Fig. 4, the EPR spectra for sample 2 is shown. In this case, the first appearance of the FMR occurs at $T \sim 350$ K, and new modes continue to appear down to ~ 260 K. For sample 2, the modes do not overlap into a single line down to 150 K. For both samples, the increase of I vs T of the FMR lines is similar to the increase found for M below T_C^* . Thus, the increase of the M below T_C^* is associated with the appearance of the FMR lines. The FMR lines are first seen at T higher than T_C^* , due to the higher sensitivity of EPR. As T approaches T_C , the main line at $g = 2.0$ shifts to lower field and its intensity grows dramatically. For $T \leq T_C$, the M extracted from the I of the main line is in excellent agreement with the M measured under similar conditions. The volume fraction required, for both samples, to explain the extra M observed at high T and the I of the FMR modes, is the same within experimental error. The hysteresis loops with virtually zero remnant field and the T dependence of the FMR modes are typical of FM materials or systems with FM regions. Thus, the origin of the features described above, are due to small regions which order ferromagnetically in the samples and are not associated with intrinsic short-range correlations as was previously claimed.

In Figs. 3 and 4, we only show the EPR spectra for $H // a$. We have measured also the angular dependence of the EPR spectra. We found no angular dependence for $T > T_C^*$.

But for $T < T_C^*$, the spectra associated to the FMR lines are only isotropic in the $[a,b]$ plane. A T dependent anisotropy is measured when H is rotated toward the c -axis. The lines shift to higher field and go through a maximum for $H // c$ ($H \sim 10$ kOe, at $T \sim 250$ K). The angular dependence measured is almost the same for both samples, suggesting that the FMR lines result from similar type of intergrowths. The difference in intensity is due to the amount of intergrowth in each sample. In sample 2, another FMR spectra is observed, corresponding to only $\sim 0.003\%$ of the sample, but that region has c as an easy axis (as found for $\text{La}_{1.4}\text{Sr}_{1.6}\text{Mn}_2\text{O}_7$). [3]

In summary, the increase of M and the I of the FMR modes varies by two orders of magnitude, from 0.03% to several %, between data reported by different groups. Thus, this effect is sample dependent, i.e. extrinsic to the $n = 2$ phase. Therefore, in agreement with Potter *et al.* [8], we conclude that the origin of the increase in M is due to RP phases with $n \geq 3$, as $n = 1$ orders antiferromagnetically. The distribution of T , at which the different FMR modes first appear, suggests the presence of intergrowths with different values of n and/or hole (Sr) concentration. In our case, these temperatures vary between ~ 290 K - 310 K and ~ 260 K - 360 K, for samples 1 and 2, respectively. That is, the intergrowths of sample 1 have a smaller distribution of n and/or holes than sample 2. The similar angular dependence found for the FMR modes for both samples is indicative of small crystals whose origin is the same. Furthermore, we did not observe an increase in the I or lineshape distortions of the $g = 2.0$ resonance of $\text{La}_{1.2}\text{Sr}_{1.8}\text{Mn}_2\text{O}_7$ above 140 K, that could be associated to short range ordering. Consequently, if any short-range ordering intrinsic with the $n = 2$ phase is present at T_C^* , it is negligible, aside from that expected between the Mn ions.

This work was supported by FAPESP grant No 95/4721-4, No 97/03065-1 São Paulo-SP-Brazil, CAPES-Brazil, NSF-INT No 9602829, and NSF-DMR No 9705155. Work done at Los Alamos was conducted under the auspices of the U.S. DOE. J.S.G. thanks Dr. K. McClellan and J.M. Roper for assistance with the crystal growths. AGF thanks Ministerio de Educacion y Cultura of Spain.

* Present address: Departamento de Física Aplicada, Universidad de Salamanca, Spain.

REFERENCES

- [1] S. N. Riddlesden, and P. Popper, *Acta Crystallgr.* **11**, 54 (1958).
- [2] Y. Moritomo, A. Asamitsu, H. Kuwahara, and Y. Tokura, *Nature (London)* **380**, 141 (1996).
- [3] T. Kimura, Y. Tomioka, H. Kuwahara, A. Asamitsu, M. Tamura, and Y. Tokura, *Science* **274**, 1698 (1996).
- [4] T. G. Perring, G. Aeppli, Y. Moritomo, and Y. Tokura, *Phys. Rev. Lett.* **78**, 3197 (1997).
- [5] J.-S. Zhou, J. B. Goodenough, and J. F. Mitchell, *Phys. Rev. B* **58**, 579 (1998); J. S. Zhou, and J. B. Goodenough, *Phys. Rev. Lett.* **80**, 2665 (1998).
- [6] T. M. Kelley, D. N. Argyriou, R. A. Robinson, H. Nakotte, J. F. Mitchell, R. Osbron, and J. D. Jorgensen, *Physica B* **241-243**, 439 (1998).
- [7] R. H. Heffner, D. E. MacLaughlin, G. J. Nieuwenhuys, T. Kimura, G. M. Luke, Y. Tokura, and Y. J. Uemura, , *Phys. Rev. Lett.* **81**, 1706 (1998).
- [8] C. D. Potter, M. Swiatek, S. D. Bader, D. N. Argyriou, J. F. Mitchell, D. J. Miller, D. G. Hinks, and J. D. Jorgensen, *Phys. Rev. B* **57**, 72 (1998).
- [9] D. C. Vier, S. B. Oseroff, C. T. Salling, J. F. Smyth, S. Schultz, Y. Dalichaouch, B.W. Lee, M. B. Maple, Z. Fisk, and J. D. Thompson, *Phys. Rev. B* **36**, 8888 (1987).
- [10] M. T. Causa, M. Tovar, A. Caneiro, F. Prado, G. Ibanez, C. A. Ramos, A. Butera, B. Alascio, X. Obradors, S. Pinol, F. Rivadulla, C. Vazquez, A. Lopez-Quintela, J. Rivas, Y. Tokura, and S. B. Oseroff, *Phys. Rev. B* **58**, 3233 (1998); M. T. Causa, G. Alejandro, M. Tovar, P. G. Pagliuso, C. Rettori, S. B. Oseroff, and M. A. Subramanian, to appear in *J. of Applied Physics* **85**, April (1999).

FIGURES

FIG. 1. The M vs T measured at 3 Oe with $H // [a, b]$ is given for both samples. The inset displays M vs T for the high T region. Notice, that the sudden increase of M occurs at different T for samples 1 and 2, ~ 280 and 330 K respectively. At 200 K the M is about one order of magnitude smaller for sample 1 (the smallest value of M reported in the literature) than in sample 2.

FIG. 2. Hysteresis loops for both samples with $H // [a, b]$ are shown. In the inset, loops for $H // c$ are shown. Notice the different in H for $H // [a, b]$ and $H // c$. The paramagnetic contribution has been subtracted in all cases.

FIG. 3. The EPR spectra for sample 1 with $H // a$ are given for several T . The resonance lines with $g = 2$ for 280 K and 240 K have been deleted to include the inset. The inset gives the I vs T of the EPR line and the FMR modes. The integrated I of the FMR modes has been multiplied by a factor of 3500 , the solid line is a guide to the eye. In the inset is not shown that the I of EPR line saturates below ~ 110 K.

FIG. 4. The EPR spectra for sample 2 with $H // a$ are given for several T . Notice that the FMR modes appear at a higher T than in sample 1 and their relative intensity to the $g = 2.0$ resonance is larger than in sample 1 (see Fig. 3).

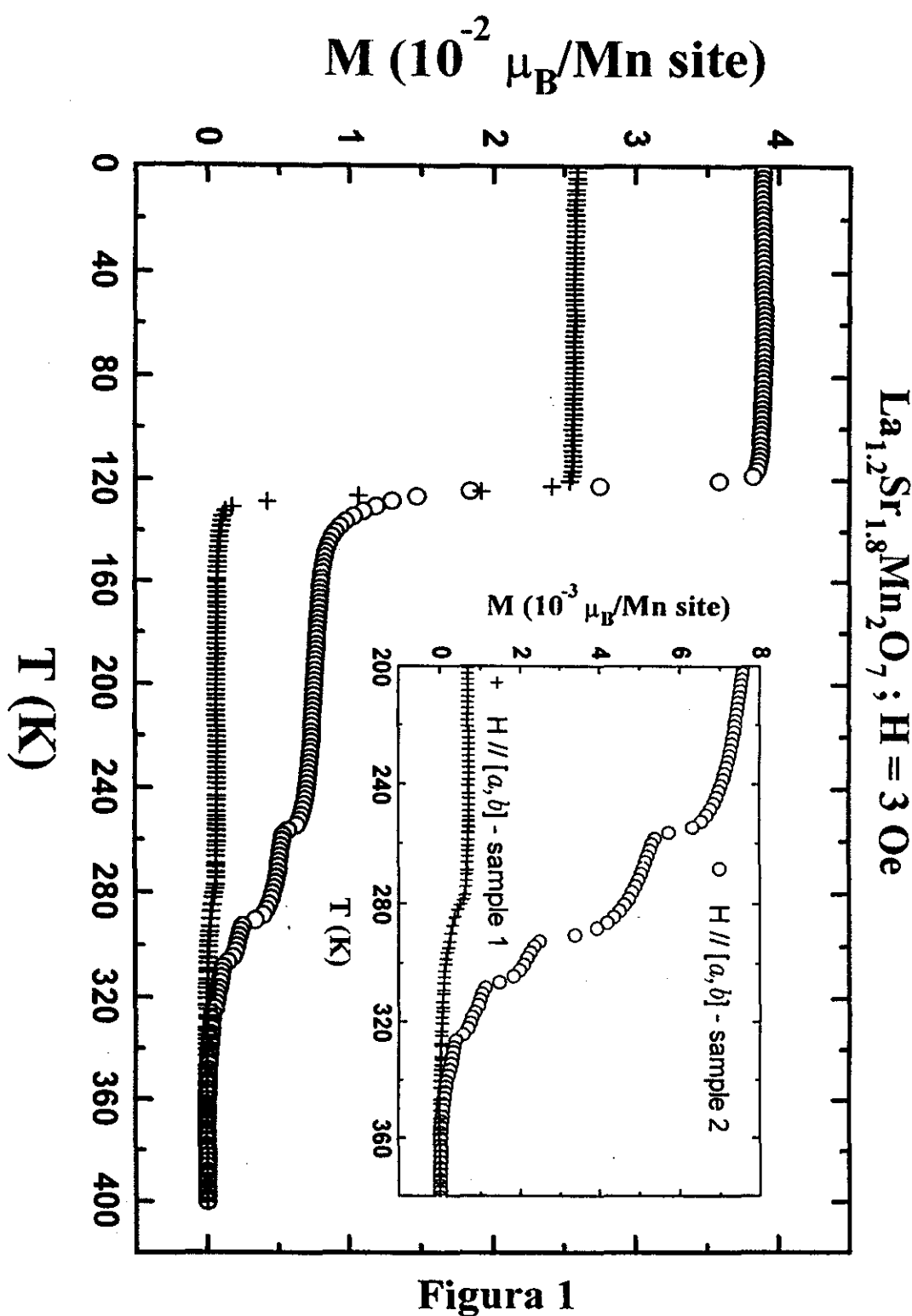


Figura 1

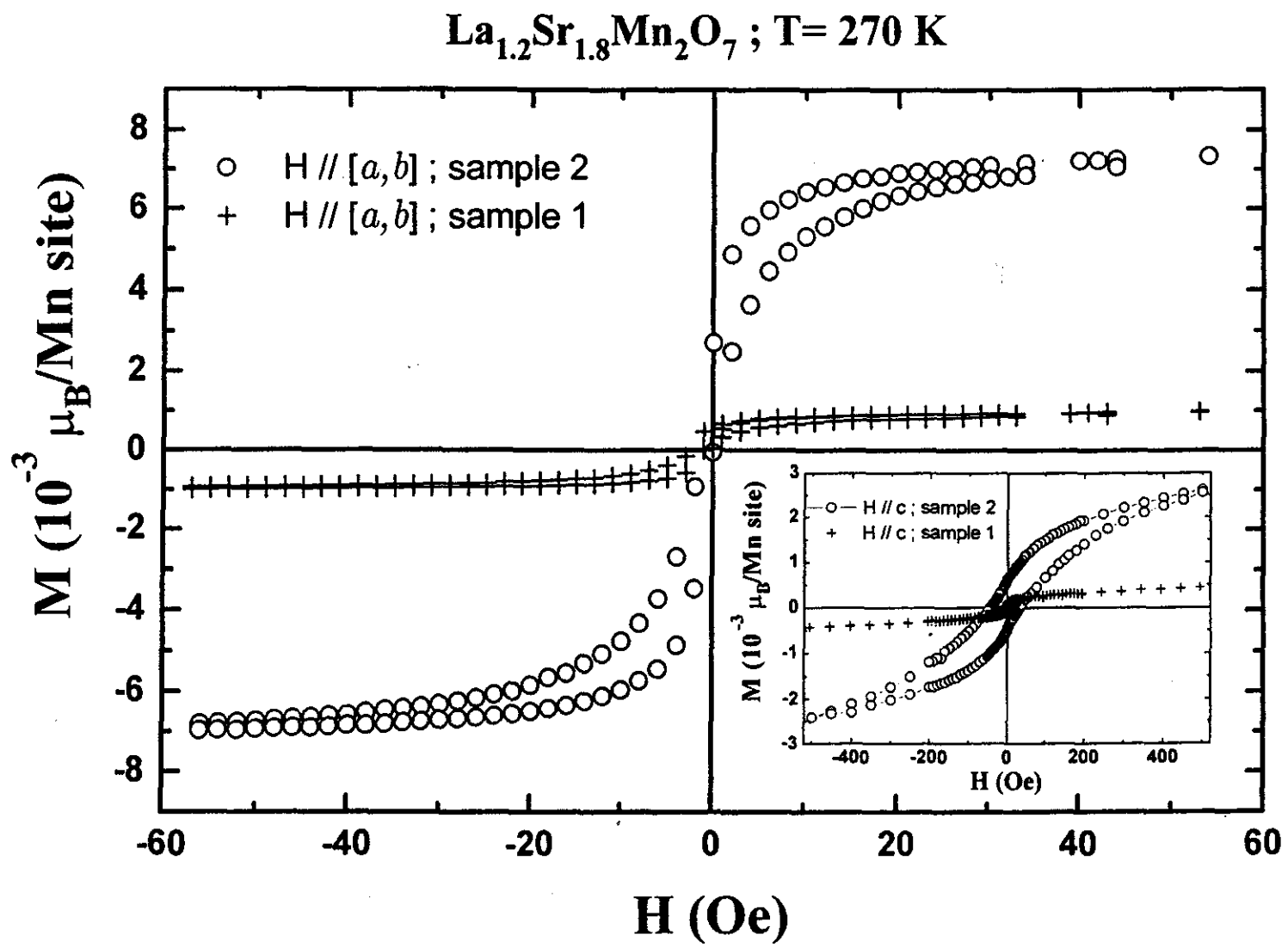


Figura 2

Abs. Derivative (arb. units)

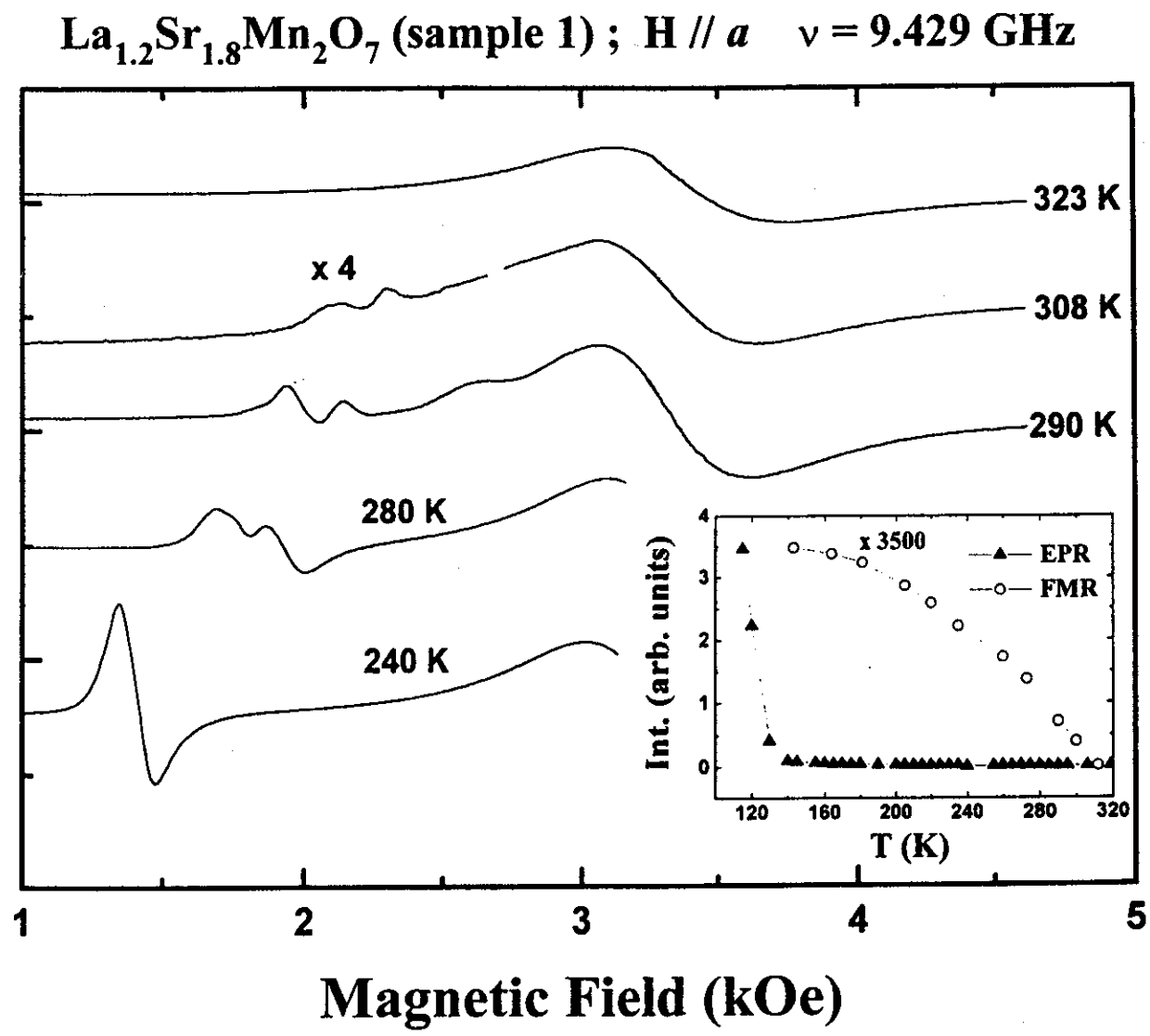


Figura 3

$\text{La}_{1.2}\text{Sr}_{1.8}\text{Mn}_2\text{O}_7$ (sample 2) $H \parallel a$ $\nu = 9.43$ GHz

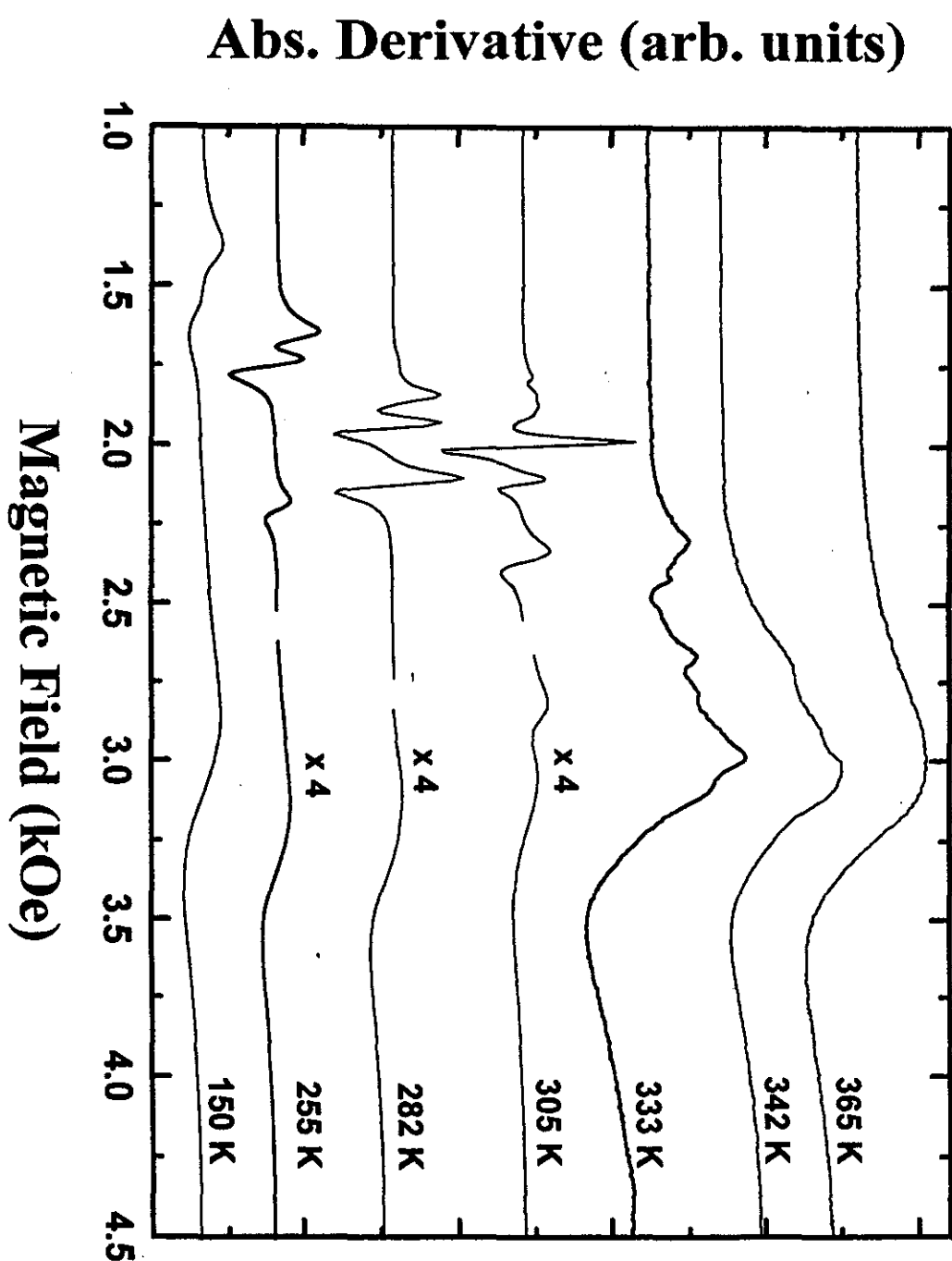


Figura 4

Capítulo 3

CONCLUSÃO GERAL

3) CONCLUSÃO GERAL

Como primeria conclusão poderíamos afirmar que para os compostos estudados a técnica de RPE se mostrou bastante funcional para os estudos de interações entre as impurezas magnéticas e os elétrons de condução além de se revelar bastante sensível a detecção de fases espúrias magnéticas. Assim, creio que os profissionais da área da fisica de estado sólido devem procurar utilizar mais frequentemente a técnica de RPE como técnica de investigação auxiliar nos seus estudos uma vez, que cada vez mais, esta técnica tem passado a ser instrumento de investigação exclusivo de químicos e biólogos.

Passamos agora a um resumo das conclusões obtidas para os diferentes sistemas estudados neste doutoramento.

Nos estudos dos compostos de $\text{Eu}_{2-x}\text{Pr}_x\text{CuO}_4$, uma sistemática de experimentos de magnetização para $0 \leq x \leq 1$ em monocrystalis crescidos em cadinhos de Pt e de Al_2O_3 com fluxos de CuO e PbO , permitiu-nos estudar o aparecimento de uma componente de WF neste materias. Modos Raman “proibidos” foram somente observados em amostras que apresentam WF.

Neste trabalho concluiu-se que para volumes de célula unitária menores que um volume crítico $V_C \approx 181.1 \text{ A}^3$ (próximo ao valor de V para Eu_2CuO_4 crescido em $\text{Al}_2\text{O}_3/\text{CuO}$) a estrutura T' destes compostos apresentam distorções locais nos planos de CuO_2 dando origem a componente WF e as modos Raman “proibidos”. Além do mais, para as amostras crescidas em Pt, as impurezas de Pt substitucionais ao Cu, favorecem as distorções locais nos planos de CuO_2 favorecendo o aparecimento do WF e dos modos Raman “proibidos”.

Para o caso dos materias supercondutores $\text{RNi}_2\text{B}_2\text{C}:Gd$ ($R = Y, \text{Lu}$), os valores obtidos para os parâmetros $\langle J_{\beta\beta}^2(q) \rangle^{1/2}$, extraídos dos estudos da dependência com temperatura da largura de linha de RPE do Gd^{+3} e do decréscimo de T_C com o aumento da concentração de impureza magnética (AG) coincidem dentro do erro experimental. Este resultado indica que os compostos $\text{RNi}_2\text{B}_2\text{C}$ ($R = Y, \text{Lu}$) comportam-se como um supercondutor BCS convencional.



Nestes compostos a interação de troca Gd^{+3} e os elétrons de condução (c-e) foi encontrada dependente do vetor de onda q , e o parâmetro $J_{fs}(0)$ é positivo para ($R = Y, Lu$) indicando que a interação Gd^{+3} - c.e. é tipo atômica. As interações elétron-elétron, se mostraram significativas para as análises dos espectros de RPE, ($\alpha = 0.3$ para Lu e ($\alpha = 0.2$ para o Y) para os materiais supercondutores RNi_2B_2C ($R = Y, Lu$).

Nos estudo de RPE do Gd^{+3} nos compostos de valência intermediária $YbInCu_4$ e no tipo Rede de Kondo $YbAgCu_4$ e sus compostos de referência (Y, Lu)(In, Ag) Cu_4 observamos um aumento do g-shift e taxa de Korringa para os compostos de Yb em relação aos de referência. Este resultado é atruído ao aumento da densidades de estados no nível de Fermi existentes para os compostos de Yb .

Para ambos os sistemas acima, a interação de troca Gd^{+3} e os c-e é dependente do vetor de onda q , e o parâmetro $J_{fs}(0)$ é positivo, indicando que a interação Gd^{+3} - c.e. é tipo atômica. No entanto, somente para o composto de valência intermediária, $YbInCu_4$, interações elétron-elétron, se mostraram significativa para as análises dos espectros de RPE. ($\alpha = 0.7(2)$). Para o composto tipo rede de Kondo não foi necessário considerar as interações elétron-elétron para analisar os dados de RPE.

Para o estudo dos compostos $LuInNi_4:Gd$ e Nd uma contribuição tipo multibanda foi necessária para as análises de RPE. A interação de troca entre a RE e os c-e é negativo para a banda-d (J_{fd}) e indicando que a interação RE - c.e. é tipo covalente, e positivo para a banda-s (J_{fs}) indicando que para este caso a interação é tipo iônica. O valor de J_{fs} é maior para o Nd^{3+} em relação ao Gd^{3+} para ambos os compostos, provavelmente devido ao maior contato com os c.c. resultado do maior raio das camadas 4f do Nd^{3+} . A banda eletrônica d para o caso do compostos de Ni, é provavelmente proveniente das camadas 3d incompletas do íon de Ni.

Como continuação deste trabalho medidas de RPE de Gd^{+3} e Nd^{3+} podem ser realizadas no compostos $YbInNi_4$, no entanto nossos resultados no compostos de Lu permitem concluir que contribuições de multi-banda eletrônica serão necessárias para o entendimento das propriedades físicas do férmion pesado $YbInNi_4$.



No composto YBiPt, observamos a ausência de korringa e g-shift nos estudos de RPE do Gd^{+3} e Nd^{+3} em concordância com o caráter semicondutor do material. O ajuste dos dados de susceptibilidade magnética nos permitiu obter os parâmetros de campo cristalino cúbico A_4 e A_6 para os compostos $Y_{0.9}Nd_{0.1}BiPt$ e $Y_{0.9}Yb_{0.1}BiPt$. Valores obtidos por outros para $YbBiPt$, $PrBiPt$ e $Y_{0.995}Er_{0.005}BiPt$ foram usados para comparação. As diferenças encontradas para os valores de A_4 e A_6 podem ser atribuídas à variação do parâmetro de rede e/ou ao aumento do caráter metálico para terras raras mais pesadas. Um limite superior para o parâmetro de campo cristalino $|b_4| \sim 1$ Oe, obtido da largura de linha, para o caso Gd, foi estimado. Nossos resultados sugerem que pequenos valores $|b_4|$ podem ser características de semicondutores da gap pequeno ou semimetais com baixa densidade de portadores.

Um possível trabalho subsequente é então a preparação de compostos dopados com Yb, $(Y, Lu)_{1-x}Yb_xBiPt:Gd$ ($0 < x < 1$), onde o caráter metálico é introduzido nos compostos pela dopagem de Yb. Os estudos de RPE destes compostos podem revelar o aparecimento de g-shift, korringa e efeitos de campo cristalino na ressonância do Gd^{3+} para as amostras mais metálicas (maior γ).

Para as diferentes amostras $R_{1-x}A_xMnO_3$ ($R = La, Pr$; $A = Ca, Sr$) os "loops" de histerese e os "splittings" de linha de RPE observados foram associados a inhomogeneidades das amostras provenientes de uma distribuição não aleatória de vacâncias, defeitos e conteúdo de oxigênio gerando principalmente uma distribuição de T_c nas amostras. Amostras com transições magnéticas bem estreitas apresentam uma única linha de RPE para $T > T_c$ e os loops de histerese desaparecem para tais temperaturas.

Também, para os cristais CMR de $La_{1.2}Sr_{1.8}Mn_2O_7$, a linha de ressonância FMR observada bem como a transição magnética a ~ 280 K foram atribuídas a fases extrínsecas provavelmente provenientes de fases de $La_{n+1}Mn_nO_{3n+1}$ com $n \neq 2$. Da análise das intensidades das linhas de EPR e FMR os volumes das fases espúrias foram estimados como $\sim 0.03\%$ do volume total da amostra # 1 e $\sim 0.25\%$ para a amostra # 2. Estes valores de porcentagem concordam com os obtidos através da comparação da magnetização de saturação das transições magnéticas a ~ 280 K e ~ 125 K. A convergência das linhas FMR para

a EPR para $T < \sim 280$ K apresenta as mesmas características dos "splittings" de linha de RPE observados para os compostos $R_{1-x}A_xMnO_3$ ($R = La, Pr$; $A = Ca, Sr$) para $T > T_c$.

Concluindo, creio que meu doutoramento propiciou uma formação muito boa no que diz respeito ao entendimento das propriedades magnéticas macroscópicas e microscópicas destes sistemas de alta correlação eletrônica, e para um futuro Post-Doc acredito que seria muito enriquecedor para a minha formação, realizar estudos de propriedades de transporte nestes sistemas, usando diferentes faixas de pressões (até 10 Kbar) e campos magnéticos (até 20 T - dc e 60 T - pulsado); estudos estes muito importantes no entendimento das propriedades físicas de sistemas de alta correlação. É meu objetivo também no pós-doutoramento aprender a desenvolver toda a sistemática de preparação e caracterização das amostras, principalmente na forma monocrystalina, trazendo para o Brasil a possibilidade de que amostras monocrystalinas de alta qualidade destes materiais possam ser preparadas aqui.



Apêndice 1

Aparato Experimental

A1.1) Espectrômetro de R.P.E.

Passamos agora a descrever de forma simplificada o aparato de laboratório utilizado para as medições de RPE. (um pouco do fômeno em si, também será abordado).

O principal elemento deste aparato é o espectrômetro de ressonância, em volta do qual toda a sistemática do experimento é planejada e montada.

Desde o seu surgimento no período subsequente a segunda guerra mundial, os espectrômetros de ressonância eletrônica e nuclear têm se tornado uma técnica bastante utilizada. Houve, como consequência, um grande avanço na tecnologia dos radares (geradores de microonda, cristais detetores, amplificadores de banda estreita para detecção em fase, etc.) e na tecnologia básica de semicondutores. O estudo da absorção e da dispersão da radiação eletromagnética causadas pela precessão de momentos magnéticos nucleares ou eletrônicos de uma amostra, submetida a um campo magnético externo aplicado, têm possibilitado o acesso a informações da dinâmica magnética interna de substâncias, que muitas vezes, não têm nem mesmo suas estruturas cristalinas conhecidas.

A ressonância paramagnética eletrônica estuda basicamente sistemas que possuem um momento magnético localizado, dentre os quais se destacam aqueles relativos a íons de elementos do grupo de transição onde as camadas parcialmente cheias possuem elétrons não emparelhados. Dentre estes, podemos destacar os elementos do grupo do Ferro (3d), do grupo do Paládio (4d), dos grupos das terras raras (4f) e do grupo dos actinídeos (5f).

As transições magnéticas entre os diferentes níveis de energia separados ("splitting") por um campo magnético externo ocorrem pela aplicação de um campo magnético oscilante (de microondas) perpendicular ao campo fixo. Podemos então definir a dependência da susceptibilidade magnética com a frequência deste campo oscilante $H_1(t)$:⁶¹

$$\chi(\nu) = \chi'(\nu) - i\chi''(\nu) \quad [A1.1]$$



Temos então uma parte real χ' que corresponde a componente do momento magnético em fase com o campo oscilante $H_1(t)$ (dispersão), e uma parte imaginária χ'' correspondente a componente em contra-fase do momento em relação ao campo (absorção). A potência média absorvida pelos momentos magnéticos é:⁶¹

$$P \propto \chi'' \cdot H_1(t)$$

[A1.2]

O princípio do espetrômetro é então, a detecção da potência absorvida em função do campo magnético H_0 aplicado (pode ser feito também em função da frequência de microonda). Portanto a descrição de seu funcionamento pode ser resumida à forma de detecção da absorção de microonda.

Uma radiação de microonda é gerada com uma frequência bem definida. Depois esta radiação é atenuada e levada até uma cavidade ressonante metálica, dentro da qual se localiza a amostra. A microonda refletida é então conduzida até um cristal detetor. A partir de então temos um sinal que pode fornecer uma função $P(H)$, desde que utilizemos uma frequência fixa, e um campo estacionário variável. A faixa de variação deste campo geralmente está entre 0 e 20.000 Gauss, partindo-se sempre do campo zero e crescendo linearmente.

A microonda é gerada por um "Klystron" (gerador baseado numa válvula com este nome) no caso do espetrômetro de fabricação da Varian, operando na faixa de 8.8 a 9.6 GHz de frequência (banda-X), e com 200mw de potência máxima. No espetrômetro Bruker a microonda é gerada por um dispositivo eletrônico conhecido como diodo Gun para cada banda S (4.0 GHz), X (9.5 GHz) e Q (34 GHz). A radiação é então direcionada por um circulador (que permite que o sinal passe num só sentido), nivelada por um sistema de controle de potência ("power leveler"), dividida em um feixe que é atenuado e mandado para a cavidade e outro que é atenuado e utilizado num acoplador direcional para a detecção do sinal refletido pela amostra. Dois sistemas de modulação diferentes frequência estão conectados em paralelo com as bobinas de modulação. O sinal detectado é pré-amplificado e enviado a unidade de



modulação, através de um sistema seletor que processa o sinal, convertendo-o numa diferença de potencial (d.c.) que é conectada ao eixo y do registrador.

Um outro sistema importante no espetrômetro é o Controle Automático de Frequência (CAF na figura-A1.1) que consiste de um pré-amplificador, um amplificador, um detetor e um refletor. Este aparato é utilizado na estabilização das flutuações entre a frequência do "Klystron" ou do diodo Gun e a frequência de ressonância da cavidade.

Isto é feito através da modulação da frequência de microondas por um sinal de 70 Hz aplicado ao refletor do "Klystron", que possibilita que se obtenha no sistema de detecção um sinal modulado em amplitude, que ao ser amplificado é comparado por detecção de fase, sendo corrigido proporcionalmente ao desvio de frequência.

A maioria dos espetrômetros de RPE têm como forma de linha registrada., a derivada da linha de absorção. Isto acontece pela utilização de um detetor sensível a fase ("lock-in detector"). Entre as vantagens obtidas (para medidas de RPE) , têm-se a possibilidade de maior precisão na medida da largura de linha (que neste caso é a distância entre os dois picos).

Utilizamos neste trabalho um espetrômetro Varian (E112) e um Bruker ELEXSYS unidos a uma cavidade ressonante retangular E-231 com modo de operação TE 102.



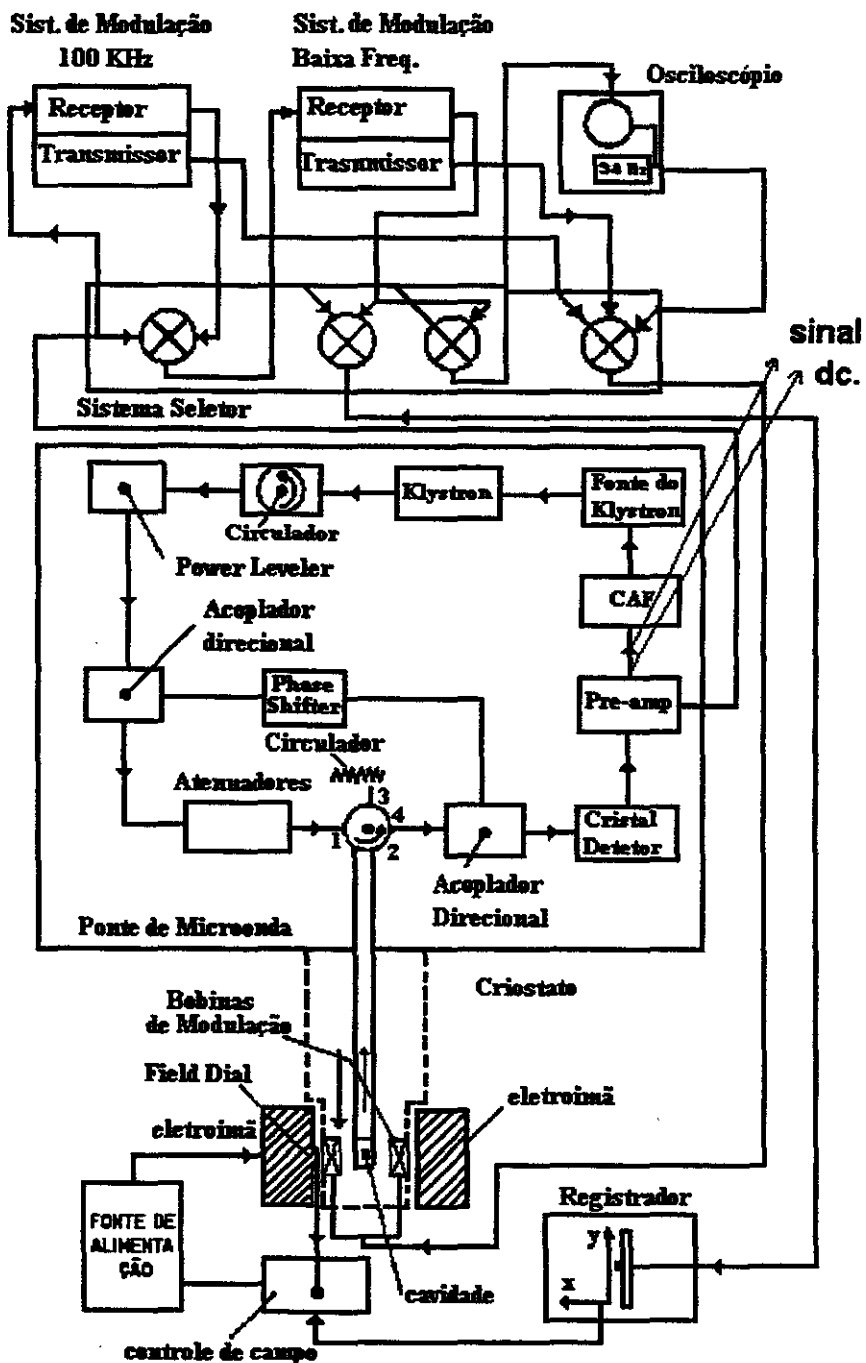


Fig-3a.1- Esquema em blocos do Espectrômetro de R.P.E.

4) REFERÊNCIAS

- 1 J.G. Bednorz and K.A. Muller, Z. Phys. **B64**, 189 (1986)
- 2 M.K. Wu, J.R. Ashburn, C.J. Torng, P.H. Hor, R.L. Meng, L.Gao, Z.J. Huang, Y.Q. Wang and C.W. Chu, Phys. Rev. Lett. **58**, 908 (1987). Proc. of Novel Mechanisms of Superconductivity (June 22-24, 1987 Berkeley) Plenum Publishing Corporation N.Y. (1987).
- 3 Y.J. Uemura, W.J. Kossler, X.H. Yu, J.R. Kempton, H.E. Schone, D. Opie, C.E. Stronach, D.C. Johnston, M.S. Alvarez and D.P. Goshorn, Phys. Rev. Lett. **59**, 1045 (1987).
- 4 K.B. Lyons, P.A. Fleury, J.P. Remeika, A.S. Cooper and T.J. Negran, Phys. Rev. **B37**, 2353 (1988).
- 5 K. Yamada, K. Kakurai, Y. Endoh, T.R. Thurston, M.A. Kastner, R.J. Birgeneau, G. Shirane, Y. Hidaka and T. Murakami, Phys. Rev. **B40**, 4557 (1989).
- 6 Y. Endoh, K. Tamada, R.J. Birgeneau, D.R. Gabbe, H.P. Janssen, M./A. Kastner, C.J. Peters, P.J. Picone, T.R. Thurston, J.M. Tranquada, G. Shirane, Y. Hidaka, M. Oda, Y. Enomoto, M. Susuki and T. Murakami, Phys. Rev. **B37**, 7443 (1988).
- 7 K. Yamada, E. Kudo, Y. Endoh, Y. Hidaka, M. Oda, M. Susuki, and T. Murakami, Solid State Commun. **64**, 753 (1987).
- 8 S. Mitsuda, G. Shirane, J.K. Sinha, D.C. Johnston, M.S. Alvarez, D. Vaknin and D.E. Monoton, Phys. Rev. **B36**, 822 (1987).
- 9 Y. Tokura, H. Takagi and S. Uohida, Nature **337**, 345 (1989).
- 10 C. Rettori, D. Rao, S. Oseroff, G. Amoretti, Z. Fisk, S-W Cheong, D. Vier, S. Schultz, M. Tovar and R.D. Zysler, Phys. Rev. **B47**, 8156 (1993).
- 11 R.D. Zysler, M. Tovar, C. Rettori, D. Rao, H. Shore, S.B. Oseroff, D.C. Vier, S. Schultz, Z. Fisk and S-W Cheong. Phys. Rev. **B44**, 9467 (1991).
- 12 C. Rettori, S.B. Oseroff, D. Rao, J.A. Valdivia, G.E. Barberis, G.B. Martins, J. Sarrao and Z. Fisk. Accepted in Phys. Rev. **B**.
- 13 R. Najarajan et. al. Phys. Rev. Lett. **72**, 274 (1994).



- 14 R. J. Cava et. al, *Nature (London)* **367**, 146 (1994); *ibid.* **367**, 252 (1994); *ibid* **367**, 282 (1994)
- 15 B. K. Cho et. al, *Phys. Rev. B* **52**, 3676 (1995); B.K. Cho et. al. *ibid B* **52**, 3684(1995).
- 16 P.C. Canfield et. al., *Physica (Amsterdam)* **C 230**, 397 (1994); D. D. Rathnayaka et. al. *Phys. Rev. B* **53**, 5688 (1996).
- 17 B. K. Cho et. al. *Phys. Rev B* **53**, 8499 (1996); B. K. Cho et. al, *ibid B* **53**, 2217(1996).
- 18 T. Ekino et. al. *Phys. Rev. B* **53**, 5640 (1996).
- 19 D. D. Lawrie and J.P. Franck, *Physica C* **245**, 159 (1995).
- 20 D. Davidov et. al., *Phys. Rev. B* **5**, 1711(1972); C. Rettori et. al., *ibid B* **7**, 1 (1973)
- 21 A. S. Nowick and B. S. Berry, *J. Phys. Chem. Solids* **36**, 1591 (1975);
Phys. Rev. Lett. **32**, 1254 (1974).
- 22 G.R. Stewart, *Rev. Mod. Phys.*, **56**, 755 (1984).
- 23 F. Gandra, S. Schultz, S.B. Oseroff, Z.Fisk and J.L. Smith, *Phys. Rev. Lett.*, **55**, 2719 (1985).
- 24 S.B. Oseroff, S. Schultz, C. Rossell, Y. Dalichaouch, M.B. Maple and Z. Fisk, *Am. Phys. Soc.*, March 1986
- 25 S.B. Oseroff, C. Rossell, S. Schultz, M.B. Maple and Z. Fisk, *Bull. Am. Phy. Soc.*, March 1987.
- 26 D.EW. MacLaughlin, C Tien, W.G. Clark, M.D. Lan, Z. Fisk, J.L. Smith and H.R. Ott,
- 27 D. Cox, *Phys. Rev. B* **35**, 4561 (1987).
- 28 E. Simanek and K. Sasahara, *J. Low Temp. Physics* **66**, 249 (1987).
- 29 A. Yoshimori and H.J. Kasai, *J. Mag. Magn. Mater.*, **31-34**, 475 (1983).
- 30 T. Gambke, B. Elschner and L.L. Hirst, *Phys. Rev. Lett.*, **40**, 1290 (1978).
- 31 M. Schlott, H. Schaeffer and B. Elschner, *Z. Phys. Cond. Matter*, **B63**, 427 (1986).

- 32 G. Heinrich, J.K. Kappler and A. Meyer, *J. Appl. Phys.*, **53**, 2155 (1982).
- 33 G.E. Barberis, D. Davidov, C. Rettori, J.P. Donoso, I. Torriani and F.C. Gandra, *Phys. Rev. Lett.*, **45**, 1966 (1980).
- 34 C. Larica and B.R. Coles, *Phil. Mag. B.*, **52**, 1097 (1985).
- 35 K. Kojima et al., *J. Mag. Mag. Mat.* **81**, 267 (1989).
- 36 C. Rossel et al., *Phys. Rev. B* **35**, 1914 (1987).
- 37 I. Felner and I. Nowik, *J. Mag. Mag. Mat.* **63&64**, 615 (1987).
- 38 I. Felner et al., *Phys. Rev. B* **35**, 6956 (1987).
- 39 E.V. Sampathkumaran et al., *Phys. Rev. B* **35**, 2035 (1987).
- 40 J.L. Sarro, R. Modler, R. Movshovich, D. Hristova, A.L. Cornelius, M.F. Hundley, J.D. Thompson, C.L. Benton, C.D. Immer, M.E. Torelli, G.B. Martins, Z. Fisk and S.B. Oseroff, *Phys. Rev. B* **57**: (13) 7785-7790 (1998).
- 41 Y. Ishikawa and Y. Noda in *Magnetism and Magnetic Materials*, edited by C.D. Graham, G.H. Lander, and J.J. Rhyme, *AIP Conf. Proc. No. 24* (AIP, New York, 1975), p.145.
- 42 C. Kittel, *Introduction to Solid State Physics*, 5th ed. (Wiley New York, 1976), p17.
- 43 R.A. Robinson, A. Purwanto, M. Kohgi, P.C. Canfield, T. Kamiyama, T. Ishigaki, J.W. Lynn, R. Erwin, E. Peterson, and M. Movshovich, *Phys. Rev. B* **50**, 9595 (1994).
- 44 A. Amato, P.C. Canfield, R. Feyerhem, Z. Fisk, F.N. Gygax, R.H. Heffner, D.E. MacLaughlin, H.R. Ott, A. Schenck, and J.D. Thompson, *Phys. Rev. A* **46**, 3151 (1992).
- 45 P. C. Canfield, J. Thompson, W.P. Beyermann, A. Lacerda, M.F. Hundley, E. Peterson, Z. Fisk, and H.R. Ott, *J. Appl. Phys.* **70**, 5800 (1991).
- 46 Z. Fisk, P.C. Canfield, W.P. Beyermann, J.D. Thompson, M.F. Hundley, H.R. Ott, E. Felder, M.B. Maple, M.A. Lopez de la Torre, P. Visani, and C.L. Seaman, *Phys. Rev. Lett.* **67**, 3310 (1991).
- 47 Z. Fisk, D. W. Hess, C.J. Pethick, D. Pines, J.C. Smith, J.D. Thompson, and J.D. Wills, *Science* **239**, 33 (1988).
- 48 G.B. Martins, D. Rao, G.E. Barberis, C. Rettori, R.J. Duro, J. Sarrao, Z. Fisk, S. Oseroff,



- J. D. Thompson, Phys. Rev. **B52**, 15062 (1995).
- 49 G.E. Barberis, D. Davidov, C. Rettori and J.F. Suassuna, Phys. Rev. **B 19**, 2385 (1979).
- 50 R.N. Mesquita, G.E. Barberis, C. Rettori, M.S. Torikachvili, M.B. Maple, Solid State Comm. **74**, 1047 (1990).
- 51 K. Chahara et al., Appl. Phys. Lett. **63**, 1990 (1993); R. von Helmolt et al., Phys. Rev. Lett. **71**, 2331 (1993); S. Jin et al., Science **264**, 413 (1994); M. McCormack et al., Appl. Phys. Lett. **64**, 3045 (1994); Y Tokura et al., J. Phys. Jpn. **63**, 3931 (1994).
- 52 G.H. Jonker and J.H. van Santen, Physica **16**, 337 (1950).
- 53 C. Zener, Phys. Rev. **82**, 403 (1951); P.G. de Gennes, Phys. Rev. **118**, 141 (1960).
- 54 J.H. Kuo, H.U. Anderson, and D.M. Sparlin, J. Solid State Chem. **83**, 52 (1989).
- 55 A. J. Millis, P. B. Littlewood, and B. I. Shraiman, Phys. Rev. Lett. **74**, 5144 (1995).
- 56 H. Y. Hwang, S.-W. Cheong, P. G. Radaelli, M. Marezio, and B. Batlog, Phys. Rev. Lett. **75**, 914 (1995).
- 57 A. Asamitsu, Y. Moritomo, Y. Tomioka, T. Arima, and Y. Tokura, Lett. to Nature **373**, 407 (1995).
- 58 S.N. Riddlesden and P. Popper, Acta Crystalligr. **11**, 54 (1958).
- 59 T. Kimura, Y. Tomioka, H. Kuwahara and Y. Tokura, Nature (London) **380**, 141 (1996).
- 60 C. D. Potter, M. Swiatek, S.D. Bader, D. N. Argyriou, J. F. Mitchell, D. G. Hinks and J. D. Jorgensen, Phys. Rev **B57**, 72 (1998).
- 61 Charles P. Poole, Jr., Electron Spin Resonance (Interscience Publishers, New York, 1964).